

Characterization of Physical and Chemical Properties of Synthetic Polymer using Ion Mobility-Mass Spectrometry

Dissertation

for the award of the degree "Doctor rerum naturalium"
of the University of Göttingen

within the doctoral program
of the Georg-August University School of Science (GAUSS)

submitted by

Shinsuke Kokubo

from Saitama, JAPAN

Göttingen, 2017

Thesis Committee

- Prof. Dr. Philipp Vana, MBA
Institute of Physical Chemistry
University of Göttingen
- Prof. Dr. Konrad Koszinowski
Institute of Organic and Biomolecular Chemistry
University of Göttingen

Members of the Examination Board

Reviewer

- Prof. Dr. Philipp Vana, MBA
Institute of Physical Chemistry
University of Göttingen

Second Reviewer

- Prof. Dr. Konrad Koszinowski
Institute of Organic and Biomolecular Chemistry
University of Göttingen

Further members of the Examination Board

- Prof. Dr. Michael Buback
Institute of Physical Chemistry
University of Göttingen
- Prof. Dr. Martin Suhm
Institute of Physical Chemistry
University of Göttingen
- Prof. Dr. Ricardo Mata
Institute of Physical Chemistry
University of Göttingen
- Dr. Florian Ehlers
Institute of Physical Chemistry
University of Göttingen

Date of the oral examination; 01.12. 2017

Preface

Nowadays plastic and elastic materials are essential material in our life. The single word of “polymer” embraces different types of material from various synthetic process with diverse functionality. Biological polymers, such as cellulose can be mainly provided from plants in nature. Since ancient time, mankind has been utilizing biological polymer for a furniture or paper. Protein and peptide, generated from living cell, play an important role in fundamental bio-activity. Synthetic polymer, which was rapidly developed since 20th century, making a revolutionary change of our life. A lot of physicists and chemists developed various kinds of synthetic process and characterization methods for physical behaviors such as phase change, phase separation and so on. These achievements enabled us to control properties and functionalities of polymer. Basic physical pictures and interaction models are required for understanding physical properties and structural analysis of synthetic polymers. These models for calculating and understanding the behavior of polymer in bulk and solution were mainly founded by two chemists, Hermann Staudinger and Paul Flory almost half century ago¹. Although these physical models describe spacious size of single molecule in a polymer –so-called “macromolecule”– using the number of polymerization degree². However, almost all conventional experiments were demonstrated using the polymer being aggregation of macromolecules with different molar mass. The experimental approach using polymer works well for understanding average properties in bulk phase. Therefore, there is still much room for developing analytical methodology for physical and chemical properties of synthetic.

Herein, one basic question arises: how can we analyze a polymer with particular molar mass? To approach this open question, the author focused on mass spectrometry (MS) in this study. MS is a powerful tool for development of new polymer because it can evaluate the absolute molar mass of the polymer³. The outstanding features of MS are high accuracy and sensitivity. Hence, MS enables the determination of the elemental composition of the sample and detection of tiny amounts of byproduct/impurities.

Besides, experimental throughput is quite high, because data acquisition time is shorter than for most other analytical methods. These advantages enables the hyphenation of MS with other analytical methods such as gas/liquid column chromatography (GC, LC), inductively coupled plasma (ICP), etc. Very recently, the hyphenation between ion mobility (IM) and MS is one of the most attractive combinations in diverse patterns of hyphenated MS techniques⁴. During measurement, sample ion drifts in a tube that is filled with an inert gas, such as helium or nitrogen at < 10 mbar. Experimental observables are the drift time and the mass-to-charge ratio (m/z). The drift time depends on the size of the sample ion.

Although the history of IM is as long as MS, it took a long time to develop a commercially available IM-MS system⁵. The bottleneck of the low yield of sample ions was solved thanks to recent development of ion trap systems technology. In the last few years, even complex and intractable species have been investigated successfully with IM-MS and the number of publications in this field is steadily growing including the application to synthetic polymer⁴.

Bowers and Wytenbach conducted the pioneering study of synthetic polymer using IM-MS in the 1990s on the dependence of polymer size with polymerization degree⁶. In their study, molecular dynamics (MD) simulation was applied to estimate the conformation of an isolated polymer. They demonstrated the feasibility of evaluating spacious size and conformation of a synthetic polymer. Recently, many groups have utilized on the other feature of IM-MS such as drift time dependence on spacious size. They propose some methodologies in terms of chromatography for structural isomers.

IM-MS evaluates spacious size and molar mass of polymer simultaneously. The isolated macromolecule enables a simpler study under similar conditions with computer simulation. This is contrary to conventional methodology such as light scattering and viscosity measurements conducted in theta solution.

In these contexts, the author came up with ideas applying IM-MS to access of understanding physical and chemical properties of synthetic polymer in a quantitative manner. Herein, the goal of this thesis is to develop analytical methods which

characterize physical and chemical properties of synthetic polymers using IM-MS. Experiment in conjunction with MD simulation was carried out to verify this idea.

This thesis is written as a final report of PhD work from April 2015 to September 2017 at the University of Göttingen, and consisted of three parts. In part I, fundamental of motivation, theory and experimental principle are described. Part II, on singly charged polymer. In part III, as a model case of multiply charged polymer, studies on a doubly charged polymer are described.

Herein, I appreciate Prof. Dr. Philipp Vana, MBA (Institute of Physical Chemistry, University of Göttingen) for giving me a chance to study and working as a first supervisor of my work in PhD course. I thank Prof. Dr. Konrad Koszinowski (Institute of Organic and Biomolecular Chemistry, University of Göttingen) for being my second supervisor. I also acknowledge all examination board members, Prof. Dr. Michael Buback, Prof. Dr. Martin Suhm, Prof. Dr. Ricardo Mata and Dr. Florian Ehlers (all at Institute of Physical Chemistry, University of Göttingen) for willingly accepting my offer.

The author wishes this study could inspire a new idea into polymer science and supports innovation of our life.

Ion mobility-mass spectrometer is like sun floating in the polymer universe.

It shows us many properties of polymer clearly, likewise, shining light on planets.

September 2017, Göttingen, Germany

Shinsuke, KOKUBO

Abstract

This thesis focuses on developing analytical methodologies based on ion mobility-mass spectrometry (IM-MS) for both physical and chemical properties of synthetic polymer. Beyond numerical experimental data, a comprehensive and visualized interpretation of polymer structure and topology was achieved by theoretical computational approach: molecular dynamics (MD) simulation and collision cross section (CCS) calculation.

In the first study (Chapter 4), the CCS of polyethylene glycol (PEG) and polypropylene glycol (PPG) were measured in dependence of the number of monomer units (n) per chain. A model equation was applied to elucidate the main factor (characteristic ratio, C_n) determining the incremental tendency of CCS against n . For PEG and PPG, C_n of 3.96 and 5.76 were obtained respectively. Detailed evaluation of the data shows that the globule model has good agreement with the literature reference values. IM-MS experiments on charged poly(methyl methacrylate) (PMMA) and polystyrene (PS) also showed good accordance with reported values, verifying sufficient versatility of the proposed method. The presented procedure is extremely quick and easy to perform and provides stunningly rapid access to the conformation data of synthetic polymers.

Rayleigh limit equation, describes physical process of electro-spray ionization, provides a useful relation between surface tension and radius of charged droplet. In the second study (Chapter 5), the lower threshold size of cation adducted polymer was analyzed by MS experiment. MD simulation gives convenient access to determine the radius of the critical stable charged polymer of diverse type in spherical dimension. This approach yielded very good result which in good agreement with the literature-known reference values of surface tension (PEG : 45.0 mN/m, PPG : 33.1 mN/m, PMMA : 40.0 mN/m and PS : 32.4 mN/m). The proposed method also provides an extremely swift and precise measurement for polymer without any external disturbances of solvents or impurities.

In the third study (Chapter 6), doubly charged ion system was investigated as a model case study of multiply charged polymer. The dependency of the effective collision cross section on n was evaluated with MD simulations. Assuming a balance between elastic and Coulomb forces inside short and asymmetric doubly-charged chains, a method for determine relative dielectric constant (ϵ_r) was developed. ϵ_r was found to be 7.87 for PEG and 6.18 for PPG, respectively. The proposed method using IM-MS is clearly carried out in the absence of solvent inside the polymer yielding intrinsic material properties.

The fourth study (Chapter 7) was designed to detect and classify isomer of star-polymer by utilizing precisely synthesized polyethylene glycol with multi-arm (star-PEG). Grafting pattern of star-PEG can be represented from experimental determined CCS of doubly charged species. Besides CCS dependency, energy resolved-ion mobility spectrometry (ER-IMS) was performed to identify the corresponding isomer. To compensate poor resolution in ion mobility spectrometry, the profile an ion mobility chromatogram (IMC) was deconvoluted with Gaussian functions was applied to extract peaks from IMC as an alternative procedure. Both IM-MS and ER-IMS measurement were demonstrated for each extracted IMC, and thus, IMC broadening could be concluded that coexisting isomers in commercial star-PEG. The cross-check in conjunction with CCS and ER-IMS analysis is powerful and reliable analytical methodology for a successful revealing isomer in star-polymer.

Abstract

Table of Contents

Preface	3
Abstract	7
Part I Background and Theory	15
Chapter 1 Introduction and Motivation	16
1.1 Mass spectrometry in polymer science	17
1.2 Drawback and challenge of mass spectrometer	17
1.3 Study on polymer using ion mobility-mass spectrometry (IM-MS)	18
1.4 Fundamental motivation of this work	19
1.5 Objective of this work	21
Chapter 2 Fundamental of Experiment	24
2.1 Fundamental principle of Ion Mobility Spectrometer (IMS)	25
2.2 Theoretical background of IMS	26
2.2.1 Ion mobility	26
2.2.2 Resolution of ion mobility spectrometry	32
2.3 Type of ion mobility (IM) spectrometer	35
2.3.1 Filter type	35
2.3.2 Drift time type	36
2.3.3 Traveling wave type	36
2.4 Comparison of IM-MS and selection	38
2.5 Introduction of Synapt G2 HDMS TM	39
2.6 Evaluation of absolute collision cross section by Synapt G2 HDMS TM	41
Chapter 3 Molecular Modeling	43

Table of Contents

3.1	Outline of molecular modeling	44
3.2	MM2.....	45
3.3	Molecular dynamics	45
3.3.1	Basic algorithm of MD simulation	45
3.3.2	Time step for MD simulation	46
3.3.3	The number of step in MD simulation of polymer	47
3.4	Calculation of <i>CCS</i>	47
 Part II Study on +1 charge adducted species		50
 Chapter 4 Collision cross section dependency on the number of		
monomer units of +1 charged polymer		51
4.1	Introduction	52
4.2	Experimental section	54
4.2.1	Materials.....	54
4.2.2	IM-MS.....	54
4.2.3	Effective <i>CCS</i> evaluation	54
4.2.4	Simulation of molecular conformation and calculation of <i>CCS</i>	55
4.3	Results and discussions	56
4.3.1	Model equation development	56
4.3.2	Theoretical validation for developed model	62
4.3.3	Experimental validation for developed model.....	64
4.3.4	Model application to other polymers	71
4.4	Conclusions	74
 Chapter 5 ESI-MS threshold polymer size.....		76
5.1	Introduction	77
5.2	Experimental section	80
5.2.1	Materials.....	80
5.2.2	IM-MS.....	81
5.2.3	Simulation of molecular conformation and calculation of <i>CCS</i>	81
5.3	Results and discussion	81

5.3.1	CCS dependency on type of alkali cation.....	81
5.3.2	Evaluation of surface tension based on CCS.....	85
5.3.3	Discrimination for sphericity of cation adducted polymer	86
5.3.4	Droplet size deviation by bulky end group.....	88
5.4	Conclusions	90
Part III	Study on +2 charge adducted species	92
Chapter 6	Collision cross section dependency on the number of monomer units of doubly charged polymer	93
6.1	Introduction	94
6.2	Experimental section	96
6.2.1	Materials	96
6.2.2	IM-MS.....	96
6.2.3	Effective CCS evaluation	96
6.2.4	Simulation of molecular conformation and calculation of CCS	97
6.3	Results and discussion.....	97
6.3.1	Classification of doubly charged species.....	97
6.3.2	Region I : Asymmetric conformation of +2 charge adducted polymer ..	100
6.3.3	Region II–III : Intermediate state between asymmetric and symmetric conformation	109
6.3.4	Region IV : Globule state in +2 charge adducted polymer	111
6.4	Conclusions	114
Chapter 7	Classification of Star polymer using IM-MS	116
7.1	Introduction	117
7.2	Experiment	118
7.2.1	Chemicals.....	118
7.2.2	Synthesis of PEG substituted tetrakis-bromomethyl-methane.....	119
7.2.3	Synthesis star-PEG with two/three PEG-arms	120
7.2.4	IM-MS.....	120
7.2.5	Simulation of molecular conformation and calculation of CCS	120

Table of Contents

7.3	Results and discussions	121
7.3.1	Mass spectrometry of synthesized star-PEG	121
7.3.2	Ion mobility spectrometry of singly charged star-PEG.....	125
7.3.3	Ion mobility spectrometry of doubly charged star-PEG	128
7.3.4	IMC profile analysis of commercial star-PEG.....	132
7.4	Conclusions	134
Conclusion Remarks		135
Bibliography.....		138
Appendix		146
Appendix I		147
Appendix II		149
Appendix III		155
Acknowledgements.....		159
About Author		162

Table of Contents

Part I

Background and Theory

Chapter 1

Introduction and Motivation

1.1 Mass spectrometry in polymer science

Polymer science is a relatively young field compared to inorganic and low molar mass organic chemistry. However, nowadays it is essential material for our daily life. Diverse mass produced commodity and novel research phase sub-nanometer sized materials are made of polymer. We believe polymer will contribute to our life with more advanced properties in the future. Therefore, research and development of novel/advanced polymer will keep proceed, the advancing modern analytical methodology of polymer will open access to a more precise picture of polymer character and behavior.

Mass spectrometry (MS) has big advantages in measuring absolute molar mass with high sensitivity. It had played a key role to discover new elements^{7,8} and compounds⁹. However, MS has one request charged molecules for sample. Ionization was the one of the highest hurdle for polymer scientist. Conventional ionization of polymer lost its original structure due to electron impact dissociation^{10,11}. In the 1980s, the development of matrix-assisted-laser-desorption- ionization (MALDI)^{12,13} and electro-spray ionization (ESI)¹⁴ dramatically accelerated research and development of polymer. Nowadays, MS is inevitable analysis for studying of polymer science^{3,15,16}.

Besides ionization method, tandem MS¹⁷ with collision induced dissociation and super accurate mass analysis enables the analysis of chemical structure and element composition of polymers¹⁸, giving further insight into new polymerization synthesis and elucidation for polymerization mechanism^{19–23}.

1.2 Drawback and challenge of mass spectrometer

In MS, the ratio of molar mass to charge (m/z) of sample is observable, this character provides both advantages and drawbacks. To elucidate detailed synthetic kinetics and functionalization of polymer, further aspects particularly for structural information is crucial. MS has difficulties to speculate microstructure and high-order structure whereas other spectroscopic methods such as nuclear-magnetic resonance spectroscopy (NMR), infra-red spectroscopy (IR), small angle x-ray scattering (SAXS) and x-ray diffraction (XRD) evaluate configuration, conformation and folding pattern of

polymer²⁴. To compensate this drawback, hyphenation of MS with other technique empowers MS as a structure analytical method. Particularly hyphenation with column chromatography enables pre-separate depending on physical and chemical interaction between sample compounds, mobile phase and stationary phase. These types of hyphenation techniques give additional information on polarity and structure.

1.3 Study on polymer using ion mobility-mass spectrometry (IM-MS)

Ion mobility-mass spectrometry (IM-MS) is a promising hyphenated technique which separate sample depending on the collision cross section with inert gas atom or molecules^{4,25}. In the 1990's, *Bower's* group (University of California, USA) has conducted pioneering work of oligomer with prototype IM-MS apparatus^{6,26}. They performed experiment with originally designed IM-MS to elucidate conformation of sodium cation (Na^+) adducted polyethylene (PEG) oligomer. They also carried out molecular dynamics simulation to get the information of PEG conformation. Besides that, IM-MS enabled separation of polymer depending on the spacious size without using chromatography. This work opens up the possibility of structural analysis in addition to absolute weight measurement with MS experiment. Compared to other hyphenated technique, IM-MS is able to achieve adequate separation in vacuum within milliseconds, order of magnitude quicker than required with HPLC-MS system (tens or hundreds of minutes scale).

However, operation and maintenance of home-build IM-MS required much expertise, thus IM-MS was widely used apparatus for general polymer science research. However, in the beginning of 21st century, IM-MS became familiar and attracted scientists in polymer physics and chemistry. Commercially available IM-MS was released from many MS product makers (Agilent technologies, SCIEX, Bruker Daltonics and Waters Corporation) with user-friendly operation. Besides that, computer technology was quickly developed in the last decade, making MD simulation and spacious size calculation much easier accessible.

In last 10 years, *Prof. Dr. Trimpin's*^{4,27–33} (Wayne State University, USA) and *Prof. Dr. Pagel's*^{34–44} (Free University of Berlin, Germany) have been actively leading study

using commercial IM-MS of Waters Corporation. A production model IM-MS can be a suitable MS as a routine technique for non-specialists to perform quantitative analysis owing to computer assistance.

1.4 Fundamental motivation of this work

Conventional studies focus much on developing commercial IM-MS with user-friendly operation, which increase the usage of IM-MS in polymer science⁴⁵. One of the most distinctive advantages of IM-MS is to evaluate spacious size of sample in vacuum phase⁴⁶. However, most studies have only done for conformational analysis and isomer separation with qualitative aspect. Few studies have quantitatively utilized IM-MS for evaluating physical and chemical properties of polymer.

Size of polymer has been conventionally evaluated using viscosity measurement and light scattering method^{47,48}. These methods were established theoretically and experimentally almost half century ago, therefore, widely used for polymer characterization. Large database in the form of handbooks⁴⁹ is available. Typically, different values coexist for particular index of polymer making the method unreliable. For instance, characteristic ratio, which represents stiffness of polymer main chain, can be theoretically identified for every polymer. On the contrary to theory, various data of characteristic ratio are available depending on type of solvent and experimental temperature. The characteristic ratio is also attributed to molar mass distribution of the sample. In synthetic polymer, different weight of macromolecules coexists due to molar mass distribution, conventional measurement has only access of the property of the macroscopic material. Therefore, we can only execute measurement with averaged observable depending on dispersion, average molar weight and so on. An alternative approach is combination with hyphenation between size excluded chromatography equipped with light scattering or viscosity detector, but SEC does not provides precise absolute molar mass.

Nowadays, correct value of index is required, because downsizing goes further and more accurate size is necessary for developing devices in electronics and medical

field. The plurality of indexes can hinder growth and development of polymer science and industry in the future.

Besides the problem of molar mass distribution of polymer, solvent molecule possibly prevents observing intrinsic properties of polymer. Conventional methods need to be carried out in liquid phase with dissolved polymer. We have to take into account interaction between polymer and solvent molecule. It is impossible to conduct experiment with bulk polymer with for example viscosity and scattering light measurement.

IM-MS surmounts these obstacles simultaneously, enables measurement of spacious size with absolute molar mass at absence of solvent. IM-MS must have potential for replacing conventional analytical methods. Within these contexts, the author considered to exploit potential of IM-MS for quantitatively evaluating physical and chemical properties of polymer.

1.5 Objective of this work

In this work, IM-MS was performed to develop analytical method regarding to following four items.

- 1) Evaluation of a characteristic ratio of polymer analyzing the contribution of each monomer unit to whole size of polymer (Chapter4)

IM-MS enables to acquire size of a particular molar mass polymer. In other words, it is possible to quantitatively evaluate incremental contribution of each monomer unit to whole size of polymer. This increment depends on the chemical property of monomer unit and strongly correlated with stiffness of polymer chain. Based on this idea, analytical method was developed for polymer stiffness represented by its characteristic ratio.

- 2) Analysis for physical and chemical property of polymer utilizing interaction between excess charge and polymer

2)-1 Obtaining surface tension (Chapter5)

According to the mechanisms of electro-spray-ionization, the minimum droplet size of polymer with excess charge can be determined by the force balance between the Coulomb repulsive force and surface tension. This method to measure surface tension of polymer was designed by evaluating the size of threshold signal on IM-MS.

2)-2 Analysis for relative dielectric constant (Chapter6)

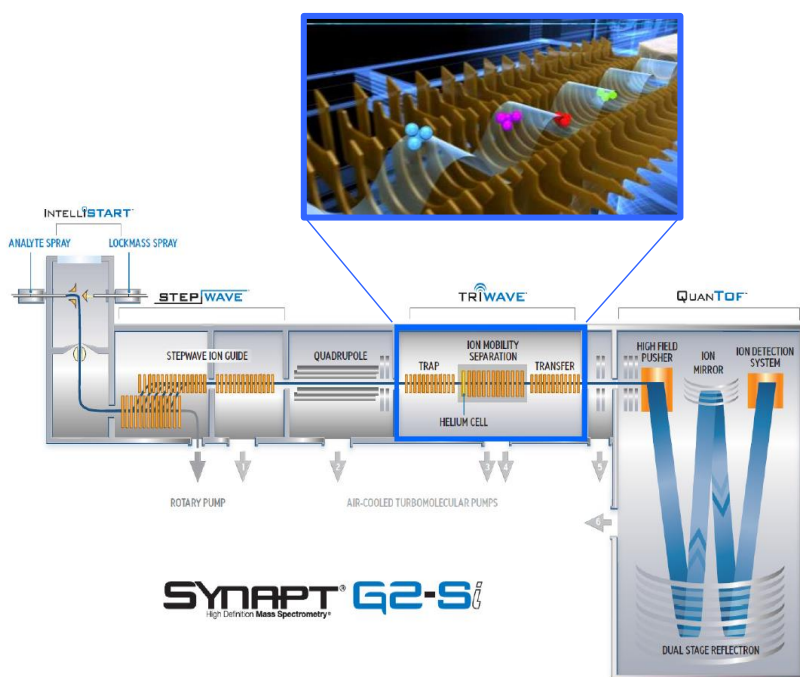
Electro-spray-ionization can efficiently produce multiply charged ions. The repulsive Coulomb force (f_c) enlarges spacious size of a polymer chain. On the other hand, a stretched out polymer chain underlies a retracting entropy elastic force (f_s) working against f_c , and they can balance each other in vacuum. Both f_c and f_s are correlated with the spacious size, which can be observed by IM-MS experiment. From these relationships, methods were developed to evaluate electronic and/or mechanical properties of the polymer chain.

2)-3 A classifying method of isomer of star shape polymer (Chapter7)

According to conventional IM-MS studies, it is known that a single excess charge can be stabilized by a polymer chain in a contracted state. In case of a multiply charged polymer, it takes larger spacious size than singly charged one. It is possible to differentiate subtle difference among isomers of a star-shape polyethylene glycol (star-PEG). Within these contexts, in this study, the isomers of star-PEGs with four hydroxyl end groups and different numbers of PEG grafted arms (PEG-arm) were originally prepared to evaluate *CCS* on the number of PEG-arm by IM-MS.

Chapter 2

Fundamental of Experiment



Reprinted with permission of Waters Corporation

2.1 Fundamental principle of Ion Mobility Spectrometer (IMS)

The advantages of mass spectrometry (MS) can be represented by high sensitivity and evaluation of absolute molar mass. Nowadays, MS is utilized in many science fields such as nano-science, biochemistry and medical diagnostics⁴. However, MS provide just only information on the ratio of molar mass to charge (m/z) without any other additional information. To broaden its application in state of art science field, the hyphenated analytical system between ion mobility spectrometer (IMS) and MS can be one of the best solutions.

Basic principle of separation in IMS can be compared to drop test of paper (Figure 2.1). Releasing two sheets of paper with same weight, the paper crumpled paper sheet can reach ground faster than the flat one. The dropping time depends on the air resistant caused by difference of the geometry. Flat paper can accept more resistant force than crumpled one, because force is proportional to area of dropping subject.

Analogous to this phenomenon, two ions with same elemental composition but different spacious size (isomers) can be separate by IMS^{50–52}. During the flight in the IMS tube, ions undergo collisions with vapor gas molecules. Ions with larger collision cross section takes more friction from vapor gas, resulting a lower drift velocity. In general, a “spread out” structure isomer drifts slower than the “collapsed” structure. IMS can separate and identify isomers from each other.

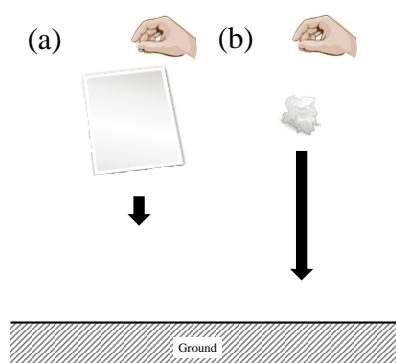


Figure 2.1

Schematic picture of paper dropping experiment. Traveling time to the ground depends on the form of paper sheet. The flat sheet of paper (a) reaches later than the crumpled paper (b).

2.2 Theoretical background of IMS

2.2.1 Ion mobility

In IMS, ions obey kinetics under a static electric field as well as in MS^{4,25}. The ion movement in IMS is strongly affected by collisions with gas molecules, whereas in MS the movement is only depending on electric field because of the absence of the gas-colliding. For instance time-of-flight type MS, an ion travels flight tube with certain velocity depending on the electric field of a vector \mathbf{E} with the magnitude $|\mathbf{E}|$. On the other hand, in IMS under same electric field of \mathbf{E} , a vector of the drift velocity of ion: $\mathbf{v}_d(\mathbf{E}/N)$ is described as a function of the field of \mathbf{E} and a molecular gas density of N . Since \mathbf{v}_d reflects the interaction between the ion and the gas molecule which strongly depends on the ion structure, the structural information is calculated from the observable of IMS: drift time. The ion movement in IMS can be classified into two conditions: the low field condition and the high field condition. As mentioned later, low electric field type IMS was used for polymer analysis in this study. Therefore, in this section, theoretical background of low field condition is described in detail.

Under low field condition, the vector of the drift velocity (\mathbf{v}_d) is described in Equation (2.1):

$$\mathbf{v}_d = K\mathbf{E} \quad (2.1)$$

Where K is defined as ion mobility which correlates with the structure of the ion. Here K can be evaluated through the movement in gas under the static electric field and we can deduce the structural information from K . Figure 2.2 shows schematic collision processes in a drift tube, where the ion and the gas molecules are regarded as a hard sphere particle with the constant collision cross section without internal motion such as vibrations and rotations.

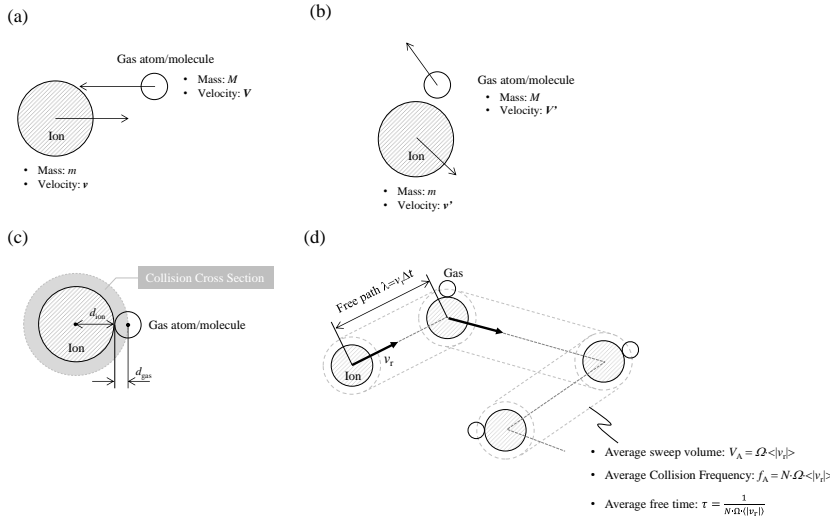


Figure 2.2

Schematic diagram of collision event in the ion mobility tube. (a) Before and (b) after collision event of ion and gas atom/molecule. (c) Experimental observable of IMS; collision cross section. (d) Successive collision events. The ion is accelerated by the electric field of ion mobility tube in free path.

The total collision energy is distributed only into the kinetic energy of each particle. The collision cross section does not depend on the electric field, gas temperature, and the kinetic energy. Figure 2.2 (a) shows the kinematic processes in the collision of the ion (mass with m) with the gas molecules (mass with M). The velocities of the ion and the colliding gas are changed from v and V into v' and V' , respectively, whereas the velocity of the center of mass v_{cm} keeps constant. As described in Fig. 2.2 (c), the radii of the ion and the gas molecule are defined as d_{ion} and d_{gas} , respectively. The collision cross section (Ω) is described as $\Omega = \pi (d_{ion} + d_{gas})^2$, which is independent of the temperature of colliding gas, velocity, and field. When the distance between the ion and the gas molecule is less than $d_{ion} + d_{gas}$, they collide with each other. Figure 2.2 (d) shows a successive collision between the ion and the gas molecules under the field. The ion is accelerated by the field during free time Δt until successive collisions event. The ion moves without collision in the path length of $\lambda = |v_r| \Delta t$, where v_r is the relative velocity of the ion to the gas molecule.

$$\mathbf{v}_r = \mathbf{v} - \mathbf{V} \quad (2.2)$$

Collision and drifts events repeat in the ion mobility tube, the total drift is obtain as an experimental observable via IMS. The field effect becomes more significant with the longer Δt . The average Δt is defined as τ , which determines the drift velocity in whole processes. τ is calculated as the inverse of the average collision frequency: $1/f_A$. Here f_A is the average number of collisions between the ion and the gas molecules in unit time. As shown in Fig. 2.2 (c), f_A is deduced from the number of the gas molecules in sweep volume V_A which is defined as $\Omega \langle |\mathbf{v}_r| \rangle$. When the ion moved in frozen gas molecules, we could obtain the frequency with $f_A = N \Omega \langle |\mathbf{v}_r| \rangle$, where N_{gas} is the molecular gas density. The average free time of τ is thus described with Equation (2.3).

$$\tau = 1/f_A = \frac{1}{N_{\text{gas}} \Omega \langle |\mathbf{v}_r| \rangle} \quad (2.3)$$

The ion moves with the constant drift velocity in ion mobility tube, the acceleration or the momentum gain by the field is lost by consecutive collision events. The momentum gain is calculated with Equation (2.4).

$$m \langle \mathbf{v} - \mathbf{v}' \rangle = \mathbf{F} \tau = q \mathbf{E} \tau \quad (2.4)$$

where \mathbf{F} is the field force applied to the ion. This momentum gain is converted into the collision gas molecule, which is described with Equation (2.5).

$$M \langle \mathbf{V}' - \mathbf{V} \rangle = M \langle \mathbf{V}' \rangle - M \langle \mathbf{V} \rangle = q \mathbf{E} \tau \quad (2.5)$$

where “ $\langle \rangle$ ” represents the average of the whole processes. Here the collision gas molecules do not move macroscopically due to electronically neutral under electric field. The averaged vector of the collision gas velocity can be regarded as zero before and after collision event.

$$\langle \mathbf{V} \rangle = 0 \quad (2.6)$$

According to Equation (2.5) and (2.6), Equation (2.7) can be obtained:

$$\langle \mathbf{V}' \rangle = \frac{qE\tau}{M} \quad (2.7)$$

Through the collision processes, trajectory of the ion can be randomly varied in space.

Therefore, time averaged \mathbf{v}_r can be regarded as zero.

$$\langle \mathbf{v}_r \rangle = \langle \mathbf{v}'_r \rangle = \langle \mathbf{v}' - \mathbf{V}' \rangle = 0, \langle \mathbf{v}' \rangle = \langle \mathbf{V}' \rangle \quad (2.8)$$

The momentum is kept constant in the collision process, which tells gives the following relation with $\langle \mathbf{v}' \rangle$ and $\langle \mathbf{V}' \rangle$ by Equation (2.9).

$$m\langle \mathbf{v} \rangle + M\langle \mathbf{V} \rangle = m\langle \mathbf{v}' \rangle + M\langle \mathbf{V}' \rangle \quad (2.9)$$

According to Equation (2.6)–(2.9), the average ion velocity just before the collision, which is the same as the magnitude of \mathbf{v}_d is described by Equation (2.10).

$$\begin{aligned} |\mathbf{v}_d| &= |\langle \mathbf{v} \rangle - \langle \mathbf{V} \rangle| = |\langle \mathbf{v} \rangle| \\ m\langle \mathbf{v} \rangle &= m\langle \mathbf{V}' \rangle + M\langle \mathbf{V}' \rangle \\ \langle \mathbf{v} \rangle &= \langle \mathbf{V}' \rangle + \frac{M}{m}\langle \mathbf{V}' \rangle = qE\tau \left(\frac{1}{M} + \frac{1}{m} \right) \\ |\langle \mathbf{v} \rangle| &= q|E|\tau \left(\frac{1}{M} + \frac{1}{m} \right) \end{aligned} \quad (2.10)$$

When the mass of ion is much smaller than that of the gas molecule, $m \ll M$, Equation (2.10) can be simplified as $\mathbf{v}_d = qE\tau/m$. In this case, the colliding gas is heavy enough to keep its position, whereas the ion moves randomly in the ion mobility tube. This process results in zero average velocity of the ion due to the collision followed by the field

acceleration to $\langle v' \rangle = qE\tau/m$ until the next collision. The velocity after collision is inversely proportional to mass of the ion.

Time dependence of the average ion velocity is schematically shown in Figure 2.3 (a) and (b)⁵. When the collision occurs every τ (Figure 2.3 (a)), the average ion velocity is represented as a periodic saw-tooth wave. Actually, the collision event does not take place periodically but randomly, where the free time varies with Poisson distribution of $p(t) = 1/t \exp(-t/\tau)$. Here, $p(t)$ is the probability function. In this situation, the average ion velocity is represented as an irregular saw-tooth wave (Figure 2.3 (b)) so that the time average is obtained as $v_d = qE\tau/(2m)$ since the average of the free time between the successive collisions is 2τ . When the mass of the ion is much larger than that of the gas molecule, $m \gg M$, Equation (2.10) is reduced to $v_d = qE\tau/M$. Ion velocity is kept almost constant through all collision events (Figure 2.3 (c)).

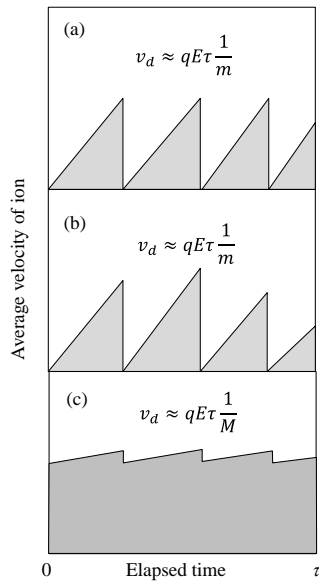


Figure 2.3

Time profile of the average velocity of ion in ion mobility tube. The profile depends on the relative weight of ion to gas. The profile can be classified into three patterns based on weight and collision event frequency. (a) $m \ll M$ with periodic collision, (b) $m \ll M$ with irregular collision and (c) $m \gg M$ with irregular collision.

For the analysis of actual IMS measurement, v_d should be obtained as a function of a gas temperature (T), the molecular gas density (N_{gas}) and the collision cross section (Ω). According to Equation (2.3), Equation (2.10) is converted into Equation (2.11).

$$|v_d| = \frac{q|E|}{N_{\text{gas}}\langle |v_r| \rangle \Omega} \left(\frac{1}{m} + \frac{1}{M} \right) \quad (2.11)$$

Taken into account the gas temperature T , the average velocity of $\langle |v_r| \rangle$ is approximated with root mean approximation by Equation (2.12).

$$\begin{aligned} \langle |v_r| \rangle &\approx \sqrt{\langle |v_r|^2 \rangle} = \sqrt{\langle (\mathbf{v} - \mathbf{V})^2 \rangle} = \sqrt{\mathbf{v}^2 - 2\langle \mathbf{v} \cdot \mathbf{V} \rangle + \mathbf{V}^2} \\ &= \sqrt{\frac{3k_{BT}}{m} + \frac{3k_{BT}}{M}} \end{aligned} \quad (2.12)$$

where $\langle \mathbf{v} \cdot \mathbf{V} \rangle$ can be treated as zero due to Equation (2.6). According to Equation (2.11) and (2.12), the drift velocity is instantly obtained by Equation (2.13).

$$|v_d| = \frac{1}{\sqrt{3}} \frac{q|E|}{N_{\text{gas}}} \left(\frac{1}{m} + \frac{1}{M} \right)^{0.5} \left(\frac{1}{k_{BT}} \right)^{0.5} \frac{1}{\Omega} \quad (2.13)$$

According to (2.1) and (2.13), the mobility K is described by Equation (2.14).

$$K = \frac{|v_d|}{|E|} = \frac{1}{\sqrt{3}} \frac{q}{N_{\text{gas}}} \left(\frac{1}{m} + \frac{1}{M} \right)^{0.5} \left(\frac{1}{k_{BT}} \right)^{0.5} \frac{1}{\Omega} \quad (2.14)$$

Equation (2.14) considers only the translational motion of ion originated from electronic field. Actually, ion and gas can diffuse in the ion mobility tube according Fick's second law⁵³. *Chapman* and *Enskog*⁵⁴ added the diffusion effect into Equation (2.14) and derivate Equation (2.15).

$$K = \frac{|v_d|}{|E|} = \frac{3}{16} \frac{q}{N_{\text{gas}}} \left(\frac{1}{m} + \frac{1}{M} \right)^{0.5} \left(\frac{2\pi}{k_B T} \right)^{0.5} \frac{1}{\Omega} \quad (2.15)$$

Thus the mobility K observed in IMS contains the information on the structure of ions which is elucidated from the collision cross section Ω in Equation (2.15).

2.2.2 Resolution of ion mobility spectrometry

Based on the mathematical description of ion mobility, we can estimate performance of ion mobility tube quantitatively. Same as a spectrometer, resolution is one of the most important indexes to design and plan research. IMS resolution (R) is defined as broadening of the ion packet which corresponds to sample ion introduced into ion mobility tube. R is defined⁵⁵ as a ratio of the drift position (L) to the width (W') on the drift direction by Equation (2.16).

$$R = \frac{L}{W'} \quad (2.16)$$

To convert this spatial definition of resolution into a more practical form, both terms are simply divided by the average drift velocity of the ion packet (v_d).

$$R = \frac{L/|v_d|}{W'/|v_d|} = \frac{t}{W} \quad (2.17)$$

where t is the drift time of the ion packet and W is the temporal width of ion packet. Assuming that this ion packet forms Gaussian shape, its width is defined as 4.7 times the standard deviation (σ). IMS resolution can be determined for an ion mobility spectrum by the Equation (2.18)

$$R = \frac{t}{2W_h} \quad (2.18)$$

where W_h is the temporal width of the ion packet measured at the half of the height of the ion peak. The width of an ion peak on the ion mobility spectrum can be attributed to four broadening factors: the initial packet width, diffusion, mutual charge repulsion and

charge-neutral interaction. In these factors, initial packet and diffusion dominantly determine the peak width. The peak width can be expressed as a function of both the initial width and the contribution of diffusion during the ion migration process,

$$W^2 = W_0^2 + W_d^2 \quad (2.19)$$

where the initial ion packet width (W_0) and diffusion broadened peak width (W_d). An expression for the diffusion broadened peak width can be derived from the normal distribution of the diffusion process,

$$\sigma' = \sqrt{2Dt} \quad (2.20)$$

where σ' is the spatial standard deviation of the diffusion process, D is the diffusion coefficient and t is the time that diffusion occurs (equivalent to the drift time). According to the *Nernst-Einstein* relation, the diffusion coefficient can be expressed in terms of mobility constant K by Equation (2.21).

$$D = \frac{kT}{q} K \quad (2.21)$$

where k is Boltzmann's constant, T is the temperature and q is the charge. Since the mobility constant K is simply the ratio of the ion velocity to the electric field, Equation (2.20) can be converted in to an expression for the spatial diffusional broadening of the peak width (W') by Equation (2.22).

$$W_d' = 4.7\sigma' = \sqrt{\frac{44.2kT|v_d|t}{q|E|}} \quad (2.22)$$

This relation can be further converted to an expression for the temporal diffusion broadened width (W_d) by dividing $v_d = L/t$.

$$W_d = \frac{W_d'}{|v_d|} = t \sqrt{\frac{44.2kT}{q|E|L}} \quad (2.23)$$

According to Equation (2.17), (2.19) and (2.23), the IMS resolution can be described by Equation (2.24).

$$R = \frac{t}{\sqrt{W_0^2 + \frac{44.2kTt^2}{q|E|L}}} \quad (2.24)$$

If spatial size of the initial ion packet is much smaller than later: $W_0 \ll W_d$, Equation (2.24) can be simplified to Equation (2.25).

$$R = \sqrt{\frac{q|E|L}{44.2kT}} \quad (2.25)$$

From this equation, that resolution is directly proportional to the magnitude of the electric field, the drift tube length and inversely proportional to the temperature. Modern instrument platform is commonly equipped with long (~1 m) drift tubes to achieve high resolution ($R \sim 50$ – 120). While $R \sim 70$ is sufficient for many applications (i.e., differentiation of chemical classes and determination of Ω values), the conformational multiplicity of biomolecules demands higher resolution⁵⁶.

2.3 Type of ion mobility (IM) spectrometer

2.3.1 Filter type

The filter type is the oldest IM spectrometer which was developed in the early 20th century. As Figure 2.4 shows, electric field was implied in the axial direction to gas streamline. Transparency of ion depends on the strength of electric field and flow velocity. IM spectrum can be obtained by scanning these parameters. This type of IM has been widely used as a differential mobility analyzer (DMA) in aerosol analysis. Beyond the analysis for mobility, DMA also provide the function to classify and collect particle. Therefore, sample particle can be measured with mobility as an ion and measure absolute size and actual shape by electron microscopy.

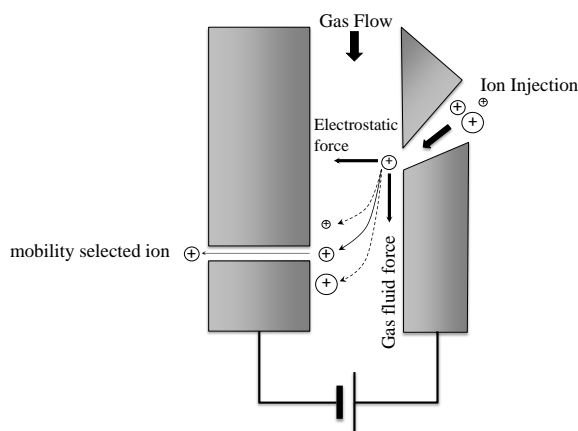


Figure 2.4

Schematic diagram of filter type ion mobility spectrometer. In the ion mobility cell, inert gas flows perpendicular to electrostatic field. Trajectory of ion depends on the mobility^{4,25}.

2.3.2 Drift time type

Sample ion species are injected as one pulsed packet and drift in the static electric field. The experimental observable is drift time which takes from starting point to detector. Drift time increases with the spacious size of the ion. Although this type of IM has the higher resolution than other ones, its sensitivity is relatively low. This problem can be caused by longer drift time (10^{-3} – 10^1 sec). Some apparatus have 2–3 m length^{57,58} IM tube and their drift time, which take up to a few seconds, are much longer than flight time of MS with up to a few hundreds of μ s. During traveling IM tube, sample ion packed could thus be diverse due to Coulomb repulsion force among ion species. To overcome this problem, commercial apparatus are equipped with ion collection trap system.

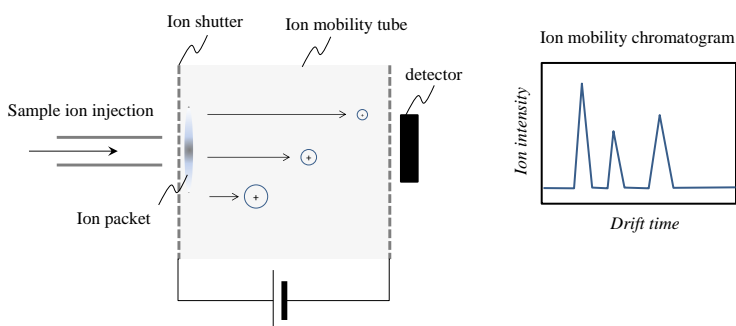


Figure 2.5

Schematic diagram of drift type ion mobility spectrometer^{4,25}. Ion is guided into electrostatic field purged with inert gas. Experimental observable is drift time which depends on the mobility of ion.

2.3.3 Traveling wave type

Traveling wave ion mobility spectrometer (TW-IMS), developed by Waters corporation⁵⁹, is like a combination ion trap and radio frequency ion guide. As shown in Figure 2.6, TWIMS is composed of parallel-aligned electrode with center hole named SRIG (Stacked Ring Ion Guide). RF field with 1 MHz frequency and voltage at a few hundreds volts is implied to all adjacent electrode. This frequency suppresses loss of ions by touch with electrodes. Ions are focused into the center of electrode hole⁶⁰. The ion focusing principle is similar to linear ion trap as well as other conventional MS. This RF

build-up enhances detection possibility of ions. In addition to this RF, bias voltages are applied along SRIG, which can transport the trapped ions to detector.

The schematic step of ion separation in TM-IMS is depicted in Figure 2.6^{25,61}. A wave form called “traveling wave (TW)” is implied to the SRIG, and TW is continuously moved with the sweep speed with hundreds of m/s. TW transfers trapped ions out of SRIG to detector in MS equipped at downstream of TW-IMS. The ions with higher mobility are effectively transferred, whereas lower ions are remained in SRIG. The mobility is measured as efficiency of passing through TW-IMS.

The distinctive advantage of TW-IMS is its high sensitivity due to the ions trapped at the center of the SRIG. On the other hand, the resolution is lower than drift time type IM, because voltage at SRIG is lower. To drive TW-IMS, DC and RF have to be implied simultaneously with high repetition rate precisely.

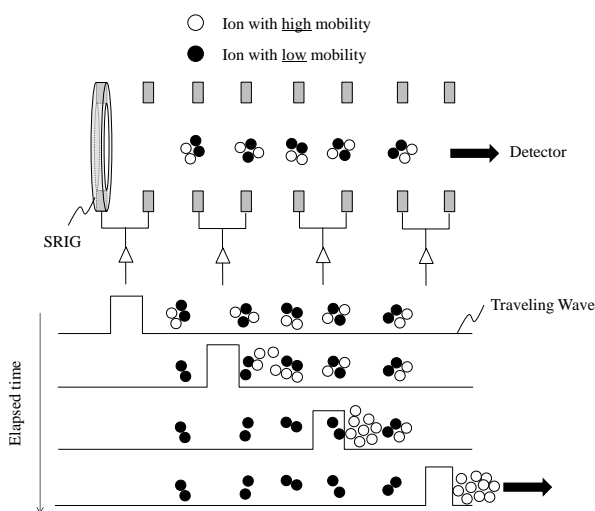


Figure 2.6

Schematic diagram of traveling wave (TW) ion mobility spectrometer^{4,25}. Stacked ring ion guide (SRIG) generates AC voltage with high frequency (~MHz) to accumulate ions at the center of each electrode. Trapped ion can be extracted by time dependent voltage along SRIG: called TW. Traveling time depends on the mobility of ion.

2.4 Comparison of IM-MS and selection

At present (2017), many types of commercially available IM-MS are released from different MS makers. Representative IM-MS and maker are listed on Table 2.1. There are also some companies offering customer specific designed instruments that meets customized experimental require. TW-IMS has advantage in high sensitive measurement that is opens up new possibility to gain information of synthetic polymer in new aspect. In 2016, Bruker Daltonics (Bremen, Germany) released new IM-MS called trapped ion mobility spectrometry (TIMS)⁵⁶. TIMS achieved high resolution with ~250 while maintain high sensitivity⁵⁶. Potential of TIMS for synthetic polymer analysis is very high, according to several reports^{56,62,63}, TIMS already made new achievements in structural analysis.

Table 2.1

Comparison of commercially available ion mobility mass spectrometer

IM-type	Maker	Advantage	Disadvantage
Filter	SCIEX	classification of particle size	sensitivity
Drift Time	Agilent technologies	resolution & calibration-free	sensitivity
Traveling Wave	Waters Corporation	sensitivity	resolution
Trap Ion	Bruker Daltonics	sensitivity & resolution	expandability

Nowadays, we can obtain highly resolved mass spectra with its resolution⁶⁴ higher than 50,000. On the other hand, ion mobility spectrometer has much lower resolution. For instance, the resolution for the traveling wave type ion mobility spectrometer of Waters Synapt⁵⁶ series has resolution at most 40. The best resolution⁵⁸ in state of the art of ion mobility spectrometer ($R \sim 1000$) is even lower than that of a common MS. In a polymer sample, macromolecule with particular molar mass is consisted of numerous atoms compared to low molar mass compounds that it can take various types of conformation. This can be explained that the magnitude of the end to end vector of macromolecule is theoretically described by Gaussian function¹. In IM-MS

experiment, each macromolecule with different conformation can be observed as different drift time. Therefore, profile of the experimentally obtained ion mobility chromatogram (IMC) can be roughly treated as Gaussian function. (Strictly saying, it is necessary to take into account diffusion of ions in IM-MS as described in Equation (2.21).) Considering an intrinsic broadening factor of IMC, resolution of the ion mobility spectrometer is actually not the limitation of the experiment. Increasing ion yield, which corresponds to ratio of “out” to “in” ion mobility tube, is much more important to perform the measurement efficiently. In general, MS measurement has to be carried out high vacuum condition ($\sim 10^{-5}$ mbar) because residual molecules disturb flight time or cause dissociation of sample molecule. On the other hand, IMS experiment is carried out under a few mbar pressure. The vacuum level of MS has to be kept 10^5 times lower than IMS⁶⁵. To generate high vacuum condition, pump must be equipped at the hyphenated part. Not only buffer gas but also sample ions can be exhausted at the same time. Due to this evacuation process, much amount of sample ions is lost. To overcome this problem, traveling wave type ion mobility spectrometer (TW-IMS) was developed in 2004 by Waters Corporation (Manchester, UK)⁵⁹.

Besides specification of IM-MS, the expandability of IM-MS with other analytical techniques has to be taken into account. Many byproducts or impurities coexist in commercially procured polymer sample. These obstacles cause serious problems of final mass-product in variety of industrial fields. Actually, IM-MS must be a powerful tool to separate and identify these contaminants, by hyphenation with HPLC or UPLC can enhance applicability of IM-MS further more. Waters has strength in knowledge, technology and the product line up that overwhelm other companies. Although a matter on expandability of IM-MS is out of this study, it is necessary to produce a good result in the long term. For these reasons, TW-IMS of Waters was adopted in this study.

2.5 Introduction of Synapt G2 HDMSTM

Experiments were carried out using Synapt G2 HDMSTM (Waters Corporation, Manchester, UK). This instrument has a hybrid quadrupole ion mobility orthogonal acceleration time of flight geometry (Figure 2.7). Ions are transported to the mobility tube

through the quadrupole analyzer. The ion mobility section comprises three consecutive, gas-filled, radio frequency ion guides named “TRIWAVE™”. Ions are accumulated in the trap TRIWAVE™ and periodically released into the mobility TRIWAVE™, where they separate according to their mobility through the action of a continuous train of DC pulses so-called “traveling-wave”. The ions separated in this way are then propelled through the transfer T-Wave using a continuous train of DC pulses into the TOF analyzer. Ion drift times are recorded by synchronization of TOF-MS acquisition with the release of ions from the trap to the mobility separator. The trap and transfer TRIWAVE™ were operated at a pressure of approximately 10^{-2} mbar of argon and the ion mobility TRIWAVE™ was operated at a pressure of 0.5–0.8 mbar of nitrogen gas. Ion mobility TRIWAVE™ was swept 200–1000 m/s and the DC pulse implied about 40 V. Data acquisition and processing were carried out using MassLynx™ software with version 4.1(Waters Corporation, Manchester, UK).

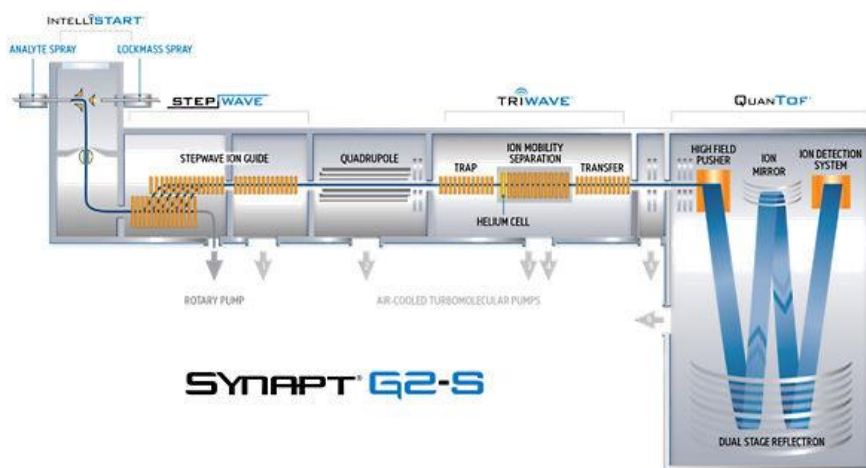


Figure 2.7
Schematic picture of IM-MS; Synapt released from Waters Corporation.
(Reprinted with permission of Waters Corporation)

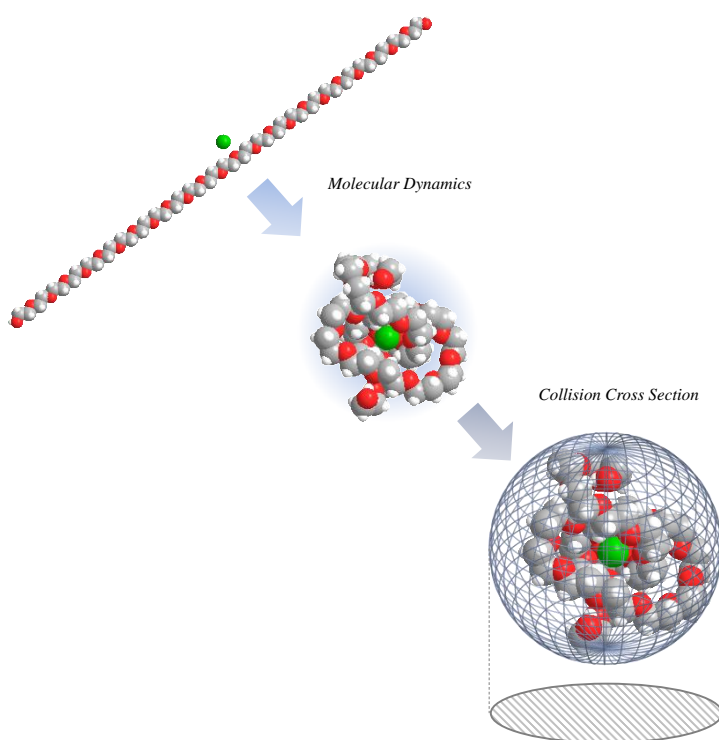
2.6 Evaluation of absolute collision cross section by Synapt G2 HDMSTM

According to Equation (2.15), except for collision cross section (*CCS*), other parameters are available. We can directly obtain the collision cross section by drift time. Here, drift time correlates with $|v_d|$ because ion travels ion mobility tube with fixed length. It is thus possible to evaluate collision cross section using drift time type IMS as mentioned in section 2.3.2⁶⁶. However, electric field of TRIWAVETM is not static but time dependent. Therefore, we cannot evaluate collision cross section via Equation (2.15) directly. Instead, an external calibration using samples with known *CCS* is usually required. According to work of Shvartsburg and Smith⁶⁷, the drift time in TRIWAVETM cannot be directly correlated to absolute *CCS*. It is crucial that the utilized calibrants are of the same molecular type (similar mass and mobility) as the analyte. Taken into account these matters, in this study, polyalanine was used to calibrate *CCS* (preparation for calibration sample is described in Appendix I). This calibration was performed with mobility parameters strictly identical to those used for measuring sample. Data processing was performed using DriftscopeTM (Version 2.7, Waters Corporation).

Chapter 3

Molecular Modeling

~Theoretical estimation of Collision Cross Section~



3.1 Outline of molecular modeling

The dimension and conformation of polymer can represent physical and chemical properties of polymer as shown exemplarily for the magnitude of end (terminal point of polymer chain) to end vector correlating stiffness of polymer^{44,45}. To access various properties of polymer, it is necessary to gain insight of polymer conformation. IM-MS enables to evaluate spacious size of sample ion, however, it does not directly show structure on molecular level. To access the molecular conformation of the polymer, theoretical approach using molecular modeling can be applied and compared with the experimental data. Fortunately, IM-MS is carried out under vacuum condition without solvent molecules, therefore, we don't need to consider position and number of solvent molecules. Nowadays a personal computer has enough capability to execute molecular modeling program with relatively good accuracy^{65,66}. Consequently, in this study, molecular modeling was utilized for obtaining structural picture of ion adducted polymer.

When we tackle in molecular modeling of a macromolecule, the number of atom and electron are too large to perform calculation of a quantum mechanics⁶⁶. Even though some of the electrons are ignored in quantum mechanical method for a macromolecular structure, large number of particles must still be considered, making the time-cost very high. Force field methods do not take into account the motions of electron and merely calculate the energy of a macromolecule as a function of the nuclear positions. Molecular mechanics (MM)^{67,68} thus works well to calculate systems containing large numbers of atoms such as a macromolecule. In some cases, force fields of MM can give proper answers that are as accurate as even the highest-level quantum mechanical methods albeit a fraction of the computer calculation running time.

The MM adopts several assumptions. Among them the most important ones is the Born-Oppenheimer approximation⁶⁶, electrons move so much faster than nuclei that the motion of them can be separated. The MM is based upon a very simple model of the interactions within a system with contributions from atomic motion such as the stretching of bonds, the opening and closing of angles and the rotations about single bonds. Although this model is rather simple, it is sufficient to describe structure of polymer and ion system with reasonable time-cost and accuracy.

Taking into account these matters, molecular dynamics simulation under internal energy potential by MM2⁶⁸ was run as molecular modeling to investigate molecular structure of polymer ion system in IM-MS.

3.2 MM2

There are several types of force field, in this study, the author adopted MM2 for molecular modeling of polymer⁶⁹. The principal MM2 force field which was developed by Allinger⁶⁸, is the one of the most popular force field for molecular modeling of polymer. This is because MM2 provides reasonable result with low time cost. Besides that, MM2 is initially installed molecular graphic soft; Chem3D (Cambridge Soft Corporation, Version14.0). Chem3D is designed for chemist, and it is thus possible to operate while checking molecular structure visually. Main components of energy term in MM2 are described in the user's manual of Chem3D precisely⁶⁹.

3.3 Molecular dynamics

Traveling time of alkali metal cation adducted polymer in TW-IMS can be estimated about 10^{-2} sec. This time scale is much longer than atomic motion regarding to rotation and vibration with $\sim 10^{-12}$ sec and $\sim 10^{-15}$ sec, respectively. Experimentally obtained CCS via IM-MS can be thus evaluated for thermally stabilized molecular structure. Taken into account it, in this study molecular dynamics (MD) simulation was applied for investigating conformation of alkali metal cation adducted polymer^{66,69}.

3.3.1 Basic algorithm of MD simulation

To obtain conformation of polymer, it is necessary to evaluate coordination position of particle in polymer. MD works well for calculating temporal development of particle position under potential based on MM2 force field. Temporal development of particle position can be calculated by solving differential equation based on Newton's motion equation:

$$\frac{\partial v_i}{\partial x_i} = m_i \frac{d^2 x_i}{dt^2} = F[x_i(t)] \quad (3.1)$$

where internal potential energy of polymer; V_i , x component of i th particle's position; x_i , and mass of particle; m_i . Differential equation can be given for y and z component as well. In case of a polymer composed of N of particles, there are $3N$ of differential equations. Analytically, it is impossible to solve these differential equations due to many-body problem. As an alternative way, differential equation can be numerically solved using a finite difference method.

There are many algorithms for integrating the equations of motion using finite difference methods, all algorithms basically assume that the position; x_i can be approximated as Taylor series expansions in very short time step; h :

$$x_i(t+h) = x_i(t) + h \frac{dx_i(t)}{dt} + \frac{h^2}{2!} \frac{d^2x_i(t)}{dt^2} + \frac{h^3}{3!} \frac{d^3x_i(t)}{dt^3} + \dots \quad (3.2)$$

The forth term regarding to h^3 can be ignored when h is very short span. The position at the time: $t-h$ can be described following equation.

$$x_i(t-h) = x_i(t) - h \frac{dx_i(t)}{dt} + \frac{h^2}{2!} \frac{d^2x_i(t)}{dt^2} \quad (3.3)$$

Adding Equation (3.2) and (3.3) instantly gives Equation (3.4).

$$x_i(t+h) = 2x_i(t) - x_i(t-h) + h^2 \frac{d^2x_i(t)}{dt^2} \quad (3.4)$$

Based on Equation (3.4), all positions of particle in polymer can be sequentially calculated every time step; h .

3.3.2 Time step for MD simulation

There are no strict rules for calculating the most appropriate time step to use in MD simulation; too small time step will cover only a limited motion; too large may cause overlaps among particles. Empirically, the timescale of some typical motions together with appropriate time steps are known as listed in Table 3.1. Polymer can be classified flexible molecules. In this study, time step less than 5×10^{-15} s was applied.

Table 3.1

The suggested time steps (in sec) for MD simulation⁶⁶

System	Types of motion	Suggested time step
Atoms	translation	10^{-14}
Rigid molecules	translation and rotation	5×10^{-15}
Flexible molecules, rigid bonds	translation, rotation, torsion	2×10^{-15}
Flexible molecules, flexible bonds	translation, rotation, torsion, vibration	10^{-15} or 5×10^{-16}

3.3.3 The number of step in MD simulation of polymer

As mentioned before, TW-IMS experiment takes about 10^{-2} sec for measuring CCS. On the other hand, time step is 10^{-15} sec, much shorter than experimental timescale. If one perform simulation to reproduce experiment completely, 10^{13} steps will be required. (It could take 3000 years, if every step is calculated with 0.01 sec.) Obviously this is too costly to perform MD simulation. In this study, step number was set 10000–40000 depending on the simulation system.

3.4 Calculation of CCS

Conventionally, CCS has been theoretically estimated by the open source software program MOBCAL^{70,71}. The MOBCAL output is based on three different models which can calculate the theoretical collisional cross section of any molecule possessing a three-dimensional coordinate file. First model, projection approximation (PA) models⁷² treats the molecule as a collection of overlapping hard spheres with radii equal to hard sphere collision distances. The orientationally averaged geometric cross section is determined by averaging the geometric cross section over all possible collision geometries. Second model is the exact hard sphere scattering models⁷⁰: the ion as a collection of overlapping hard spheres with radii equal to hard-sphere collision distances. The orientationally averaged momentum transfer cross section is calculated by

determining the scattering angles between the incoming buffer gas atom trajectory and the departing buffer gas atom trajectory. In the third model, trajectory Method (TM) models⁷¹, the ion as a collection of atoms, each one represented by a 12-6-4 Lennard-Jones potential. The effective potential is obtained by summing over the individual atomic contributions. Trajectories are run in this potential to obtain the scattering angle (the angle between the incoming and departing buffer gas atom trajectory). The orientationally averaged collision integral is determined by averaging over all possible collision geometries. We have to choose proper model fitting to experimental result. In 2009, Waters released Windows-based IM-MS data processing software program “DriftscopeTM” equipped with *CCS* calculating function⁷³. Compared to MOBCAL, it is easy to operate input and export of data file. The *CCS* calculation algorithm is modified PA model of MOBCAL. Although accuracy of calculated *CCS* by PA is generally less than TM⁷¹, PA yields relatively good accordance with experimentally obtained *CCS* of large molecule such as macromolecule and protein⁷⁴.

Part II

Study on +1 charge adducted species

Chapter 4

Collision cross section dependency on the number of monomer units of +1 charged polymer

~Novel evaluating method for characteristic ratio of polymer~

Summary

Ion mobility mass spectrometry (IM-MS) was used for measuring singly charged sodium cation (Na^+) adducted polyethylene glycol (PEG), polypropylene glycol (PPG), polymethyl methacrylate (PMMA) and polystyrene (PS). The collision cross sections (CCS) of all polymers were measured in dependence of the number of monomer units per chain, which could directly be related to the value of chain stiffness, i.e., the characteristic ratio (C_n). The evaluation of the data according to the globule model, which assumes that the chain in the gas phase exhibits spherical dimensions, yield C_n of 3.96 for PEG, 5.76 for PPG, 8.65 for PMMA and 7.85 for PS, which are in very good agreement with the literature-known reference values. The presented method is extremely quick and easy to perform, providing stunningly rapid access to the conformation data of synthetic polymers.

Adapted with permission from S. Kokubo, P. Vana, *Macromolecular Chemistry and Physics*, **2017**, 218, 1600373, Copyright 2017, Wiley-VCH.

4.1 Introduction

By designing and synthesizing polymer material it is often essential to precisely evaluate its molar mass distribution and the conformation of the individual polymer chains. The spacious dimension of chains is of special interest, as it directly governs intrinsic properties such as viscosity, density, and swelling properties of polymers^[1,47]. Based on the knowledge on molecular level, the conformational character of polymer chains is frequently described by specific parameters, such as the characteristic ratio, C_n ^[78–81]. C_n is defined as the ratio of the mean square unperturbed end-to-end distance for a real chain to the value expected for a freely jointed chain with the same number of bonds, of the same mean square length – and the persistence length, l_p ^[82,83] – defined as the length over which correlations in the direction of the tangent are lost. Conventionally, these parameters are evaluated from the combination of a variety of different observables such as the radius of gyration obtained by static light scattering, the intrinsic viscosity, and the hydrodynamic radius measured by dynamic light scattering. Those experiments are generally very laborious and time-consuming and are generally performed in solution phase under theta conditions, which are hard to handle, as this condition is particularly sensitive to temperature and to the type of solvent with small deviations from ideality leading to polymer precipitation.

In order to alleviate these restrictions, mass spectrometry is appropriate as a new and much easier way for studying chain dimensions and C_n of polymers. A very powerful method for getting precise information both on molar mass and spacious size of polymer is ion mobility-mass spectrometry (IM-MS)^[45,84]. The IM-MS technique enables the measurement of m/z values and spacious size of molecules at the same time. *Bowers'* group, for instance, measured the collision cross section (CCS) of positively charged single sodium ion (Na^+) adducts of polyethylene glycol (PEG) consisting of 9, 13 and 17 monomer units with IM-MS and they elucidated individual spacious structures of these polymers by performing MD simulations^[6]. *Memboeuf et al.*, on the other hand, performed a first principle calculation of similar systems and derived the CCS of PEG consisting of 1 to 17 monomer units^[85]. These experimental and theoretical results

showed good agreement with each other and provide us with the crucial information of how the size and the shape of PEG correlate with its specific molar mass.

Based on these backgrounds, polyglycols were adopted as the reference polymers. Polyglycols, with PEG and polypropylene glycol (PPG) as the most prominent representatives, are very popular polymers, as they are hydrophilic and harmless to biological system⁸⁶. At the same time, they are easily ionized in soft-ionization MS, which makes them ideal candidates for method development studies. In this work, the potentials of IM-MS were exploited for simultaneously measuring both the size and the molar mass of polymer without the disturbances of solvent and neighboring polymers. It was thus possible to develop a new methodology for obtaining C_n by evaluating the contribution of each individual monomer unit to the increment of CCS. To verify versatility of the proposed methodology, IM-MS were demonstrated for polymethyl methacrylate (PMMA) and polystyrene (PS).

4.2 Experimental section

4.2.1 Materials

Ethylene glycol (Aldrich), PEG (Aldrich, average $M_n \sim 400$ and $M_n \sim 1000$), propylene glycol (Aldrich) and PPG (Aldrich, average $M_n \sim 425$, $M_n \sim 1000$ and / $M_n \sim 2000$) were used without further purification and any salt added. These materials were dissolved in methanol (Fluka, LC-MS CHROMASOLV) yielding polymer solutions having concentrations of ca. 100 ppm.

PMMA (Polymer Standards Service, average $M_n \sim 620$ and $M_n \sim 1730$) and PS (Polymer Standards Service, average $M_n \sim 435$, $M_n \sim 1020$, $M_n \sim 1790$ and $M_n \sim 3280$) were used without further purification and any salt added. These materials were dissolved in acetone (Fluka, LC-MS CHROMASOLV) yielding polymer solutions having concentrations of ca. 100 ppm.

The all polymer solutions were charged to a 100 μ l syringe and injected into an electron-spray ionization (ESI) source running with a 5 μ l/min flow rate.

4.2.2 IM-MS

ESI was applied to IM-MS, and measurements were carried out with a Synapt G2 HDMSTM (Waters Corporation). ESI source temperature was 80 °C, the capillary voltage was 3.5 kV, desolvation temperature was 150 °C and the cone voltage was 40 V. The flow rate of helium in the cell located in front of the tri-wave ion mobility cell was set to 180 mL/min. Nitrogen flow in the ion mobility cell was set to 90 mL/min. The ion mobility spectrometer wave velocity and its wave height was optimized to 600 m/s and 40 V. CCS data were calibrated using polyalanine^[66] under the same measurement condition as for the PEG and PPG samples.

4.2.3 Effective CCS evaluation

The CCS, which is a primal experimental observable of ion mobility spectrometry, needs to be corrected in case the sample dimension and the buffer gas dimension is in the same order of magnitude^[87]. For evaluating the effective CCS of the sample (CCS_{eff}) it is then necessary to subtract the CCS of the buffer gas, as is demonstrated in **Figure 4.1**. In

this study, IM-MS experiments were carried out with nitrogen as a buffer gas. The radius of the nitrogen molecule can be treated as 2.5 Å by using the van der Waals coefficient b (0.0387 L/mol)^[88]. CCS_{eff} can thus be obtained via Equation (4.1).

$$CCS_{\text{eff}}[\text{Å}] = \left\{ \left(\frac{CCS[\text{Å}]}{\pi} \right)^{0.5} - 2.5[\text{Å}] \right\}^2 \pi \quad (4.1)$$

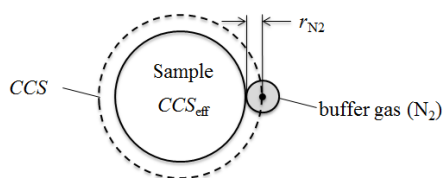


Figure 4.1

Correlation of CCS and CCS_{eff} when considering a buffer gas (nitrogen in this work) as collision partner that has dimension in the same order of magnitude as the sample.

4.2.4 Simulation of molecular conformation and calculation of CCS

Molecular dynamics (MD) simulation was performed to get information about the PEG and PPG conformation in the gas phase. MD simulations were performed by Chem3D Pro (Cambridge Soft Corporation, Version13.0) with the MM2 interaction^[68,71]. The initial condition of the polymer was set with stretched-out main chain and the Na^+ placed almost at the center of mass of all monomer units. MD simulations were running with a 2.0 fs step interval over 40000 steps at 300 K. Based on the coordination of the MD simulated polymer, the CCS was calculated by DriftscopeTM (Waters Corporation, Version 2.7). The amount of CCS was evaluated as an averaged area of different projection areas.

4.3 Results and discussions

4.3.1 Model equation development

PEG and PPG were mainly observed as single sodium cation (Na^+) adducts in the respective mass spectrum (**Figure 4.2**). No sodium salts were added to the sample solutions, the used PEG and PPG and/or the used solvent apparently contained sodium salt as a contaminant which is sufficient for efficient ionization, as is frequently observed in mass spectrum of synthetic polymers.

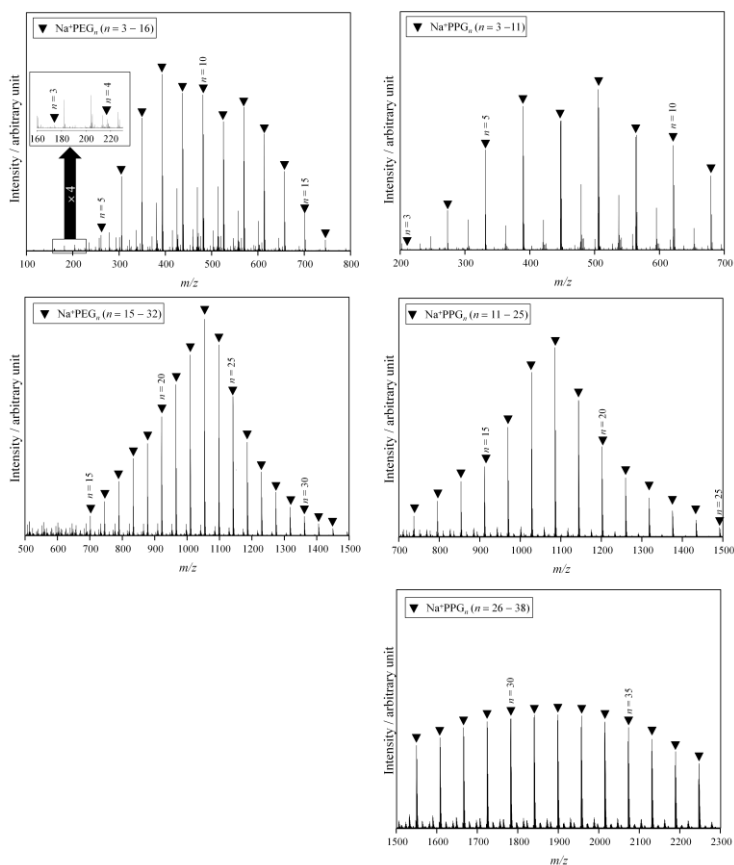


Figure 4.2

ESI time-of-flight mass spectra of PEG and PPG. The singly charged species for Na^+PEG_n and Na^+PPG_n are marked with black triangles.

Figure 4.3 shows the CCS profiles of the studied PEG and PPG samples. Each of these individual spectra are obtained from ion mobility measurements of each individual peak occurring in Figure 4.2 without any shoulder and splitting structure. The peak maximum positions, i.e., the ion mobility and thus the cross section of these PEG and PPG ions, are clearly proportional to the number of monomer unit in the respective chains. This is analogous to the fact that polymer size is proportional to the number of monomer units.

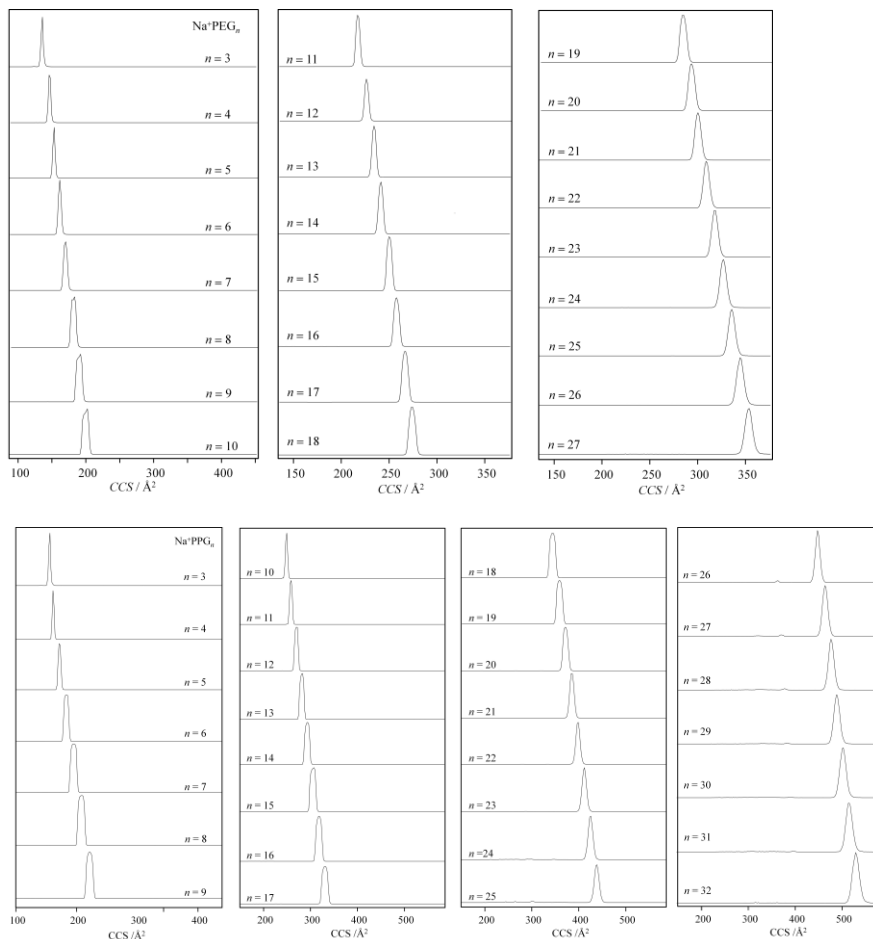


Figure 4.3

The collision cross section (CCS) profiles of singly charged Na^+PEG_n ($n = 3\text{--}27$) and Na^+PPG_n ($n = 3\text{--}32$).

It is well-known that the size of a freely-rotating polymer chain can be represented by the end-to-end vector, \mathbf{R} . The square of end to end distance, $|\mathbf{R}|^2$ is described with the characteristic ratio C_n , the bond vector, \mathbf{l} and the number of bonds, k_n , as follows^[1,47].

$$|\mathbf{R}|^2 = \sum_{i=1}^n \sum_{j=1}^n \langle \mathbf{l}_i \cdot \mathbf{l}_j \rangle = C_n |\mathbf{l}|^2 k_n \quad (4.2)$$

If the experimentally obtained CCS_{eff} could be related to $|\mathbf{R}|^2$, one can evaluate the stiffness of the polymer chain, i.e. C_n values, by analyzing CCS_{eff} as a function of monomer unit number. Based on this idea, a model equation was derived to connect CCS_{eff} with the number of bonds, k_n . To do so, it is first necessary to consider the dimensional transformation of \mathbf{R} , because this vector occurring in the three-dimensional space, whereas CCS_{eff} is a two dimensional observable. \mathbf{R} needs thus to be projected from 3D-space to a two-dimensional plane. This is done by projecting each individual bond vector \mathbf{l}_i , yielding a two-dimensional vector $\mathbf{l}_{p,i}$ can be described with projection angle θ_i via Equation (4.3).

$$\mathbf{l}_{p,i} = \mathbf{l}_i \cos \theta_i \quad (4.3)$$

The complete projected end-to-end vector \mathbf{R} , i.e., \mathbf{R}_p can then be obtained by summation over all individual 2D vectors:

$$\mathbf{R}_p = \sum_{i=1}^{k_{\text{eff}}} \mathbf{l}_{p,i} = \sum_{i=1}^{k_{\text{eff}}} \mathbf{l}_i \cos \theta_i \quad (4.4)$$

k_{eff} represents the effective number of bond which contributes to the projected \mathbf{R}_p . k_{eff} is smaller than the true k_n , as not all bonds in the 3D coil will contribute to the 2D-projection forming CCS_{eff} . Some of the bonds will be hidden inside the polymer coil or at the far side of the coil. It is thus necessary to take into account how many bonds effectively take part in the growing of CCS_{eff} with increasing chain length. This consideration is naturally dependent on the polymer dimension. In this study, during traveling through the ion mobility cell, polymer segment- Na^+ and segment-segment

interactions occur mainly under no solvent condition, as the chain is held in near-vacuum. This dimension could thus – in a first assumption – be considered as being similar to the globule state^[85] forming a spherical structure.

In order to evaluate the effective number of bonds k_{eff} , a model case was considered. As for such a globular coil with the total volume V , which contains k_n spherical elements with the volume v . These k_n element can aggregate forming a sphere – under a first assumption – with no vacant space. In this model case, the radius of the globule, R_{globule} , can be described via Equation (4.5).

$$R_{\text{globule}} = \left\{ \left(\frac{3}{4\pi} \right) V \right\}^{1/3} \quad (4.5)$$

The projection area of this spherical globule, $S_{\text{p,globule}}$, is given by Equation (4.6).

$$S_{\text{p,globule}} = \pi R_{\text{globule}}^2 = \pi \left(\frac{3}{4\pi} V \right)^{2/3} \quad (4.6)$$

By using the relation $V = k_n v$, it follows that

$$S_{\text{p,globule}} = \pi \left(\frac{3}{4\pi} k_n v \right)^{2/3} \quad (4.7)$$

The projection area of the k_n spherical elements, s , can be described by the v as follows:

$$s = \pi \left(\frac{3}{4\pi} v \right)^{2/3} \quad (4.8)$$

The overall projection, $S_{\text{p,globule}}$, can then be obtained as summation over the effectively participating elements:

$$S_{\text{p,globule}} = k_p s \quad (4.9)$$

Here, k_p corresponds to an effective number of elements which contributes to the extent of the projection area. According to Equation (4.7), (4.8) and (4.9), k_p follows as

$$k_p = k_n^{2/3} \quad (4.10)$$

Now it is possible to correlate the squared Equation (4.4), which yields the square of the projected end-to-end vector, in a similar fashion as in Equation (4.2), with the characteristic ratio and the effective number of bonds,

$$|\mathbf{R}_p|^2 = \sum_{i=1}^{k_p} \sum_{j=1}^{k_p} \langle \mathbf{l}_i \cdot \mathbf{l}_j \rangle \cos \theta_i \cos \theta_j = C_{k_n} |\mathbf{l}|^2 (\overline{\cos \theta})^2 k_p \quad (4.11)$$

with $\overline{\cos \theta}$ being the angular averaged $\cos \theta$. During the flight in the ion mobility cell, sample species undergo many collisions with nitrogen molecule. Under this condition, the sample species will randomly rotate and its projection angle will be variable in the range from 0 to 2π radian with equal probability for all values. It is thus possible to calculate the angular averaged $\overline{\cos \theta}$ via Equation (4.12):

$$\overline{\cos \theta} = \int_0^{2\pi} |\cos \theta| d\theta / \int_0^{2\pi} d\theta = 2/\pi \quad (4.12)$$

According to Equation (4.10), (4.11) and (4.12), the projection length of the end-to-end distance of a polymer chain is instantly obtained:

$$|\mathbf{R}_p|^2 = C_{k_n} |\mathbf{l}|^2 (\overline{\cos \theta})^2 k_p = C_{k_n} \left(\frac{2}{\pi}\right)^2 l^2 k^{2/3} \quad (4.13)$$

Although $|\mathbf{R}_p|$ cannot be directly observed via IM-MS, *Chirot et al.* reported that the radius of gyration, R_g , of a polymer can be empirically related to its CCS^[89]. On the other hand, R_g is proportional to the magnitude of the end-to-end distance, $|\mathbf{R}|$, which can be connected to $|\mathbf{R}_p|$ according to Equation (4.13). In the globule state, it is known that the relation between $|\mathbf{R}|$ and the radius of gyration R_g is described by $|\mathbf{R}|^2 = 5/3 R_g^2$ ^[48]. The magnitude of R_g does not depend on the projection angle, because R_g is an isotropic parameter which represents the dislocation of the polymer chain from its gravity point.

Hence, it is possible to connect the square of R_g with the square of projection length of the end-to-end vector, R_p , via Equation (4.14).

$$|R_p|^2 = \frac{5}{3} R_g^2 \quad (4.14)$$

Furthermore, taking into account the empirical relation $R_g^2 \approx CCS_{\text{eff}} / 6$ ^[89], CCS_{eff} can approximately be correlated with the number of bonds, k_n , via Equation (4.15):

$$\frac{5}{18} CCS_{\text{eff}} = C_{k_n} \left(\frac{2}{\pi} \right)^2 l^2 k_n^{2/3} \quad (4.15)$$

As for PEG and PPG, the monomer units along the back bones are containing three individual bonds; one C–C (1.53 Å ^[21]) and two C–O (1.43 Å ^[21]). These two types of bond are very similar in length within 0.1 Å. An arithmetic mean length of them (1.463 Å ^[90]) can be thus regarded as a bond length of PEG and PPG. Moreover, the number of bonds can be finally converted into the number of monomer units, n , which gives Equation (4.16).

$$\frac{5}{18} CCS_{\text{eff}} = \left(\frac{2}{\pi} \right)^2 C_n (1.463)^2 (3n)^{2/3} \quad (4.16)$$

with CCS_{eff} in Å². This globule model equation connects experimentally obtained CCS_{eff} values with the number of monomer units, n . The correlation factor of this equation contains the characteristic ratio, C_n , which can thus easily be extracted by plotting $5/18 \times CCS_{\text{eff}}$ against $n^{2/3}$.

4.3.2 Theoretical validation for developed model

In order to validate the proposed method, it was applied to calculated cross-section data of PEG_{*n*} and PPG_{*n*}, which was obtained by molecular dynamics (MD) simulation for isolated chains. Please note that in this first approach, no ionizing cation was taken into account, which is mandatory for MS. For each degree of polymerization, a *CCS* was calculated by DriftscopeTM and transformed into *CCS*_{eff} for collision with nitrogen according to Equation (4.1). **Figure 4.4** shows the corresponding $5/18 \times CCS_{\text{eff}}$ against $n^{2/3}$ plot, according to Equation (4.16). Both plots for PEG_{*n*} (*n* = 1–35) and PPG_{*n*} (*n* = 1–35) – described by Equation (4.17) and (4.18) – exhibit excellent linearity with correlation coefficients more than 0.99. The intercept values are only very slightly deviating from zero, as expected from Equation (16).

$$\frac{5}{18} CCS_{\text{PEG}n} = 6.57n^{2/3} - 0.17 \quad (4.17)$$

$$\frac{5}{18} CCS_{\text{PPG}n} = 8.61n^{2/3} - 1.50 \quad (4.18)$$

According to Equation (4.16), the slope value of Equation (4.17) and (4.18) can directly be related to the characteristic ratio, *C_n*, and the bond length, *l*. The average bond length of PEG was taken as 1.463 Å^[90], as described above, and also taken for PPG in a first assumption. Consequently, *C_n* can be easily obtained as 3.64 and 4.77 for PEG and PPG, respectively. These calculated results show good agreement with literature known *C_n* values^[49,79–81,91,92] (**Table 4.1**). This finding confirms that the globule model equation Equation (4.16) enables to quantitatively obtain stiffness data of PEG and PPG by measuring collision cross section data as function of chain length. Next, Equation (4.16) was applied to IM-MS results and evaluated *C_n* experimentally.

Table 4.1

The characteristic ratio, C_n , of PEG and PPG as obtained in this study (bold text) compared to literature values. (RT; room temperature)

Polymer	C_n	Method	Temperature / K	Reference
PEG	3.64	calculated CCS_{eff} on PEG	300	this work
	3.96	globule model fitting	RT (ca.300)	this work
	4.8	viscosity measurement	298–323	[79]
	4.2–5.5		325	[93]
	5.1–5.7		298–323	[81]
	3.6–5.5	<i>ab initio</i> calculation	303–323	[91]
PPG	4.73	calculated CCS_{eff} on PPG	300	this work
	5.76	globule model fitting	RT (ca. 300)	this work
	4.85	viscosity measurement	323	[49]
	5.05		323	[49]
	6.01		323	[78]
	5.88–6.16	<i>ab initio</i> calculation	323	[92]

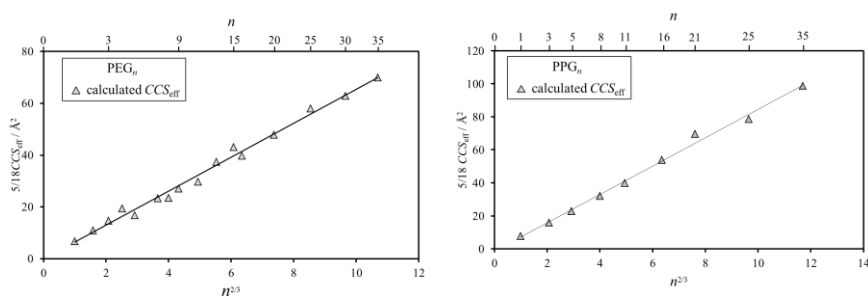


Figure 4.4

Calculated data of $5/18 \times CCS_{\text{eff}}$ of PEG_n ($n = 1-35$) and PPG ($n = 1-35$) against $n^{2/3}$ according to Equation (4.16). The black lines are linear fittings.

4.3.3 Experimental validation for developed model

Experimentally obtained CCS_{eff} of Na^+PEG_n and Na^+PPG_n from IM-MS measurements were also treated according to the globule model as described above. In contrast to the simulated data (Figure 4.4), the plots of $5/18 \times CCS_{\text{eff}}$ of Na^+PEG_n ($n = 3-27$) and Na^+PPG_n ($n = 3-32$) (Figure 4.5) are deviating from linearity, especially in the low molar mass regime for the range $n^{2/3} \leq 4$ ($n \leq 8$) for PEG and PPG, whereas good linearity is observed for longer chains. The major difference between the simulated data above and the experimental data is the presence of an attached cation, which is essential for MS. Thus, the polymer species were simulated again, this time with an attached sodium cation.

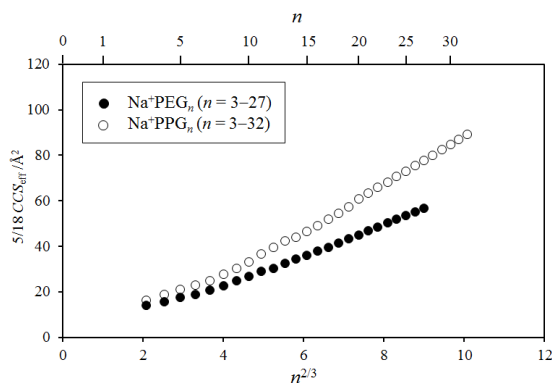


Figure 4.5

Experimentally obtained $5/18 \times CCS_{\text{eff}}$ of Na^+PEG_n ($n = 3-27$) and Na^+PPG_n ($n = 3-32$) against $n^{2/3}$ according to Equation (4.16).

Inspection of **Figure 4.6**, in which this simulated data (grey squares) is plotted together with the experimental data (circles), showing a very good match between simulation and experiment and proves that the existence of the attached cation has a distorting impact on the data evaluation. It is thus clear that the presence of the Na^+ cation affects electronically the steric structure and thus the CCS_{eff} of the polymer chain. On the example of trimer species, this effect can be demonstrated.

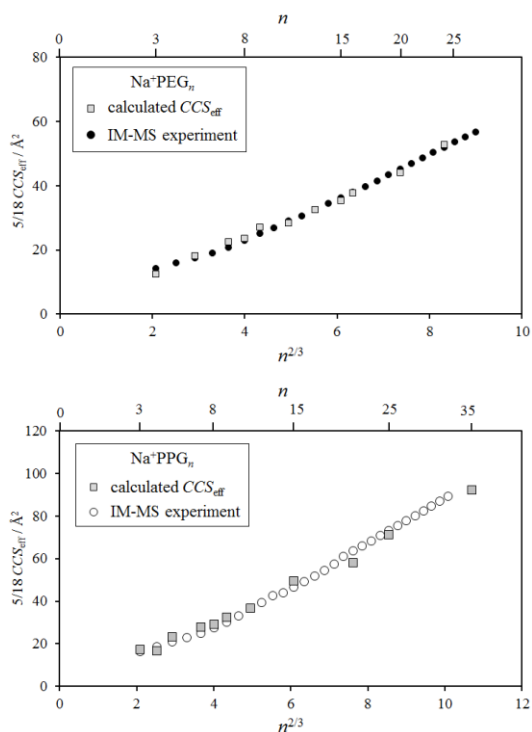


Figure 4.6

Comparison of experimentally obtained and theoretically calculated $5/18 \times \text{CCS}_{\text{eff}}$ data of Na^+PEG_n and Na^+PPG_n against $n^{2/3}$.

According to steric energy estimation by MM2 based MD simulation, the linear stretched-out conformation of a PEG₃ (LPEG₃, $CCS_{\text{eff}} = 53.4 \text{ \AA}^2$) is 22 kJ/mol more stable than the crown-ether type conformation (CPEG₃, $CCS_{\text{eff}} = 49.8 \text{ \AA}^2$), as shown in **Figure 4.7**. The larger conformation is thus the more stable one. When attaching a sodium cation, however, the smaller, crown-ether type conformation ($CCS_{\text{eff}} = 49.8 \text{ \AA}^2$) becomes the far more stable one in comparison to the linear with $CCS_{\text{eff}} = 64.4 \text{ \AA}^2$. Comparison with the experimentally obtained $CCS_{\text{eff}} = 50.5 \text{ \AA}^2$ of trimers, which is very close to the calculated crown-ether type value, indicates that the sodium cation is indeed inducing a contraction to the polymer chains, which can be attributed to the electronically attractive interaction between positively charged Na^+ and negatively charged lone pair electrons of the oxygen atoms in the PEG chain. The contraction can clearly be observed until Na^+PEG_8 with a calculated CCS_{eff} of 81.9 \AA^2 in comparison to the value of 84.4 \AA^2 for the neutral species.

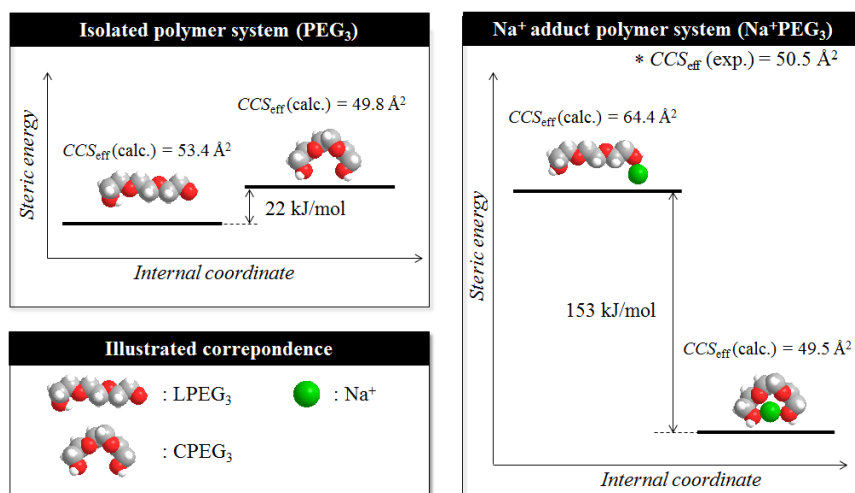


Figure 4.7

The calculated steric energy diagram of PEG₃ and Na⁺PEG₃. All atoms and ions are represented by a space filling model. Carbon, hydrogen, oxygen and sodium cation (Na^+) are indicated gray, white, red, and green, respectively.

It now needs to be evaluated, how this contraction affects the chain stiffness measurement according to Equation (4.16) and if the higher molar mass data, which shows good linearity, can be used for C_n measurements. According to the MD simulation, Na^+ locates almost at the gravity center of the Na^+PEG_8 and Na^+PPG_8 , sandwiched by two 12-crown-4 type chain conformations (see left hand side of **Figure 4.8**). This type of monomer unit coordination around the sodium cation provides a highly symmetric and close-packed conformation, which can be understood as a ‘first solvation layer’ for Na^+ . Actually, when looking at the conformation of Na^+PEG_9 and Na^+PPG_9 , it becomes clear that the ninth monomer unit coordinates on the outside of the first solvation layer (see right hand side of Figure 4.8).

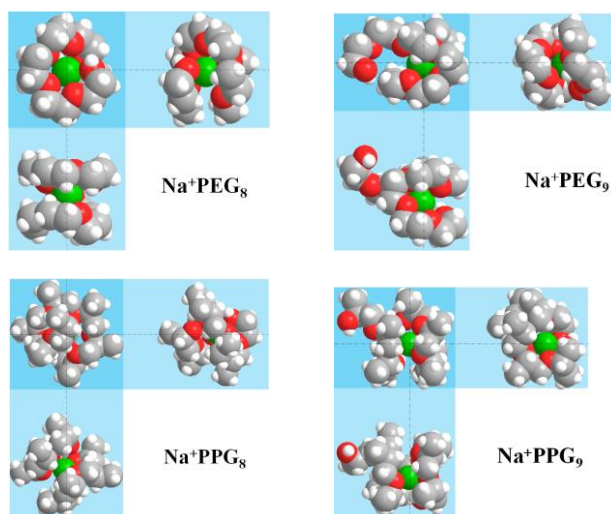


Figure 4.8

Three-plane pictures of Na^+PEG_n and Na^+PPG_n ($n = 8$ and 9), which were obtained by MD simulations. Carbon, hydrogen, oxygen, and sodium cation (Na^+) are indicated by gray, white, red, and green, respectively.

The monomer units for $n \geq 9$ are consequently located at the outside of the ‘first solvation layer’ and build a second layer. According to *ab initio* calculation results for Na^+PEG_n ($n = 3-17$)^[85], the incremental ratio of the binding energy between Na^+ and the monomer

units changes at chain length of ca. nine and the electrostatic energy of Na^+ seems almost to be saturated at longer species. This result is in good agreement with the picture that the electrostatic field of Na^+ is almost shielded by the first solvation layer until $n = 8$. It may thus be concluded that monomer units with $n \geq 9$ behave like a neutral polymer in a less electronically perturbed field, which is especially true for the increment of CCS_{eff} with n , which is the basis for the proposed method. A picture emerges, in which the core of the polymer chain up to $n = 8$ is contracted in comparison to the ideal, neutral species, but in which the second polymer layer with $n \geq 9$ behaves more like an ideal species with respect to its size increment. This picture is in good harmony with our results (see Figure 4.6), where a deviation from the linearity is observed with short chains, but good linearity is observed at higher degrees of polymerization. When considering only the data of $n \geq 9$, the plots of Na^+PEG_n ($n = 9\text{--}27$) and Na^+PPG_n ($n = 9\text{--}32$) (see Figure 4.6) show correlation factors of more than 0.998 yielding Equation (4.19) for PEG and Equation (4.20) for PPG.

$$\frac{5}{18}\text{CCS}_{\text{eff}, \text{Na}^+\text{PEG}_n} = 6.86n^{2/3} - 5.36 \quad (4.19)$$

$$\frac{5}{18}\text{CCS}_{\text{eff}, \text{Na}^+\text{PPG}_n} = 10.33n^{2/3} - 15.36 \quad (4.20)$$

The intercept values are obviously not zero, as expected from Equation (4.16), which is in line with the picture that the polymer coil contains a more compact core. The slope values, however, are in good agreement with the values of Equation (4.19) and (4.20), which were derived from the calculation of ideal, neutral species.

For the method being fast and easy, the experimentalist needs to know from which n value on the CCS data can be used for obtaining C_n values, when studying an unknown polymer. In order to provide a practical guideline for this choice, the increment of CCS_{eff} defined Equation (4.21) was used.

$$\Delta\text{CCS}_{\text{eff}}(n) = \text{CCS}_{\text{eff}}(n+1) - \text{CCS}_{\text{eff}}(n) \quad (4.21)$$

which is plotted in **Figure 4.9**.

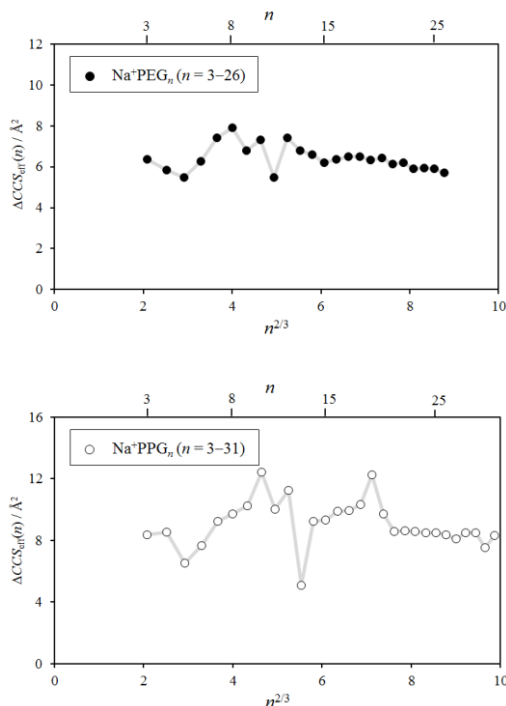


Figure 4.9

The evolution of the increment of the collision cross section, $\Delta CCS_{\text{eff}}(n)$ for Na^+PEG_n ($n = 3-26$) and Na^+PPG_n ($n = 3-31$) with $n^{2/3}$.

It can be seen that this increment is fluctuating at small chain lengths, which is indication for the influence of the cation and the slowly occurring first and second layer of polymer segments. For PEG, $\Delta CCS_{\text{eff}}(n)$ gets constant for $n \geq 16$ and for PPG for $n \geq 21$, respectively. These values are obviously the ones, from which on the impact of the sodium cation can be neglected and the polymer coil approaches a spherical shape, which is a prerequisite of the globule model. This spherical shape is clearly not occurring when the second polymer segment layer is very small (e.g. when $n = 9$, as indicated in Figure 4.8), although the electronic impact of the cation is already diminishing. When evaluating plots for PEG with $n \geq 16$ and PPG with $n \geq 21$, according to this guideline, an extremely good linearity with correlation factors of more than 0.9999 was found (**Figure 4.10**) and Equation (4.22) and (4.23) were obtained for PEG and PPG, respectively.

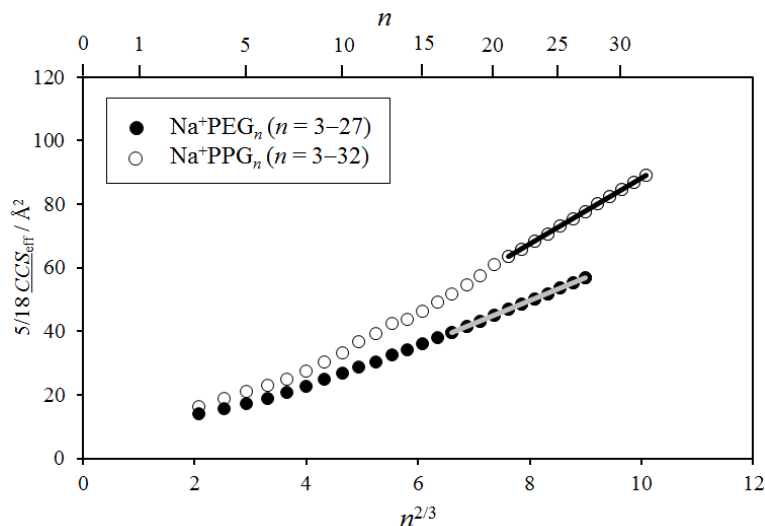


Figure 4.10

Experimentally obtained $5/18 \times CCS_{\text{eff}}$ of Na^+PEG_n and Na^+PPG_n against $n^{2/3}$. The gray and black linear lines correspond to the linear fitting for Na^+PEG_n ($n = 16-27$) and Na^+PPG_n ($n = 21-32$).

$$\frac{5}{18} CCS_{\text{Na}^+\text{PEG}_n} = 7.15n^{2/3} - 7.58 \quad (4.22)$$

$$\frac{5}{18} CCS_{\text{Na}^+\text{PPG}_n} = 10.39n^{2/3} - 15.63 \quad (4.23)$$

According to Equation (4.16), the slope of Equation (4.22) and (4.23) gave C_n values of 3.96 and 5.76 for PEG and PPG, respectively (see Table 4.1). These values are in very good agreement with earlier reported values, as evidenced by comparison with literature values collated in Table 4.1. The globule model is consequently a very suitable way of evaluating characteristic value, C_n , of synthetic polymer chains using ion mobility-mass spectrometry.

In the next section, versatility was checked by applying for other polymers with more bulky pendant group and lower polarity.

4.3.4 Model application to other polymers

To verify the versatility of formulated globule equation, IM-MS experiment were demonstrated with Na^+ adducted PMMA and PS. In comparison with PEG and PPG, the properties of both polymers are very different in possessing bulky side chain group and polarity. At first, according to the practical guideline, $\Delta\text{CCS}_{\text{eff}}(n)$ of both polymers were evaluated (**Figure 4.11**). $\Delta\text{CCS}_{\text{eff}}$ of Na^+PMMA_n ($n \geq 17$) and Na^+PS_n ($n \geq 15$) decrease almost constantly with increasing n .

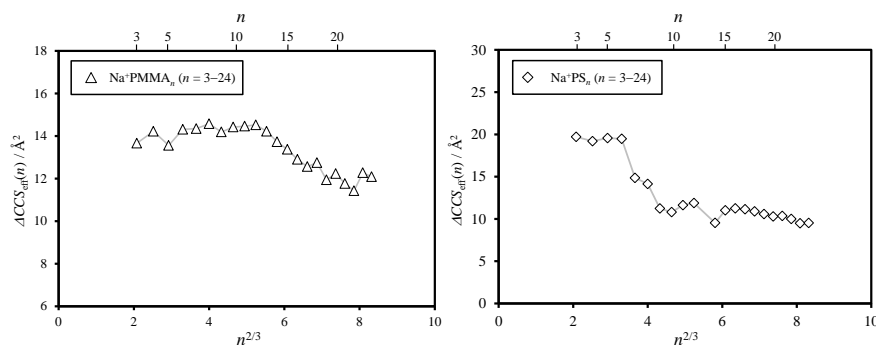


Figure 4.11

The evolution of the increment of the collision cross section, $\Delta\text{CCS}_{\text{eff}}(n)$ for Na^+PMMA_n ($n = 3-24$) and Na^+PS_n ($n = 3-24$) with $n^{2/3}$.

Second, $5/18 \times \text{CCS}_{\text{eff}}$ of both polymers were plot against $n^{2/3}$ (**Figure 4.13**). The least-square fitting were applied for all plot of Na^+PMMA_n ($n \geq 17$) and Na^+PS_n ($n \geq 15$). Both fitting lines showed extremely good linearity with correlation factors of more than 0.9999 with Equation (4.24) and (4.25).

$$\frac{5}{18} \text{CCS}_{\text{Na}^+\text{PMMA}_n} = 13.84n^{2/3} - 15.54 \quad (4.24)$$

$$\frac{5}{18} \text{CCS}_{\text{Na}^+\text{PS}_n} = 11.82n^{2/3} + 4.52 \quad (4.25)$$

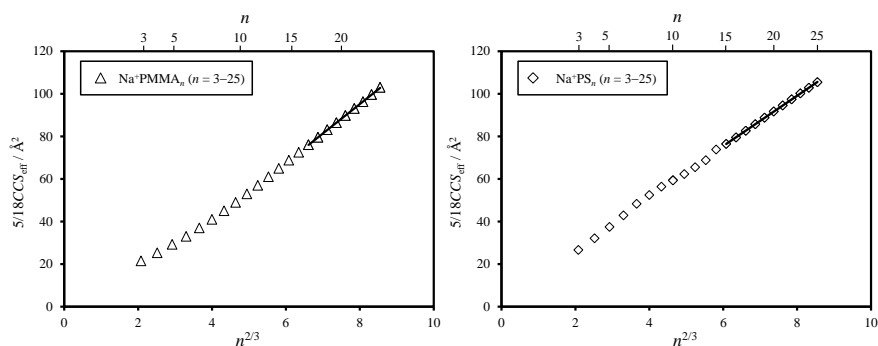


Figure 4.12

Experimentally obtained $5/18 \times CCS_{\text{eff}}$ of Na^+PMMA_n and Na^+PS_n against $n^{2/3}$. The gray and black linear lines correspond to the linear fitting for Na^+PMMA_n ($n = 17-25$) and Na^+PS_n ($n = 15-25$).

By Inserting slope values of Equation (4.24) and (4.25) into Equation (4.15), C_n of PMMA and PS were calculated. It is noted that the bond length (l) has to be adopted with 1.53 \AA^{90} due to C-C merely building main chain of PMMA and PS. Consequently, C_n was instantly obtained with 9.19 and 7.85 for PMMA and PS, respectively. These values showed good accordance with reported values (**Table 4.2**). Both methacrylate and phenyl hindering free rotation of polymer main chain, enlarging stiffness of PMMA and PS. The stiffness is observable as incremental ratio of CCS_{eff} against each monomer units. The proposed methodology for evaluating C_n could be universally applied for synthetic polymer.

Table 4.2

The characteristic ratio, C_n , of PMMA and PS as obtained in this study (bold text) compared to literature values. (RT; room temperature)

Polymer	C_n	Method	Temperature/K	Reference
PMMA	8.65	globule model fitting	RT (ca.300)	this work
	6.35	viscosity measurement	306	[94]
	7.85		296	[95]
	7.95		301.5	
	8.65		298	
PS	7.85	globule model fitting	RT (ca.300)	this work
	7.2	viscosity measurement	323	[95]
	9.4		298	
	9.15	light scattering	323	
	10.8	SAXS	298	

4.4 Conclusions

IM-MS was performed for PEG, PPG, PMMA and PS, and measured the increment of the collision cross section of the polymer with the degree of polymerization in order to evaluate the intrinsic stiffness of the polymer chains. According to MD simulations and experimental results, the globule model is excellently suited for describing the conformational dimensions of PEG and PPG under these conditions. From the experimentally obtained values of the characteristic ratio C_n of 3.96 for PEG, 5.76 for PPG were determined, respectively, showing excellent agreement with earlier reported values. To verify versatility of proposed method, IM-MS experiment were demonstrated with Na^+ adducted PMMA and PS. The experimentally obtained C_n of 8.65 for PMMA, 7.85 for PS, respectively, also showed good accordance with reported values. These results support the power of the here presented method. The proposed method is extremely fast and easy to perform, but caution regarding the dimension of the polymer chain in the short chain-length regime needs to be exercised when evaluating the true stiffness of synthetic polymers.

Chapter 5

ESI-MS threshold polymer size

~The minimum droplet size depends on surface tension of polymer~

Summary

Ion mobility-mass spectrometry was used for measuring singly charged polyethylene glycol (PEG), polypropylene glycol (PPG) and polymethyl methacrylate (PMMA) via electrospray ionization. The collision cross-sections of polymer ions were measured for the smallest polymer ion with spherical dimension. The acquired data were analyzed according to Rayleigh limit model, which assumes that minimum spherical polymer chain coil with excess charge. This process yielded very good agreement with the literature-known reference. Surface tension of 45.0 mN/m for PEG, 33.1 mN/m for PPG, 40.0 mN/m for PMMA and 32.4 mN/m for PS were obtained.

5.1 Introduction

Ionization source is one of the most important techniques in a mass spectrometry to measure molar weight of polymer samples^{3,5}. Particularly, an electro-spray-ionization (ESI)⁵ can produce ion with wide range of molar mass with producing less fragmentation. The hyphenation of ESI and mass spectrometer (ESI-MS) opened new avenues for quantitative characterization of polymer, because ESI-MS enabled to evaluate absolute molar mass and its distribution. As a fundamental analysis, this technique contributed to elucidate reaction mechanism of polymer synthesis such as controlled radical polymerization techniques³.

The first experiment of original ESI was carried out by in the 18th century⁵ and its physical process for producing ionized droplet could be described by Rayleigh⁹⁶. The charged droplets detached from the Taylor cone disintegrates by losing its weight through evaporation of the solvent. Right after the disintegration, the excess charges in both the parent charged droplets. **Figure 5.1** shows the sequential droplet fission processes of the charged parent droplet (N is the number of excess charges, R : the radius of the droplet / μm)⁵.

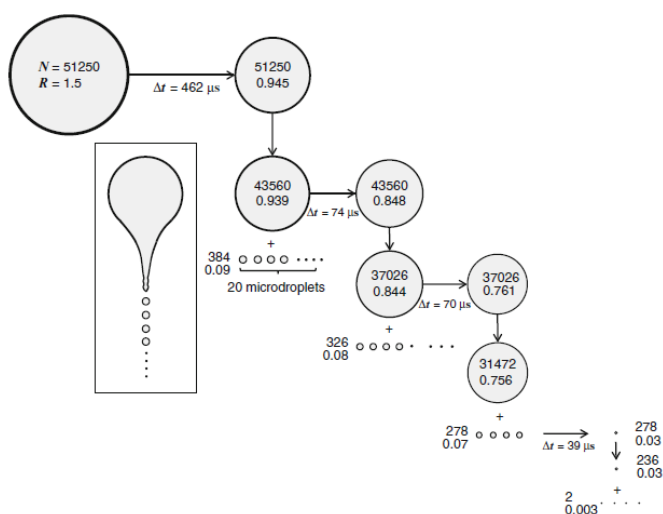


Figure 5.1

Schematic representation of time history of parent and offspring droplets⁵.

(Reprinted with permission from Springer)

In Figure 5.1, the parent droplet with the radius R of 1.5 μm holds the excess charges N of 51250. At the moment of droplet fission, the parent droplet changes to a fig-like shape, as shown in the inset and the jet fission produces fine secondary droplets. This uneven fission process is similar to the formation of charged droplets from the Taylor. In droplet fission, about 20 secondary droplets with R of about 1/10 of that of the parent droplet are formed (about 1/1000 in volume). In this fission event, about 15 % of the charge and 2 % of the mass are lost from the parent droplet^{25,97,98}, meaning that the charge density increases significantly in the secondary off-spring droplets. Two forces are balanced in droplet, one is Coulomb force and the other one is internal force with surface tension (γ). The relation between the excess charge Q and the radius r for the spherical droplet at Coulomb instability (the Rayleigh equation) is thus given in (8.12).

$$\frac{N^2 Q^2}{16\pi\epsilon_0 R^2} = 4\pi\gamma R$$

$$R^3 = \frac{N^2 Q^2}{64\pi^2 \gamma \epsilon_0} \quad (5.1)$$

Here, surface tension is one of the most important indexes describing solubility or compatibility of different types of polymer. For instance, *Helfand* and *Tagami*⁹⁹ proposed physical theory about the correlation of surface tension and solubility, which is helpful for designing and controlling physical and chemical properties of blend polymer. According to Equation (5.1), the radius of charged droplet instantly enables to calculate surface tension. One of the most promising candidate for evaluating charged droplet size can be ion mobility mass spectrometry (IM-MS). In a last decade, a combination of ESI and IM-MS (ESI-IM-MS) attracts polymer scientist due to its very distinctive capability in characterizing structure and measuring size and molar mass simultaneously^{4,45,100}. Here, spacious size is quantitatively obtained as collision cross-section (CCS) which corresponds to averaged projected area of sample ion⁷³. As described in Chapter 4, it is known that it takes globule state in spherical dimension¹⁰¹. It is noticeable that globule forming polymer ion with the smallest CCS is a proposed model for Rayleigh limit

droplet. And its radius can be experimentally evaluated from using CCS^{101} . Applying radius of Rayleigh limit droplet to Equation (5.1) provides easily and quickly accessible to evaluate surface tension of polymer.

Based on this idea, ESI-IM-MS of very common polymer was performed, polyethylene glycol (PEG), polypropylene glycol (PPG) and polymethyl methacrylate (PMMA) to evaluate radius of Rayleigh limit droplet. Besides ESI-IM-MS experiment, MD simulation was carried out to discriminate the sphericity of cation adducted polymer for Rayleigh limit approach.

5.2 Experimental section

5.2.1 Materials

Polyethylene glycol (PEG, Aldrich, average $M_n \sim 400$), polypropylene glycol (PPG, Aldrich, average $M_n \sim 425$), polymethyl methacrylate (PMMA, Polymer Standard Service, average $M_n \sim 620$) and polystyrene (PS, Polymer Standard Service, average $M_n \sim 376$) were used in this study (**Figure 5.2**). All sample polymers were utilized without further purification. PEG and PPG were dissolved in methanol (Fluka, LC-MS CHROMASOLV) yielding polymer solutions having concentrations of ca. 100 ppm. PMMA and PS were dissolved in acetone (Sigma-Aldrich, CHROMASOLV Plus for HPLC) and prepared concentration with ca. 100 ppm. To produce smaller cation adducted polymer, lithium (Li) was adopted as a cation. LiCl (Aldrich, purity $\geq 99\%$) was dissolved in methanol and prepared with 1 mmol/L of concentration. The sample solution was prepared by mixing 1 mL of polymer solution with 0.01 mL of LiCl methanol solution. The sample solutions were charged to a 250 μL syringe and injected into an electron-spray ionization (ESI) source running with a 5 $\mu\text{L}/\text{min}$ flow rate.

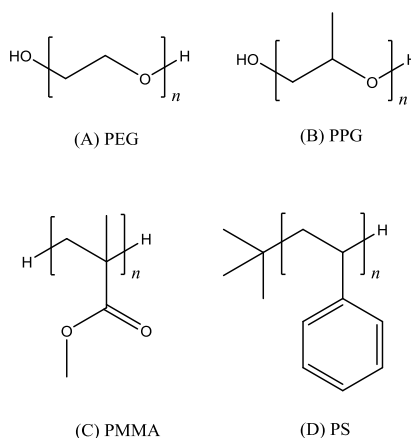


Figure 5.2

The chemical structures correspond to (A) polyethylene glycol (PEG), (B) polypropylene glycol (PPG), (C) polymethyl methacrylate (PMMA) and (D) polystyrene (PS), respectively.

5.2.2 IM-MS

ESI was applied to IM-MS, and measurements were carried out with a Synapt G2 HDMSTM (Waters Corporation). ESI source temperature was 80 °C, the capillary voltage was 3.0 kV, desolvation temperature was 120 °C and the cone voltage was 40 V. The flow rate of helium in the cell located in front of the tri-wave ion mobility cell was set to 180 mL/min. Nitrogen flow in the ion mobility cell was set to 90 mL/min with temperature at 300 K. The ion mobility spectrometer wave velocity and its wave height was optimized to 600 m/s and 40 V. *CCS* data were calibrated using polyaniline⁶⁶ under the same measurement condition as for all polymer samples.

5.2.3 Simulation of molecular conformation and calculation of *CCS*

Conformational information about Li cation (Li^+) adducted polymers is obtained by comparing the experimental *CCS* and theoretical *CCS*. Chem3D Pro (Cambridge Soft Corporation, Version13.0) was used to generate the candidate conformational structures. Based on theoretically obtained conformation, *CCS* was evaluated by DriftscopeTM (Version 2.7, Waters Corporation). Although DriftscopeTM prepares atomic diameter for carbon, hydrogen and oxygen atom, there is no available data for Li^+ . The atomic diameter was adopted by 1.18 \AA^{102} for Li^+ according to Pauling's ionic radius to calculate *CCS* of Li^+ adducted polymers. The initial condition of the polymer was set with stretched-out main chain. The position of Li^+ was set at center in the main chain. MD simulations were running with a 2.0 fs step interval over 40000 steps at 300 K.

5.3 Results and discussion

5.3.1 *CCS* dependency on type of alkali cation

All polymers were observed as mono-cation of Li^+ and/or Na^+ adducts in the respective mass spectrum (**Figure 5.3**). Although no sodium salts were added to all sample polymer solutions, the used polymer sample solution apparently contained Na^+ as a contaminant which is sufficient for efficient ionization, as is frequently observed in mass spectrum of synthetic polymers¹⁰³.

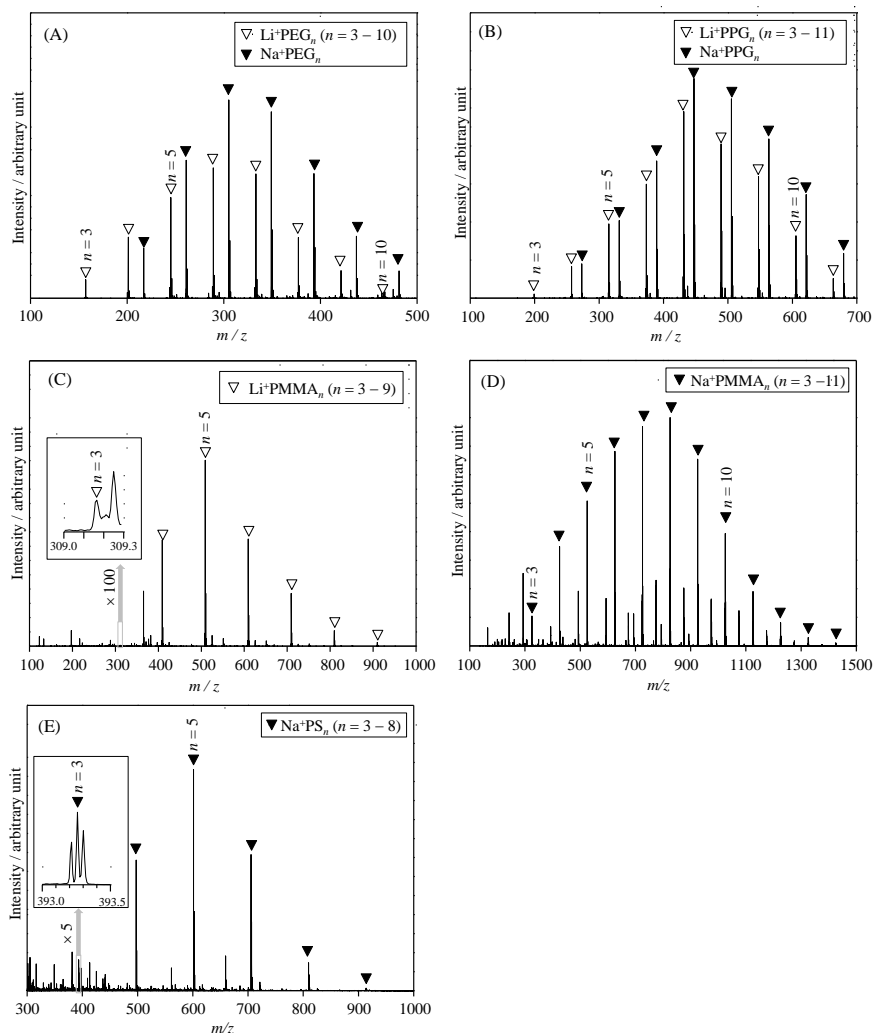


Figure 5.3

Time of flight mass spectra of (A) PEG, (B) PPG (C) (D)PMMA and (E) PS. All polymers were observed as a Li⁺and/or Na⁺ adduct.

Except for the PS, minimum cation adducted polymers were observed with trimer, which was consistent with former studies^{101,104}. PS was also observed with Na⁺ adduct with trimer, but no signals on IM-MS with Li⁺. A former IM-MS study of PS ionized by MALDI¹⁰⁴ that detected Li⁺PS₃ and Na⁺PS₃. Ionization mechanism is possibly attributed to the difference of ionization mechanism of ESI compared to MALDI. Although Li⁺ and Na⁺ have different radius, CCS of both Li⁺ and Na⁺ attached PS showed almost same value¹⁰⁴. In this study, Na⁺PS₃ was thus treated as the smallest cation adducted PS.

Meanwhile, experimentally obtained representative CCS of Li^+ adducted PEG, PPG and PMMA were summarized in **Table 5.1**. Our adopted parameter for Li^+ are likely reliable, because theoretically calculated CCS of Li^+ adducted polymer showed good accordance with experimentally results (**Table 5.2**).

Table 5.1

Comparison of experimentally obtained CCS of PEG, PPG and PMMA with Li^+ and Na^+ .

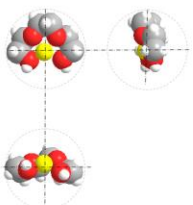
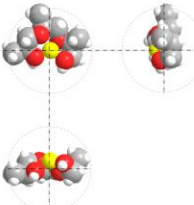
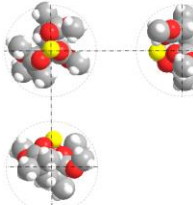
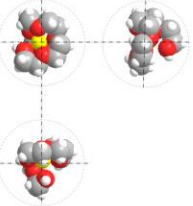
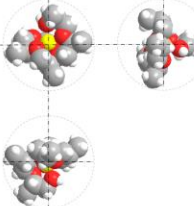
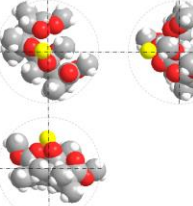
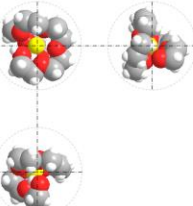
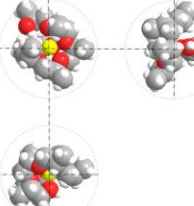
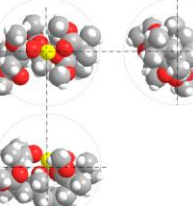
n	$CCS / \text{\AA}^2 (R_{\text{eff}} / \text{\AA})$	
	Li^+PEG_n	Na^+PEG_n
3	131.8 (4.0)	133.9(4.0)
4	141.3(4.2)	144.3(4.3)
6	161.3(4.7)	162.24(4.7)

n	$CCS / \text{\AA}^2 (R_{\text{eff}} / \text{\AA})$	
	Li^+PPG_n	Na^+PPG_n
3	144.9 (4.3)	147.7 (4.4)
4	158.6 (4.6)	161.9 (4.7)
6	185.0 (5.2)	189.2 (5.3)

n	$CCS / \text{\AA}^2 (R_{\text{eff}} / \text{\AA})$	
	Li^+PMMA_n	Na^+PMMA_n
3	170.2 (4.9)	172.9 (4.9)
4	191.7 (5.3)	194.3 (5.4)
6	233.6 (6.1)	236.5 (6.2)

Table 5.2

Three-plane pictures of Li^+PEG_n , Li^+PPG_n and Li^+PMMA_n ($n = 3, 5$ and 6) were obtained by MD simulations. Carbon, hydrogen, oxygen and Li^+ are indicated by gray, white, red and yellow, respectively. Each circle with dotted gray line was depicted centering at the gravity of polymer ion with effective radius (R_{eff}). The experimentally and theoretically (in parentheses) obtained collision cross section (CCS) of Li^+ adducted polymers. Both values showed good agreement with relatively small error ($< 5.7\%$). The sphericity (S) of Li^+ adducted polymers were calculated by Equation (5.4).

n	Li^+PEG_n	Li^+PPG_n	Li^+PMMA_n
3			
	$CCS = 129.6 \text{ (127.5)} \text{ \AA}^2$	$CCS = 144.9 \text{ (147.9)} \text{ \AA}^2$	$CCS = 170.2 \text{ (172.1)} \text{ \AA}^2$
	$R_{\text{eff}} = 3.92 \text{ \AA}$	$R_{\text{eff}} = 4.29 \text{ \AA}$	$R_{\text{eff}} = 4.86 \text{ \AA}$
	$S = 0.694$	$S = 0.679$	$S = 0.797$
5			
	$CCS = 150.1 \text{ (150.2)} \text{ \AA}^2$	$CCS = 171.6 \text{ (181.4)} \text{ \AA}^2$	$CCS = 214.3 \text{ (231.0)} \text{ \AA}^2$
	$R_{\text{eff}} = 4.41 \text{ \AA}$	$R_{\text{eff}} = 4.89 \text{ \AA}$	$R_{\text{eff}} = 5.72 \text{ \AA}$
	$S = 0.752$	$S = 0.768$	$S = 0.745$
6			
	$CCS = 161.6 \text{ (160.7)} \text{ \AA}^2$	$CCS = 185.0 \text{ (190.1)} \text{ \AA}^2$	$CCS = 233.59 \text{ (247.0)} \text{ \AA}^2$
	$R_{\text{eff}} = 4.67 \text{ \AA}$	$R_{\text{eff}} = 5.17 \text{ \AA}$	$R_{\text{eff}} = 6.12 \text{ \AA}$
	$S = 0.806$	$S = 0.841$	$S = 0.721$

It should be noticed that *CCS* of both Li^+ and Na^+ adducted polymer showed similar values, nevertheless ion radius of Li^+ (60 pm^{102}) is smaller than Na^+ (95 pm^{102}). This result indicates that polymer reaches most contracted state. Actually, spacious size of Na^+ adducted PEG and PPG is smaller than globule state formed by only electronically neutral polymer chain^{85,101} (See also Chapter 4). Na^+ adducted polymer, they can exceed lower limit of spacious size corresponding to globule state due to electrostatic interaction between cation and lone pair electron of oxygen atom. Na^+ adducted PEG, PPG and PMMA do not contract furthermore, therefore, Li^+ adducted ones showed almost same *CCS* with Na^+ adducted. Hence, in this study, Li^+ adducted polymers except for PS are mainly analyzed and discussed in the following sections.

5.3.2 Evaluation of surface tension based on *CCS*

Equation (5.1) describes that dielectric substance forms the smallest sphere with excess charges. As for IM-MS measurement in vacuum phase, mono-cation adducted polymer chain forms globule state with a spherical geometry. The threshold polymer size on MS can be a proposed smallest *CCS* with sphere so-called “Rayleigh limit droplet”. If the radius of Rayleigh limit droplet were evaluated, one could instantly obtain γ using Equation (5.1). Using experimentally obtained *CCS* data, it is possible to estimate radius of Li^+ adducted polymer because *CCS* corresponds to the averaged projected area of globular coil. Evaluating the effective radius (R_{eff}) and effective *CCS* (CCS_{eff}) of the sample, it is then necessary to subtract the *CCS* of the buffer gas^[87]. In this study, IM-MS experiments were carried out with nitrogen as a buffer gas. The radius of the nitrogen molecule can be obtained as 2.5 \AA by using the van der Waals coefficient b (0.0387 L/mol)^[88]. R_{eff} and CCS_{eff} can thus be obtained via Equation (5.2) and (5.3), respectively.

$$R_{\text{eff}}[\text{\AA}] = \left(\frac{CCS[\text{\AA}^2]}{\pi} \right)^{0.5} - 2.5[\text{\AA}] \quad (5.2)$$

$$CCS_{\text{eff}}[\text{\AA}^2] = \pi R_{\text{eff}}^2 \quad (5.3)$$

Applying experimentally obtained CCS of the smallest ion: Li^+PEG_3 , Li^+PPG_3 , Li^+PMMA_3 and Na^+PS_3 into Equation (5.1)–(5.3), γ of each polymer was obtained (Table 5.3).

Table 5.3

Comparison of surface tension values. Surface tension of each polymer is calculated by Equation (5.1)–(5.3) using CCS of threshold ion.

polymer	threshold ion	surface tension / $\text{mN}\cdot\text{m}^{-1}$	
		this work	reference
PEG	Li^+PEG_3	76.1	42.5-42.9 ^{105–108}
PPG	Li^+PPG_3	58.1	31.1-31.7 ^{107,109–112}
PMMA	Li^+PMMA_3	40.0	41.1 ⁹⁵
PS	Li^+PS_3	27.2	32.4-40.7 ^{95,113,114}

γ of PMMA was obtained 40.0 mN/m which was relatively good accordance with reported value of 41.1 mN/m. On the other hand, PEG, PPG and PS were obtained with 76.1 mN/m and 58.1 mN/m and 27.2 mN/m, respectively. γ of PEG, PPG and PS were largely deviated from literature reported values. Here it should be noted MD simulated structures in Table 5.2, Li^+PEG_3 and Li^+PPG_3 are not a spherical structure but more oblate-shaped, whereas Li^+PMMA_3 formed almost spherical structure. In the next section, discrimination methodology for sphericity of cation adducted polymer was considered.

5.3.3 Discrimination for sphericity of cation adducted polymer

To discriminate sphericity in a quantitative manner, spherical index (S) was adopted by Equation (5.4)¹¹⁵.

$$S = \sqrt{\frac{D_t}{D_c}} \quad (5.4)$$

Here, D_i is the largest inscribed circle diameter and D_c is the smallest circumscribed circle diameter. In this study, classification of sphericity was used¹¹⁵, and set criteria for $S \geq 0.775$ as a spherical droplet which satisfies Rayleigh limitation equation. D_c was determined using MD simulated structure for all polymers to cover whole structures of Li^+ and Na^+ adducted polymer (**Figure 5.4**). The diameter of inscribed circle; D_i was determined from the snap shot of Li^+ and Na^+ adducted polymer which gave the smallest projected area. This profile of the snapshot does not always give smooth profile because magnitude of whole size is comparable order of atomic size. In this study, the profile was smoothed by connecting hydrogen atoms which located on the original profile line of projected area as depicted Figure 5.4.

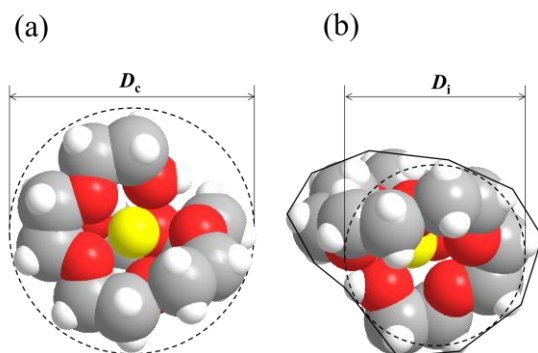


Figure 5.4

The dotted line in (a) and (b) correspond to the circle with D_c and D_i , respectively, in case of Li^+PEG_6 . The black line in (b) shows smoothed profile of projected view giving the smallest area in Li^+PEG_6 . Carbon, hydrogen, oxygen, and sodium cation (Li^+) are indicated by gray, white, red, and yellow, respectively.

The calculated S of Li^+PEG_3 and Li^+PPG_3 did not match the requirement for sphericity (Table 5.2). With increasing number of monomer units, sphericity of Li^+PEG_6 and Li^+PPG_6 finally reach criteria for the smallest sphere. Applying CCS of Li^+PEG_6 and Li^+PPG_6 to Equation (5.1)–(5.3), γ for PEG and PPG could be calculated with 45.0 mN/m and 33.1 mN/m, respectively. These values showed good accordance with literature values with 42.5–42.9 mN/m^{105–108} for PEG and 31.1–31.7 mN/m for PPG^{107,109–112}.

5.3.4 Droplet size deviation by bulky end group

Experimentally obtained R_{eff} of Na^+PS_3 had smaller surface free energy than literature value although the sphericity is sufficient (**Table 5.4**). According to Equation (5.1), larger radius gives smaller surface free energy. In case of PS, Na^+PS_3 is the smallest polymer ion size thus impossible to give larger surface free energy any more. Here, one should take note to polymer structure. Main chain of applied PS sample consisted with tert- C_4H_9 and hydrogen atom at both ends from its synthesis. One can deduce that tert- C_4H_9 enlarges CCS of Na^+PS_3 . To inspect quantitative contribution of tert- C_4H_9 to whole Na^+PS_3 , theoretically calculated CCS_{eff} of Na^+PS_3 with and without tert- C_4H_9 (Na^+PSH_3) were compared to each other (The chemical formula of PSH_3 is depicted in Figure 5.5).

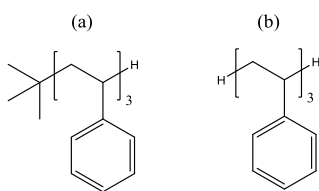


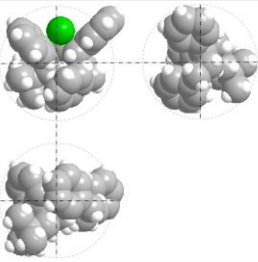
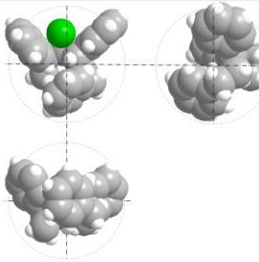
Figure 5.5

Comparison of chemical formula of (a) PS_3 and (b) PSH_3 .

CCS_{eff} of Na^+PS_3 was calculated with 202.5 \AA^2 giving very close to experimentally obtained one with 202.3 \AA^2 . Next, CCS of Na^+PSH_3 , in which tert- C_4H_9 was substituted with hydrogen atom, was calculated with 185.4 \AA^2 . Based on CCS of Na^+PSH_3 , R_{eff} was calculated with 5.2 \AA . Theoretically obtained R_{eff} of Na^+PSH_3 was $\sim 0.3 \text{ \AA}$ smaller than that of Na^+PS_3 , at the same time, sphericity of Na^+PSH_3 lies in a good acceptable level (Table 5.4). Consequently, by using 5.2 \AA for R_{eff} , surface tension of PSH could be obtained as 34.3 mN/m . This value was quite well consistent with the literature reported value of $32.4\text{--}40.7 \text{ mN/m}$.

Table 5.4

Three-plane pictures of Na^+PS_3 and Na^+PSH_3 were obtained by MD simulations. Carbon, hydrogen, oxygen and Na^+ are indicated by gray, white, red and green, respectively. Each circle with dotted gray line was depicted centering at the gravity of polymer ion with effective radius (R_{eff}). The experimentally and theoretically (in parentheses) obtained collision-cross section (CCS) of Na^+ adducted polymers.

Na^+PS_3	Na^+PSH_3
	
$\text{CCS} = 199.6 \text{ (202.5) } \text{\AA}^2$	$\text{CCS} = - (185.4) \text{ } \text{\AA}^2$
$R_{\text{eff}} = 5.53 \text{ } \text{\AA}$	$R_{\text{eff}} = 5.18 \text{ } \text{\AA}$
$S = 0.780$	$S = 0.780$

5.4 Conclusions

Initial objective was to obtain surface tension of synthetic polymer using Rayleigh limit equation which was described for the minimum polymer droplet with excess charge. To approach this objective, IM-MS was performed using ESI for PEG, PPG, PMMA and PS with Li^+ and Na^+ salt. It is noticeable that two regulations should be considered.

1) Sphericity

The minimum polymer ion, which gave the smallest *CCS*, does not always take spherical dimension. To verify dimension of polymer ion, MD simulation assists to characterize steric structure and discriminate sphericity.

2) End group

CCS containing contribution of polymer chain and end group. If necessary, end group have to be substituted with hydrogen atom.

Taking account of these two matters, surface tension can be obtained in good agreement with the literature reported value for PEG with 45.0 mN/m, PPG with 33.1 mN/m, PMMA with 40.0 mN/m and PS with 34.3 mN/m, respectively.

The IM-MS in conjunction with MD simulation enables to evaluate surface tension of synthetic polymer from different type. The proposed method provides an extremely swift and precise measurement for polymer without any external disturbances of solvents or impurities.

Part III

Study on +2 charge adducted species

Chapter 6

Collision cross section dependency on the number of monomer units of doubly charged polymer

~Obtaining the dielectric constant and characteristic ratio of polymers~

Summary

Ion mobility-mass spectrometry (IM-MS) of doubly-charged polyethylene glycol (PEG) and polypropylene glycol (PPG) was performed after electrospray-ionization mass spectrometry. The dependency of the effective collision cross section on the number of monomer units was evaluated with the help of MD simulations. Assuming a balance between elastic and coulomb forces inside short, asymmetric doubly-charged chains, a method was developed to evaluate the dielectric constant, which was found to be 7.87 for PEG for $n = 14$ –28 and 6.18 for PPG for $n = 13$ –20. From the same experiment at higher chain lengths the characteristic ratio C_n of 4.30 for PEG ($n \geq 63$) and 5.54 for PPG ($n \geq 56$) could be evaluated according to an earlier reported method, which was demonstrated here to also work with doubly-charged species. The proposed method enables an extremely swift and precise measurement both of ε and C_n of polymer which strong tolerance of solvent or impurities.

Reproduced with permission from S.Kokubo and V. Vana, *Macromolecular Chemistry and Physics*, 2017, 1700126. Copyright 2017, Wiley-VCH.

6.1 Introduction

An accurate structure and molecular weight control using cutting-edge polymerization techniques allows polymers becoming one of the most important materials in nano-science and advanced chemical industries. At the same time, analytical methods for precise determination of the properties of these tailored polymers need to be further developed. Within this context, mass spectrometry of polymers is a powerful and established method,⁹ which recently has made the step to the next level by introducing ion mobility-mass spectrometry (IM-MS), by which the spacious size of polymers can be evaluated quantitatively²⁰. IM-MS enables to measure the drift time of sample in an ion mobility cell, which is filled with an inert gas. The experimental observable, i.e., drift time depends on the collision cross section (CCS) of the sample. CCS represents the spacious size of polymer coils which are, however, not disturbed by solvent molecules and other polymer chains because IM-MS is performed of isolated single macromolecules in vacuum. Therefore, CCS provides intrinsic property information of polymers, which can be advantageous when comparing with other methods such as viscosity and light scattering measurements in solution. These conventional methods deliver molar mass averages, whereas IM-MS gives data for individual chains and property changes with chain length can provide access to specific chain dimension parameters. In a previous study⁹⁸, IM-MS of polyethylene glycol (PEG) and polypropylene glycol (PPG) were performed after electrospray-ionization (ESI) and measured CCS as function of chain length. By applying a globule model CCS was connected with the number of monomer units, n , with the characteristic ratio, C_n . The derived model equation described the IM-MS result very well and experimentally obtained C_n values showed extremely good agreement with literature reported data.

ESI is one of the most widely used and powerful ionization methods for polymers, due to its softness and high ionization efficiency and mild ionization conditions. ESI also have the ability to produce multiply charged species^{21,113}. The multiply charged ions are sometimes advantageous for high molar mass molecules, e.g., mono-disperse proteins, as it brings m/z values down to lower values for an easier detection. Multiply charged ions are, on the other hand, not frequently used for synthetic polymers, which inherently show

molar mass dispersion, as singly and multiply charged species may overlap, complicating the spectrum interpretation. It should be mentioned that, however, in IM-MS it is possible to turn the disadvantage of multiply charged species observed after ESI into an advantage: according to conventional studies on polyethylene glycol (PEG) using IM-MS^{24,25,65,114,115}, the dimension of the polymer coil depends on both number of charges and polymerization degree (n). In small n region, PEG takes partially rod like structure in which globule and stretched out monomer unit coexist. With increasing n , all monomers are attracted by the charge and finally complete a globule structure. As for doubly charged PEG –two sodium cations (Na^+) adducted PEG $((\text{Na}^+)_2\text{PEG}_n)^-$ with $n < \sim 30$ should form a stretched out structure²⁵ due to the repulsive Coulomb force (f_c) between the two Na^+ ions. On the other hand, a stretched out polymer chain underlies a retracting entropy elastic force (f_s) working against f_c . Under the first assumption in vacuum, f_c and f_s balance each other. Both f_c and f_s are correlated with the spacious size, which can be interpreted via CCS in the IM-MS experiment. Knowledge on these parameter enable the evaluation and understanding of the electronic and mechanical properties of the polymer chain. Besides that, $(\text{Na}^+)_2\text{PEG}_n$ with $n > 60$ show globule structure²⁵ similar as observed by singly charged PEG.⁹⁸ According to our previous study,⁹⁸ it is thus also possible to evaluate C_n of PEG by applying the globule model equation to doubly charged polymer species. Based on these consideration, IM-MS was performed with focus on doubly charged PEG and polypropylene glycol (PPG) to obtain the CCS dependency on n . Molecular dynamics (MD) simulation were also carried out and compared with experimentally values of CCS. Furthermore, the dielectric constant of the tested polymers were derived.

6.2 Experimental section

6.2.1 Materials

PEG (Aldrich, average $M_n \sim 1000, 1450, 2000, 3000$) and PPG (Aldrich, average $M_n \sim 1000, 2000, 2700$) were used without further purification and any salt added. These materials were dissolved in methanol (Fluka, LC-MS CHROMASOLV) yielding polymer solutions having concentrations of ca. 100 ppm. The PEG and PPG solutions were charged to a 100 μ l syringe and injected into an electrospray ionization (ESI) source running with a 5 μ l/min flow rate.

6.2.2 IM-MS

ESI was applied to IM-MS Synapt G2 HDMSTM (Waters Corporation). Prior to IM-MS measurement, MS was calibrated using a methanol solution of sodium iodide (100 mg/mL) ESI source temperature was 80 °C, the capillary voltage was 3.5 kV, desolvation temperature was 150 °C and the cone voltage was 40 V. The flow rate of helium in the cell located in front of the tri-wave ion mobility cell was set to 180 mL/min. Nitrogen flow in the ion mobility cell was set to 90 mL/min. The ion mobility spectrometer wave velocity and its wave height was optimized to 600–1000 m/s and 40 V. CCS data were calibrated using polyalanine⁶³ under the same measurement condition as for the PEG and PPG samples.

6.2.3 Effective CCS evaluation

The CCS, which is a primal experimental observable of ion mobility spectrometry, needs to be corrected in case the sample and the buffer gas size is in the same order of magnitude⁸⁴. For evaluating the effective CCS of the sample (CCS_{eff}) it is then necessary to subtract the CCS of the buffer gas. In this study, IM-MS experiments were carried out with nitrogen as a buffer gas. The radius of the nitrogen molecule can be obtained as 2.5 Å by using the van-der-Waals coefficient b (0.03913 L/mol)⁸⁵. CCS_{eff} can thus be obtained via Equation (6.1).

$$CCS_{\text{eff}}[\text{\AA}] = \left\{ \left(\frac{CCS[\text{\AA}]}{\pi} \right)^{0.5} - 2.5[\text{\AA}] \right\}^2 \pi \quad (6.1)$$

6.2.4 Simulation of molecular conformation and calculation of CCS

Molecular dynamics (MD) simulation was performed to get information about the PEG and PPG conformation in the gas phase. MD simulations were performed by Chem3D Pro (Cambridge Soft Corporation, Version13.0) with the MM2 interaction.⁶⁵ The initial condition of the polymer was set with stretched-out main chain and two Na⁺ placed at both ends of polymer chain. MD simulations were running with a 2.0 fs step interval over 10000 –40000 steps at 300 K. Based on the coordination of the MD simulated polymer, the CCS was calculated by the software Mobcal^{70,71} equipped with Drift Scope (Waters Corporation, Version 2.7). The amount of CCS was evaluated as an averaged area of different projection areas.

6.3 Results and discussion

6.3.1 Classification of doubly charged species

In the mass spectra of PEG and PPG were observed as adducts with one or more sodium cations (Na⁺) (**Figure 6.1**). The used sample polymer and/or solvent apparently contained sodium salt as a contaminant coming from polymer sample, solvent and MS calibration reagent in sample flow line. The amount of sodium cation is sufficient for producing multiply charged ionization efficiently, as is frequently observed in MS of polymers¹⁰⁰. From each individual ionic species being present in the MS, the drift time is subsequently measured in an ion mobility tube. In the present study, drift times for the doubly charged species (Na⁺)₂PEG_{*n*} and (Na⁺)₂PPG_{*n*} were specifically measured. The peak positions of these peaks obviously shifted to later drift times with increasing number of monomer units (*n*). From calibration, the effective cross section was obtained for all doubly-charged species, CCS_{eff} (see Equation (6.1)), and plotted them against *n* (see **Figure 6.2**).

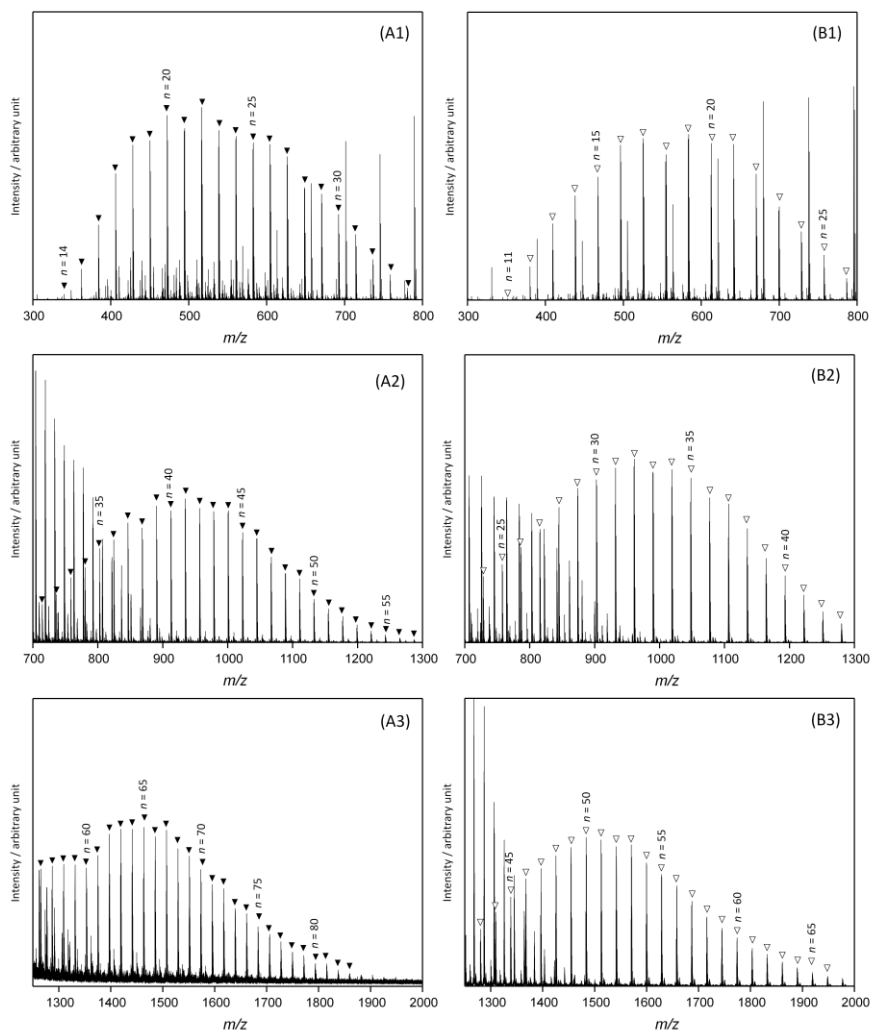


Figure 6.1

ESI time-of-flight mass spectra of PEG on left-hand-side and PPG on right-hand-side. The doubly charged species for $(\text{Na}^+)_2\text{PEG}_n$ and $(\text{Na}^+)_2\text{PPG}_n$ are marked with black in (A1) – (A3) and white triangles in (B1)–(B3), respectively.

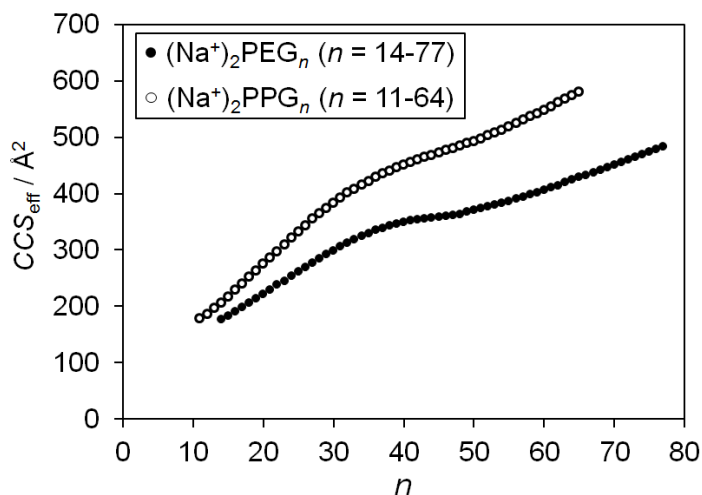


Figure 6.2

The effective collision cross sections (CCS_{eff}) of doubly-charged species $(\text{Na}^+)_2\text{PEG}_n$ ($n = 14-77$) and $(\text{Na}^+)_2\text{PPG}_n$ ($n = 11-64$) vs. number of monomer units (n).

The characteristics of these curves are significantly different than that of singly charged species⁹⁸: mono Na^+ -adducted PEG and PPG showed a very steady increase of CCS_{eff} vs. n dependency for $n > 8$.⁹⁸ For the doubly charged $(\text{Na}^+)_2\text{PEG}_n$ and $(\text{Na}^+)_2\text{PPG}_n$, on the other hand, it can clearly be seen as an s-shaped curve with an inflection point around $n = 40$. The reason for this may be a change of coil structure with increasing chain length. *Trimpin et al.*²⁴ suggested that the coil structure of multiply charged PEG chains in IM-MS depends on the number of monomer units: with $n < 40$, PEG shows a stretched out conformation whereas with $n > 60$ the chain forms a more globular coil²⁴. In this work, Equation (6.2) was used to calculate the incremental change of CCS_{eff} (**Figure 6.3**).

$$\Delta CCS_{\text{eff}}(n) = CCS_{\text{eff}}(n+1) - CCS_{\text{eff}}(n) \quad (6.2)$$

$\Delta CCS_{\text{eff}}(n)$ can roughly be divided into 4 regions.

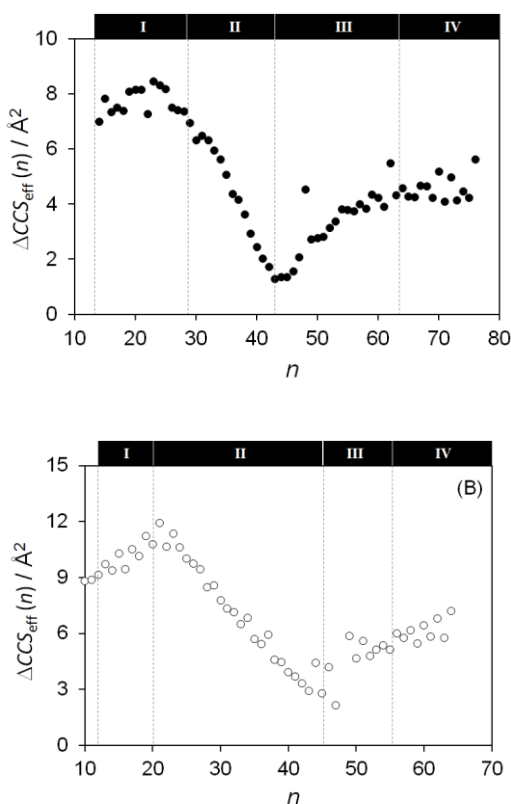


Figure 6.3

The evolution of the increment of the collision cross section with chain length, $\Delta CCS_{\text{eff}}(n)$, for (A) $(\text{Na}^+)_2\text{PEG}_n$ ($n = 14-76$) and (B) $(\text{Na}^+)_2\text{PPG}_n$ ($n = 14-63$).

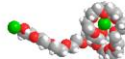
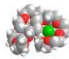
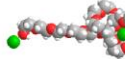
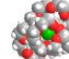

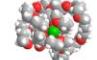
6.3.2 Region I : Asymmetric conformation of +2 charge adducted polymer

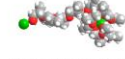
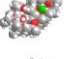
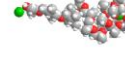
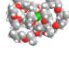
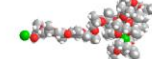
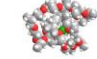
In region I, $\Delta CCS_{\text{eff}}(n)$ kept almost constantly and marked maximum value in all regions as far as measured in this study. As for singly charged species, mono Na^+ adduct, $\Delta CCS_{\text{eff}}(n)$ of Na^+PEG_n ($n = 14-22$) and Na^+PPG_n ($n = 13-20$) were ca. 6 \AA^2 and 8 \AA^2 , respectively⁹⁸. On the other hand, as for doubly charged species, $\Delta CCS_{\text{eff}}(n)$ of $\text{Na}_2^{2+}\text{PEG}$ ($n = 14-22$) and $\text{Na}_2^{2+}\text{PPG}_n$ ($n = 13-20$) were more than 7 \AA^2 and 10 \AA^2 , respectively, both were larger than singly charged species. These discrepancies of CCS_{eff} are attributed to the Coulomb repulsive force between the two attached Na^+ . In mono Na^+ adduct systems, an attractive force is dominant and the polymer chain forms a contracted globular structure. However, a second attached Na^+ changes the force balance and

enlarges the spacious size of the polymer chain.¹¹⁶ MD simulations of $(\text{Na}^+)_2\text{PEG}_n$ and $(\text{Na}^+)_2\text{PPG}_n$ ($n = 15$, and 20) were performed to study this effect. All MD simulations clearly gave structures, which are pronouncedly different from singly charged species as indicated in **Table 6.1**. The singly charged species forms a collapsed coil wrapping around Na^+ , whereas the doubly charged species forms an asymmetric, almost fully stretch out rod-like structure^{24,65,115} in which one Na^+ is located at one end of the polymer chain and the other being part of a more collapsed globular region at the other end of the chain. The calculated values of CCS_{eff} based on these MD simulations show excellent agreement with experimental values (Table 6.1).

Table 6.1

The comparison of CCS_{eff} between doubly and singly charged PEG in region I. Experimentally obtained and calculated (in parentheses) CCS_{eff} are shown below the simulated structures, which are snapshots with carbon, hydrogen, oxygen, and sodium cation (Na^+) indicated in grey, white, red, and green, respectively.

n	$(\text{Na}^+)_2\text{PEG}_n$	Na^+PEG_n
15	 183.3 Å ² (185.5 Å ²)	 130.2 Å ² (126.8 Å ²)
20	 219.5 Å ² (224.1 Å ²)	 162.1 Å ² (158.2 Å ²)
25	 261.7 Å ² (261.2 Å ²)	 192.7 Å ² (192.1 Å ²)

n	$(\text{Na}^+)_2\text{PPG}_n$	Na^+PPG_n
15	 223.8 Å ² (220.9 Å ²)	 167.4 Å ² (172.7 Å ²)
20	 278.3 Å ² (272.5 Å ²)	 213.7 Å ² (211.9 Å ²)
25	 315.9 Å ² (327.8 Å ²)	 254.3 Å ² (256.4 Å ²)

It is clear that this asymmetric structure must contain information about the physical properties of polymer as a dielectric substance.

According to the MD simulation results, both Na^+ are located near the terminal end of the polymer chain (see snap shot in Table 6.1). In such a conformation, the Coulomb force, f_e between two Na^+ can be described by Equation (6.3).

$$f_e = \frac{e^2}{4\pi\epsilon_0\epsilon_r|R|^2} \quad (6.3)$$

with the elementary charge, e , the electric constant, ε_0 , and the relative dielectric constant of the polymer, ε_r . On the other hand, the entropy elastic force, f_s , acts in the stretched out polymer as follows⁴⁴,

$$f_s = \frac{3kT}{C_n l^2 x} |\mathbf{R}| \quad (6.4)$$

with the Boltzmann constant, k , temperature, T , characteristic ratio, C_n , bond length of consecutive atoms along the polymer chain, l , and the number of bonds, k_n . These two forces could – at a first glance – considered being balanced, which leads to an expression for the squared end-to-end vector \mathbf{R} Equation (6.5).

$$|\mathbf{R}|^2 = \left(\frac{e^2 C_n l^2 k_n}{12\pi\varepsilon_0\varepsilon_r kT} \right)^{2/3} \quad (6.5)$$

For PEG and PPG, each monomer unit has three bonds along the main chain, so that $k_n = 3n$. Equation (6.5) can thus be rewritten with the number of monomer units, n :

$$|\mathbf{R}|^2 = \left(\frac{e^2 C_n l^2 n}{4\pi\varepsilon_0\varepsilon_r kT} \right)^{2/3} \quad (6.6)$$

In case of doubly charged system, \mathbf{R} of the whole polymer chain corresponds to a combination of the end-to-end vector of the globular part, $\mathbf{R}_{\text{globule}}$, and of the rod part, \mathbf{R}_{rod} .

$$\mathbf{R} = \mathbf{R}_{\text{globule}} + \mathbf{R}_{\text{rod}} \quad (6.7)$$

The square magnitude of \mathbf{R} can then be described by Equation (6.8);

$$\begin{aligned} |\mathbf{R}|^2 &= (\mathbf{R}_{\text{globule}} + \mathbf{R}_{\text{rod}})^2 \\ &= |\mathbf{R}_{\text{globule}}|^2 + |\mathbf{R}_{\text{rod}}|^2 + 2|\mathbf{R}_{\text{globule}}||\mathbf{R}_{\text{rod}}|\cos\theta \end{aligned} \quad (6.8)$$

In the IM-MS experiment, the temperature of the ion mobility cell was kept constant at 300 K. Under this experimental condition, the polymer takes various conformations due to molecular dynamics the part of Equation (6.8) with $\cos\theta$ is thus averaged and cancels out, leading to

$$|\mathbf{R}|^2 = |\mathbf{R}_{\text{globule}}|^2 + |\mathbf{R}_{\text{rod}}|^2 \quad (6.9)$$

It is then necessary to consider the dimensional transformation of \mathbf{R} , because this vector occurs in the three-dimensional space, whereas CCS_{eff} is a two dimensional observable. \mathbf{R} needs thus to be projected from 3D-space to a two-dimensional plane. According to our previous study⁹⁸ the magnitude of the 2D-projected end-to-end vector \mathbf{R} , i.e., \mathbf{R}_p can be described by Equation (6.10).

$$|\mathbf{R}_p| = \frac{2}{\pi} |\mathbf{R}| \quad (6.10)$$

\mathbf{R}_p can also, like in Equation (6.9), be written as a combination of the rod and globular part of the chain:

$$\mathbf{R}_p = \mathbf{R}_{p,\text{globule}} + \mathbf{R}_{p,\text{rod}} \quad (6.11)$$

leading to the equivalence of Equation (6.9)

$$|\mathbf{R}_p|^2 = |\mathbf{R}_{p,\text{globule}}|^2 + |\mathbf{R}_{p,\text{rod}}|^2 \quad (6.12)$$

\mathbf{R}_p is proportional to the gyration radius, R_g , and the factor of proportionality depends on the shape of the polymer chain. When the polymer forms a globular structure, the square magnitude of $\mathbf{R}_{p,\text{globule}}$, is correlated with R_g by Equation (6.13)⁴⁵.

$$|\mathbf{R}_{p,\text{globule}}|^2 = \frac{5}{3} R_g^2 \quad (6.13)$$

In addition, taking into account the empirical relation $R_g^2 \approx CCS_{\text{eff}} / 6^{86}$, CCS_{eff} can approximately be described via Equation (6.14):

$$|\mathbf{R}_{\text{p, globule}}|^2 = \frac{5}{18} CCS_{\text{eff, globule}} \quad (6.14)$$

On the other hand, in case of a rod-like polymer, the end to end distance of polymer, $\mathbf{R}_{\text{p, rod}}$, is correlated with R_g by Equation (6.15)⁴⁵.

$$|\mathbf{R}_{\text{p, rod}}|^2 = 12R_g^2 \quad (6.15)$$

As well as with the globular polymer, taking into account the empirical relation $R_g^2 \approx CCS_{\text{eff}}/6^{86}$ it follows that

$$|\mathbf{R}_{\text{p, rod}}|^2 = 2CCS_{\text{eff, rod}} \quad (6.16)$$

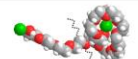
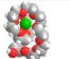

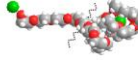
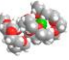
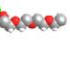
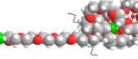
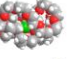

Combining Equation (6.10), (6.12), (6.14) and (6.16), Equation (6.17) is obtained.

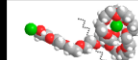

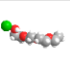
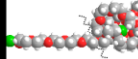
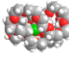
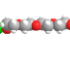
$$\frac{5}{18} CCS_{\text{eff, globule}} + 2CCS_{\text{eff, rod}} = \left(\frac{2}{\pi}\right)^2 |\mathbf{R}|^2 \quad (6.17)$$

As $CCS_{\text{eff, globule}}$ and $CCS_{\text{eff, rod}}$ are not able to be obtained experimentally, but estimated them by using MD simulations. **Table 6.2** shows snap-shots of MD simulated $(\text{Na}^+)_2\text{PEG}_n$ and $(\text{Na}^+)_2\text{PPG}_n$, indicating the clear separation between globular and rod-like chain regions of doubly charged polymer ions.

Table 6.2

The comparison of experimental and simulated CCS_{eff} for $(Na^+)_2PEG_n$ and $(Na^+)_2PPG_n$ ($n = 15, 20$ and 25), respectively. Molecular structures are snap-shots of MD simulations. The zigzag dotted line corresponds to the boundary between the ‘globular’ and the ‘rod-like’ region. CCS_{eff} data are given beneath the structures.

Exp.	Calc.		
	Whole	Globule	Rod
$(Na^+)_2PEG_{15}$			
183.3 Å ²	185.5 Å ²	112.7 Å ²	75.8 Å ²
$(Na^+)_2PEG_{20}$			
219.6 Å ²	224.1 Å ²	144.0 Å ²	76.5 Å ²
$(Na^+)_2PEG_{25}$			
261.7 Å ²	261.2 Å ²	162.0 Å ²	99.1 Å ²

Exp.	CCS_{eff} Calc.		
	Whole	Globule	Rod
$(Na^+)_2PEG_{15}$			
183.3 Å ²	185.5 Å ²	112.7 Å ²	75.8 Å ²
$(Na^+)_2PEG_{25}$			
261.7 Å ²	261.2 Å ²	162.0 Å ²	99.1 Å ²

The experimental and calculated CCS_{eff} values are in excellent agreement for the three simulated chain lengths, indicating the significance of the MD procedure. When separating the two regions of the chain (see zig-zag line in Table 6.2), one can obtain individual $CCS_{eff,globule}$ and $CCS_{eff,rod}$ values: $(Na^+)_2PEG_{20}$, for instance, can be divided into a rod part of 4 monomer units with a $CCS_{eff,rod}$ of 76.5 Å² and a globular part of 16 monomer units with a $CCS_{eff,globule}$ of 144.0 Å². The summation of these two values ($CCS_{eff,sum}$) gave 220.4 Å², which also showed good agreement with the calculated CCS_{eff} of the complete chain (224.1 Å²). These values indicate a ratio between globular and rod-like part of 0.61 to 0.39. The ratio for the other investigated PEG chains of different chain length are very similar and allow for the calculation of an average value of 0.61 (globular) to 0.39 (rod-like). By applying the same procedure to PPG, average values of 0.47 (globular) to 0.53 (rod-like) can be obtained (see Table 6.2). Using these data and

taking Equation (6.6) into account, Equation (6.17) can be rewritten to Equation (6.18) and (6.19).

$$0.949 \times CCS_{\text{eff,PEG}} = \left(\frac{2}{\pi}\right)^2 \left(\frac{e^2 C_n l^2 n}{4\pi\epsilon_0\epsilon_r kT}\right)^{2/3} \quad (6.18)$$

$$1.19 \times CCS_{\text{eff,PEG}} = \left(\frac{2}{\pi}\right)^2 \left(\frac{e^2 C_n l^2 n}{4\pi\epsilon_0\epsilon_r kT}\right)^{2/3} \quad (6.19)$$

Based on Equation (6.18) and (6.19); $0.949 \times CCS_{\text{eff,PEG}}$ and $1.19 \times CCS_{\text{eff,PPG}}$ was plotted against $n^{2/3}$, which exhibited good linearity with correlation coefficients more than 0.99 (**Figure 6.4**), yielding the following best linear fits, Equation (6.20) and (6.21):

$$0.949 CCS_{\text{eff,PEG}} = 28.84 n^{2/3} \quad (6.20)$$

$$1.19 CCS_{\text{eff,PPG}} = 43.51 n^{2/3} \quad (6.21)$$

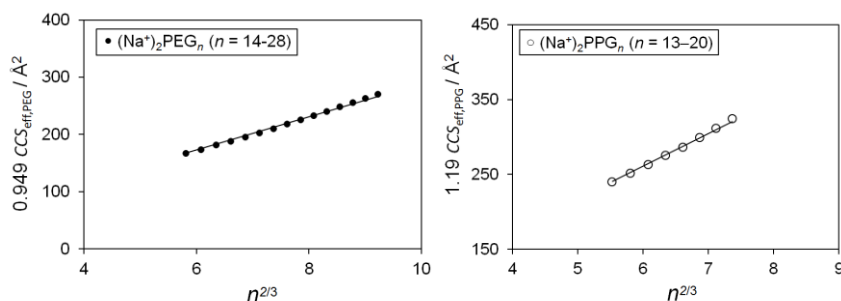


Figure 6.4

Experimentally obtained $0.949 \times \text{CCS}_{\text{eff}}$ of $(\text{Na}^+)_2\text{PEG}_n$ ($n = 14-28$) and $1.19 \times \text{CCS}_{\text{eff}}$ of $(\text{Na}^+)_2\text{PPG}_n$ ($n = 14-20$) against $n^{2/3}$. The linear lines are best linear fits.

All physical constants in Equation (6.18) and (6.19), except the relative dielectric constant, ϵ_r , are well known, as mentioned above. Here, C_n was used with 3.96 for PEG ($n = 16-27$) and 5.76 for PPG ($n = 21-32$)⁹⁸, which covers the same range of chain length, and a bond length of 1.463 Å both for PEG and PPG.⁸⁹ It is possible to estimate ϵ_r of PEG and PPG being 7.98 and 6.18, respectively. ϵ_r of PEG is slightly smaller than a relative old literature value of 8.95–10.95 of PEG having similar chain length ($M_n = 1000-1540$).¹¹⁷ This deviation might be attributed to the contaminant of more than one weight percent of water in the PEG, which *Koizumi et. al.* used for their study¹¹⁷. ϵ_r of water with ca. 80 is higher than that of PEG. Our IM-MS experiments were clearly carried out in the absence of any water inside the polymer yielding intrinsic material properties. The ϵ_r value of PPG of 6.18 also showed small deviation from the literature reported ϵ_r of 5.59 for PPG of $M_n = 2000$.¹¹⁸ Here our experimentally obtained ϵ_r value is slightly higher than the literature value, although deviations may even not be statistical significant. This very small deviation may, however, be explainable by the molar mass of the studied polymers. The smaller the chain length of polyglycols, the larger the relative dielectric constant¹¹⁷. The monomer unit of PPG, i.e., propane-1,2-diol, shows $\epsilon_r = 28.360$ ¹¹⁹ which is much higher than that of the polymer PPG. ϵ_r of PPG thus consequently decreases with the number of monomer units. As the literature value of PPG was obtained by *Sengwa*¹¹⁸ for PPG with $n \sim 34$, which is higher than the values of $n =$

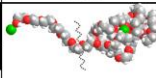
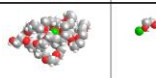

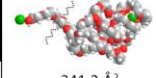
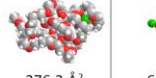

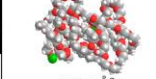
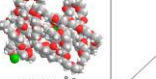
13–20 used in this study, the small deviations are well in line with this chain length effect.

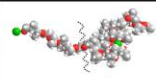
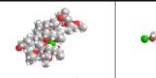

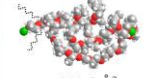
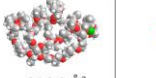
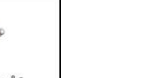
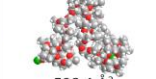
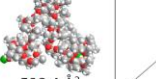
6.3.3 Region II–III : Intermediate state between asymmetric and symmetric conformation

In the chain length region II (see Figure 6.3) which corresponding to $n = 23$ –43 for PEG and $n = 21$ –45 for PPG, $\Delta CCS_{\text{eff}}(n)$ continuously decreases and reaches a minimum value around $n = 40$, which is then followed by region III, in which $\Delta CCS_{\text{eff}}(n)$ again is rising. These two regimes clearly describe a transition state between the rod-like/globular structures of region one and the pure globular coils of $(\text{Na}^+)_2\text{PEG}_n$ with $n \geq 63$ and of $(\text{Na}^+)_2\text{PPG}_n$ with $n \geq 59$, as described by *Trimpin et al.*²⁴ In order to better understand this transition, MD simulations were performed again (see **Table 6.3**).

Table 6.3

The comparison of experimental and simulated CCS_{eff} for $(\text{Na}^+)_2\text{PEG}_n$ ($n = 35, 40$ and 65) and $(\text{Na}^+)_2\text{PPG}_n$ ($n = 35, 40$ and 60). Molecular structures are snap-shots of MD simulations. The zigzag dotted line corresponds to the boundary between the ‘globular’ and the ‘rod-like’ region. CCS_{eff} data are given beneath the structures.

Exp.	Calc.		
	Whole	Globule	Rod
$(\text{Na}^+)_2\text{PEG}_{35}$			
329.7 Å ²	335.4 Å ²	213.3 Å ²	108.0 Å ²
$(\text{Na}^+)_2\text{PEG}_{40}$			
349.8 Å ²	341.2 Å ²	276.2 Å ²	61.9 Å ²
$(\text{Na}^+)_2\text{PEG}_{65}$			
428.8 Å ²	419.8 Å ²	419.8 Å ²	

Exp.	Calc.		
	Whole	Globule	Rod
$(\text{Na}^+)_2\text{PPG}_{35}$			
409.7 Å ²	416.5 Å ²	265.5 Å ²	163.0 Å ²
$(\text{Na}^+)_2\text{PPG}_{40}$			
435.8 Å ²	441.8 Å ²	396.0 Å ²	49.3 Å ²
$(\text{Na}^+)_2\text{PPG}_{60}$			
534.4 Å ²	538.4 Å ²	538.4 Å ²	

$(\text{Na}^+)_2\text{PEG}_{35}$ shows a globular and a rod-like like in region I. When increasing the chain length to 40, it can clearly be seen that the relative size of the rod-like part is decreasing in relation to the globular part. This structural change is directly reflected in $\Delta CCS_{\text{eff}}(n)$ and ends a pure globular structures, exemplified in Table 3 at $n = 65$ and 60 , respectively. But *what is the main driving force of this internal dimensional change?* A major cause is attributed to breaking balance of the Coulomb force between two Na^+ in polymer chain. In vacuum, Na^+ in globular part is electronically stabilized by coordination of lone pair electrons of oxygen atom²². When the number of monomer unit

reaches enough much to shield electronic field of an excess charge; Na^+ , fewer entropy elastic force can be balanced with the Coulomb repulsion force. Under this situation, polymer chain prefers globular structure to rod structure because steric energy of former one is more stable than that of latter one⁹⁸. In Region III, $(\text{Na}^+)_2\text{PEG}_n$ ($n = 43\text{--}62$) and $(\text{Na}^+)_2\text{PPG}_n$ ($n = 46\text{--}59$) might correspond to a transition state from partially to fully contract chain structure.

6.3.4 Region IV : Globule state in +2 charge adducted polymer

All monomer units begin to take part in globule structure from $(\text{Na}^+)_2\text{PEG}_{63}$ and $(\text{Na}^+)_2\text{PEG}_{60}$, and then, $\Delta\text{CCS}_{\text{eff}}(n)$ keeps almost constant value against n . The MD simulations of $(\text{Na}^+)_2\text{PEG}_{65}$ and $(\text{Na}^+)_2\text{PPG}_{60}$ show a contracted shape structure according to a globular state (see Table 6.3). From here on (region IV, see Figure 6.3) $\Delta\text{CCS}_{\text{eff}}(n)$ stays constant again, indicating that the principal structure remains unchanged with further increasing chain length. According to Chapter 4, $5/18 \times \text{CCS}_{\text{eff}}$ can then be correlated with $n^{2/3}$ by the globular model Equation (6.22):

$$\frac{5}{18} \text{CCS}_{\text{eff}} = C_n \left(\frac{2}{\pi}\right)^2 l^2 k_n^{2/3} \quad (6.22)$$

with C_n , l and k_n representing the characteristic ratio, the bond length and the number of bonds, respectively. In case of PEG and PPG, each monomer unit has three bonds along the main chain, i.e., $k_n = 3n$, and Equation (6.22) can be rewritten by Equation (6.23), inserting the bond length of 1.463 \AA ⁸⁷

$$\frac{5}{18} \text{CCS}_{\text{eff}} = \left(\frac{2}{\pi}\right)^2 C_n (1.463 \text{ \AA})^2 (3n)^{2/3} \quad (6.23)$$

Evaluating the plots of $5/18 \times \text{CCS}_{\text{eff}}$ against $n^{2/3}$ showed extremely good linearity with correlation factors of more than 0.999 (**Figure 6.5**), yielding the best linear fits Equation (6.24) and (6.25) for PEG and PPG, respectively.

$$\frac{5}{18}CCS_{\text{eff,PEG}} = 7.75n^{2/3} - 6.25 \quad (6.24)$$

$$\frac{5}{18}CCS_{\text{eff,PPG}} = 9.85n^{2/3} - 2.34 \quad (6.25)$$

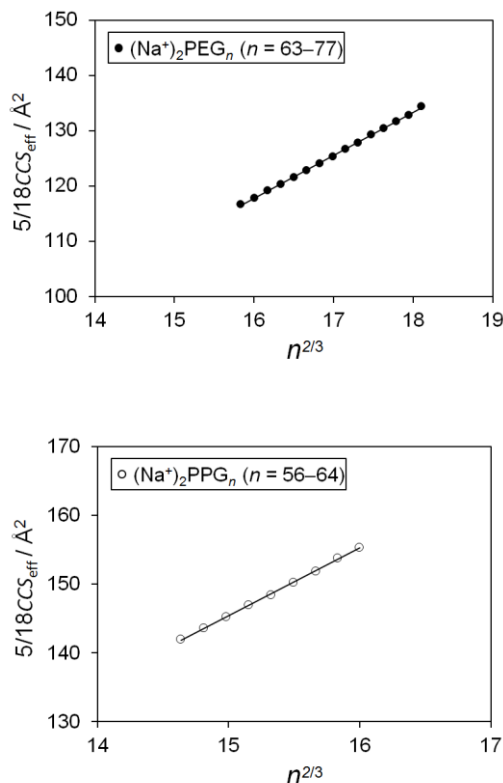


Figure 6.5

Experimentally obtained $5/18 \times CCS_{\text{eff}}$ of $(\text{Na}^+)_2\text{PEG}_n$ ($n = 63-77$) and $(\text{Na}^+)_2\text{PPG}_n$ ($n = 56-64$) against $n^{2/3}$. Black lines are best linear fits.

Please note that the occurrence of an intercept deviating from zero in Equation (6.24) and (6.25) is well understood and are indicative of an interaction between Na^+ and lone pair electrons of oxygen in the polymer chain and do not affect the data analysis.^{82,98} According to Eq. (6.23), the slope of Eq. (6.24) and Eq. (6.25) then give C_n values of 4.30 and 5.46 for PEG and PPG, respectively. These values are in very good agreement with earlier reported values^{98,46,75-78,89} as evidenced in **Table 6.4**. Our earlier developed method using the globular model in IM-MS can thus also be employed to obtain the characteristic ratio of polymers from doubly charged species.

Table 6.4

The characteristic ratio, C_n , of PEG and PPG as obtained in this study (bold text) compared to literature values.

Polymer	C_n	Method	Temperature/K	Reference
PEG	4.30	globule model fitting (Na⁺)₂PEG_n (n = 63–77)	RT (ca.300)	this work
	3.96	globule model fitting Na ⁺ PEG _n (n = 16–27)	RT (ca.300)	[98]
	4.8		298–323	[76]
	4.2–5.5	viscosity measurement	325	[90]
	5.1–5.7		298–323	[78]
	3.6–5.5	<i>ab initio</i> calculation	303–323	[88]
PPG	5.46	globule model fitting (Na⁺)₂PPG_n (n = 56–64)	RT (ca.300)	this work
	5.76	globule model fitting Na ⁺ PPG _n (n = 21–32)	RT (ca. 300)	[98]
	4.85		323	[46]
	5.05	viscosity measurement	323	[46]
	6.01		323	[75]
	5.88–6.16	<i>ab initio</i> calculation	323	[89]

6.4 Conclusions

IM-MS of doubly charged PEG, $(\text{Na}^+)_2\text{PEG}_n$ ($n = 14-77$), and PPG, $(\text{Na}^+)_2\text{PPG}_n$ ($n = 11-64$) was demonstrated to evaluated the increment dependency of the effective collision cross section, CCS_{eff} , on the number of monomer units, n with the help of MD simulation. The CCS_{eff} dependency on n for $(\text{Na}^+)_2\text{PEG}_n$ ($n = 14-22$) $(\text{Na}^+)_2\text{PPG}_n$ ($n = 13-20$), can be represented with the relative dielectric constant, ϵ_r . The obtained values for ϵ_r were 7.98 and 6.18 for PEG and PPG, respectively. Although no available reference data for PPG, PEG result showed relatively good agreement with earlier reported values. As for larger polymer, which corresponding $(\text{Na}^+)_2\text{PEG}_n$ ($n = 64-77$) and $(\text{Na}^+)_2\text{PPG}_n$ ($n = 59-64$), can take globule structure. By fitting experimentally measured CCS_{eff} data to globule model, the characteristic ratio C_n of 4.30 and 5.46 for PEG and PPG, respectively, were obtained and showed excellent agreement with earlier reported values. The proposed methodology enables us to evaluate intrinsic dielectric properties of polymer. In addition to MS advantage for sensitivity and absolute accuracy, combination with ion mobility raises analytical possibility of MS in polymer science field.

Chapter 7

Classification of Star polymer sing IM-MS

~Possibility in characterization of topology~

Summary

Ion mobility-mass spectrometry (IM-MS) is performed for detecting and classifying isomers of star-polymer by utilizing originally synthesized polyethylene glycol with multi-arm (star-PEG). Grafting pattern of PEG-arm in star-PEG can be represented with collision cross section (*CCS*) of doubly charged star-PEG. Besides *CCS* dependency, energy resolved-ion mobility spectrometry (ER-IMS) is performed to identify isomers. Herein ER-IMS is an identification technique in which isomeric components are individually activated in the gas phase by imposed at collision- induced dissociation (CID) energy. By analyzing the amount of dissociated product at varied CID activation energy, ER-IMS can distinguish the isomer. As a model sample study for isomer analysis, commercial star-PEG is performed by IM-MS and it shows broad ion mobility chromatogram (IMC) with some shoulder peaks distinct from originally prepared star-PEG. This is because the resolution of commercially available IM-MS is limited at the design of the instrument and usually cannot be upgraded at-will without extensive modifications. To compensate the poor resolution in IMS, the IMC profiles are deconvoluted with Gaussian functions. This treatment works well for extracting several peaks from IMC as an alternative. Both IM-MS and ER-IMS measurement are demonstrated for each extracted IMC, and thus the IMC broadening can conclude the coexisting isomers in sample star-PEG. The cross-check in conjunction with *CCS* and ER-IMS analysis is powerful analytical methodology for a successful revealing isomer in star-polymer.

7.1 Introduction

Star-polymer is one of the most active research targets in topological polymer design. It shows different viscoelastic property from linear polymer^{45,120–122}. So-called “reputation” of the star polymer can be characterized by the ratio of the number of monomer units in each arm of the star-polymer to the number of monomers in an entanglement star-polymer^{45,120}. Besides hydrodynamic character, star-polymer possesses multiple end groups which is possible to enhance the performance of functional materials, for example, highly reactive catalyst and strong surfactant¹²³. The property of star polymer depends on the molecular topology particularly for the number of arm and chain length of each arm. Therefore, analysis of detailed structural and topological behavior of these polymer is crucial for developing tailored polymer material with star-polymer¹²⁴.

The number of arm can be designed from the core part of star, for instance, glycerin and pentaerythritol provide three and four arms, respectively¹²⁴. However, all functional group is not always grafted same number of polymer chain. Spectrometry such as NMR and IR work well for characterizing chemical structure but is not able to distinguish isomer with same chemical formula but different topology or chain length distribution. *Kuki* et al performed tandem mass spectrometer for some star-polymer to distinguish the polymer with different distribution of chain length¹²⁵. Product ion via collision induced fragmentation, which is well known from the MSⁿ experiment, can be well applied here for investigate structure of polymer in most case.

In this study ion mobility mass spectrometry (IM-MS) was performed to measure molecular weight and spacious size simultaneously^{20,42,51}. Experimentally, spacious size is quantitatively observable as a collision cross section (CCS) which corresponds to average projected area of sample ion. CCS can be theoretically obtained from structure via molecular-dynamics (MD) simulation^{70,71,81}. Comparing experimentally and theoretically obtained CCS, it is possible to speculate conformation and dimension of polymer ion precisely^{98,126}.

Recently several groups conducted IM-MS to the isomer of oligosaccharides to identify molecular structure using dependency their spacious size on the sugar configuration in oligomer^{32,127}. Besides size evaluation, some studies proposed analytical

method for distinguishing isomeric oligosaccharides by deconvolution of peak on the ion mobility chromatogram (IMC). They scanned product ion species of sugar molecule against collision-induced-dissociation (CID) process and identified each isomer on IMC. This method was very useful to characterize structure of oligosaccharides. According to our former study¹²⁶, spacious size of doubly charged linear PEG was enlarged by Coulomb repulsive force between two charges. Therefore, it is possible to magnify the subtle difference between isomers of a star-shape polyethylene glycol (star-PEG) as well. Actually, *Trimpin* et al demonstrated IM-MS on star-PEG and found several signals for doubly charged species with different spacious size on IMC²⁰. If these peaks on IMC were derived from the isomeric polymer, IM-MS could be a crucial solution to detect the isomer of star-PEG.

In this study, isomers of star-PEGs with four hydroxyl end group and different number of PEG grafted arm (PEG-arm) were originally prepared to evaluate *CCS* on the number of PEG-arm by IM-MS. MD simulations of cation adducted star-PEGs were also performed to investigate their conformation. In addition to *CCS* measurements, tolerance of doubly charged system against CID energy was examined as an additional cross-check option for characterizing isomer and classifying molecular structure of star-PEG in case of analysis for structure unknown sample.

7.2 Experiment

7.2.1 Chemicals

Tetrakis-bromomethyl-methane (TBMM, Sigma-Aldrich, 96 %), polyethylene glycol (Sigma-Aldrich) with average molecular weight 200 (PEG200), 300 (PEG300) and 400 (PEG400), sodium hydroxide (1 mol/L solution, Sigma-Aldrich), ethanol (Honeywell Riedel-de Haën, 99.8 %) were used as received. Sodium (> 99.8 %, in kerosene, Sigma-Aldrich) was washed with pentane prior to use.

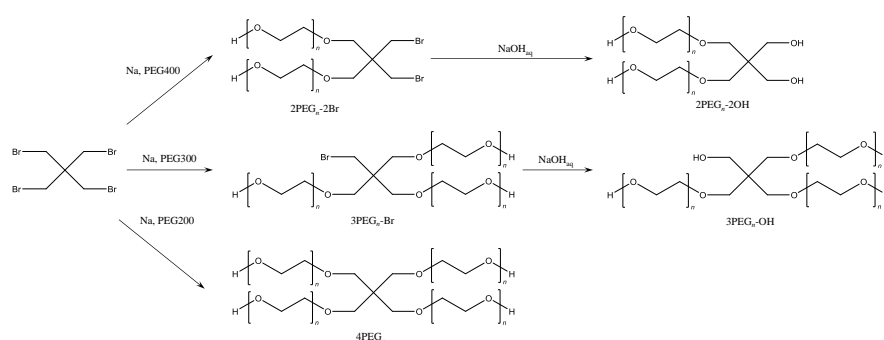
7.2.2 Synthesis of PEG substituted tetrakis-bromomethyl-methane

In a typical experiment, sodium was added to PEG under argon at room temperature. The mixture was then heated up to 120 °C for 1 hour until no observable sodium left. Tetrakis-bromomethyl-methane (TBMM) was added to the mixture and reaction was allowed to proceed at 160 °C under reflux overnight. The product mixture was used for next synthesis and MS-analysis without any treatment. The detailed experimental conditions and scheme are given in Table 7.1 and Scheme 7.1, respectively.

Table 7.1

Reaction conditions of the synthesis of different PEG substituted TBMM.

Product abbreviation	2PEG _n -2OH	3PEG _n -OH	4PEG _n
Type of PEG	PEG400	PEG300	PEG200
Approx. Equiv. of PEG	8.00	16.00	16.00
Equiv. of sodium	2.00	3.00	4.00
Equiv. of TBMM	1.00	1.00	1.00



Scheme 7.1

Schematic representation of the synthetic approach to star-PEG with 2–4 arms.

7.2.3 Synthesis star-PEG with two/three PEG-arms

In a typical reaction, 10 g of reaction mixture from the synthesis of PEG substituted TBMM (containing 3.0 mmol of 2PEG_n-2Br or 2.0 mmol 3PEG_n-Br with excess of unreacted PEG) was dissolved in 100 ml water-ethanol mixture (1:1). NaOH (1 mol/L solution, 3.3 mmol for 2PEG_n-2Br and 2.2 mmol for 3PEG_n-Br) was added to the mixture and the hydrolyze reaction was carried out under reflux overnight. After reaction, solvent was removed in vacuum. The polymeric mixture was used for MS-analysis without further treatment.

7.2.4 IM-MS

Electrospray ionization (ESI) was applied to IM-MS; Synapt G2 HDMSTM (Waters Corporation). ESI source temperature was 80 °C, the capillary voltage was 3.5 kV, desolvation temperature was 150 °C and the cone voltage was 40 V. The flow rate of helium in the cell located in front of the tri-wave ion mobility cell was set to 180 mL/min. Nitrogen flow in the ion mobility cell was set to 90 mL/min. The ion mobility spectrometer wave velocity and its wave height was optimized to 600 m/s and 40 V. CCS data were calibrated using polyaniline⁶³ under the same measurement condition as for the PEG and PPG samples.

7.2.5 Simulation of molecular conformation and calculation of CCS

Molecular dynamics (MD) simulation was performed to get information about the star-PEG conformation in the gas phase. MD simulations were performed by Chem3D Pro (Cambridge Soft Corporation, Version14.0) with the MM2 interaction⁶⁵. The initial condition of the polymer was set with stretched-out main chain and two Na⁺ placed at the ends of polymer chain. MD simulations were running with a 2.0 fs step interval over 40000 steps at 300 K. Based on the coordination of the MD simulated polymer, the CCS was calculated by the software MOBCAL^{70,71} equipped with DriftscopeTM (Waters Corporation, Version 2.7). The amount of CCS was evaluated as an averaged area of different projection areas.

7.3 Results and discussions

7.3.1 Mass spectrometry of synthesized star-PEG

Mass spectra of synthetic intermediates, in which Br are partially substituted with PEG, are shown in **Figure 7.1**. Br worked as a marker for checking how many Br atoms of TBMM were substituted with PEG by monitoring isotope pattern on time of flight mass spectrum (TOF-MS). Two/three Br of TBMM were substituted with PEG, isotope patterns of them were perfectly consistent with theoretically calculated one obtained using molecular weight calculation program of Chem3D. Bi- and tri- PEG substituted TBMM ($2\text{PEG}_n\text{-2Br}/3\text{PEG}_n\text{-Br}$) could be synthesized by our synthetic procedure and confirmed by MS. Tetra PEG subtitled TMBB was also confirmed by TOF-MS (**Figure 7.2 (C)**), which has no Br isotopically peaks. This supports that four Br of TBMM are substituted with four PEG chains.

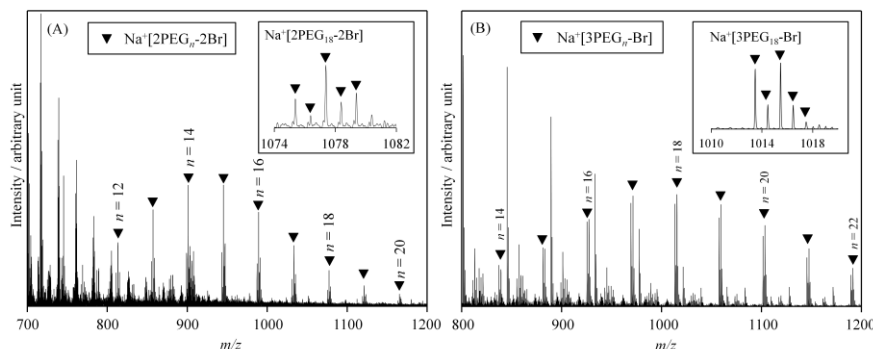


Figure 7.1

TOF-MS of the unhydroxylated star-PEG : (A) 2arm-PEG ($2\text{PEG}_n\text{-2Br}$), (B) 3arm-PEG ($3\text{PEG}_n\text{-Br}$). One sodium cation (Na^+) adduct of them are displayed with black colored triangle. Insertion of (A) and (B) are the magnified TOF-MS of one Na^+ adducted 2arm-PEG ($\text{Na}^+[2\text{PEG}_{18}\text{-2Br}]$) and 3arm-PEG ($\text{Na}^+[3\text{PEG}_{18}\text{-Br}]$). Isotope pattern of them are perfectly consistent with theoretically calculated one.

TOF-MS of linear PEG (reactant) enable to speculate how the chain length of each arm is distributed in synthesized star-PEG. The synthetic intermediates with Br: $2\text{PEG}_n\text{-2Br}$ and $3\text{PEG}_n\text{-Br}$ were observed with maximum intensity with $n = 14\text{--}16$ and $n = 17\text{--}19$, respectively (Figure 7.1). Assuming that the length distributed is homogeneous,

each arm should consist of PEG_n ($n = 8-10$) for $2\text{PEG}_n\text{-2Br}$ ($n = 14-16$) and PEG_n ($n = 7-8$) for $3\text{PEG}_n\text{-Br}$ ($n = 17-19$), respectively. According to TOF-MS of raw chemical PEG400 and PEG300 (**Figure 7.3**), this rough estimation gives very good accordance with the main component of PEG400 and PEG300 being PEG_n ($n = 8-10$) and PEG_n ($n = 6-8$), respectively. Therefore, 2arm- and 3arm-PEG should possess homogeneous length PEG chain for each arm.

The mass spectra of OH terminated star-PEG are shown Figure 7.2. The detected signal intensity of doubly charged ones were larger than singly charged ones, indicating that polymer sample contains enough much Na^+ from the synthesis to produce doubly charged polymers. Although 2arm-PEG ($2\text{PEG}_n\text{-2OH}$) and 3arm-PEG ($3\text{PEG}_n\text{-OH}$) were detected with low intensity, they are enough much to implement ion mobility spectrometry. Insertion of Figure 7.2 (A) and (B) shows the intensity TOF-MS for doubly charged $2\text{PEG}_{18}\text{-2OH}$ ($(\text{Na}^+)_2[2\text{PEG}_{18}\text{-2OH}]$) and $3\text{PEG}_{18}\text{-OH}$ ($(\text{Na}^+)_2[3\text{PEG}_{18}\text{-OH}]$), respectively. Both of isotope pattern are consistent with expectation from the synthesis design. The most abundant component of TOF-MS signal for 4arm-PEG (4PEG_n) was observed with $n = 17-18$ (Figure 7.2 (C)). Considering main component of reactant PEG 200 being PEG_4 and PEG_5 , the chain length of 4PEG can be regarded as almost homogeneously.

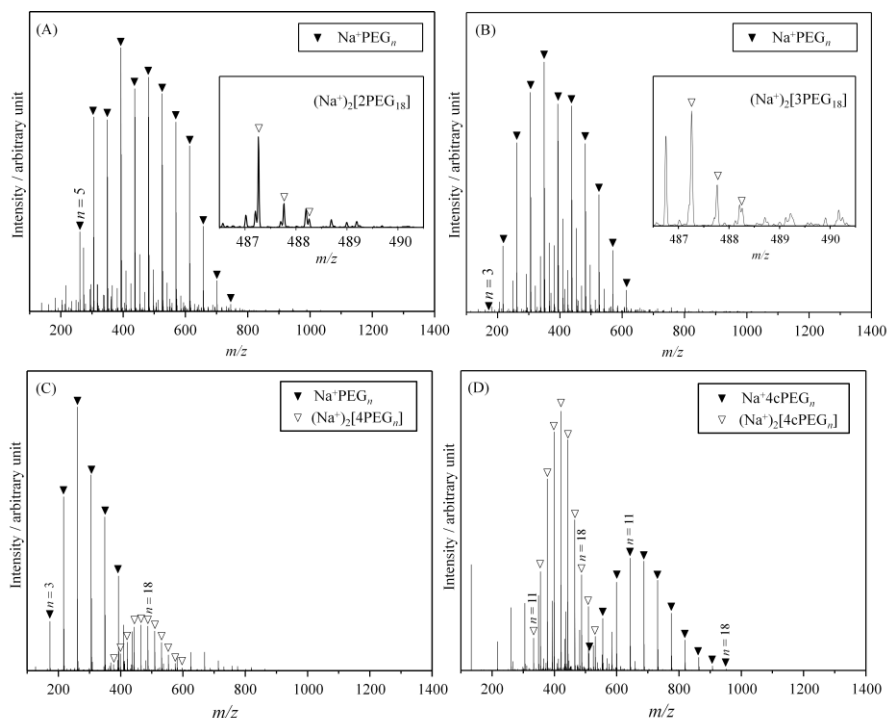


Figure 7.2

TOF-MS of hydroxylated star-PEG; (A) 2arm-PEG (2PEG_n-2OH), (B) 3arm-PEG (3PEG_n-OH), (C) 4arm-PEG (4PEG_n) and (D) commercial 4arm-PEG (4cPEG_n). One and two sodium cation (Na⁺) adduct of them are displayed with black and white colored triangle, respectively. Insertion of (A) and (B) are the TOF-MS with 100 times magnified intensity of two Na⁺ adducted 2arm-PEG ((Na⁺)₂[2PEG₁₈-2OH]) and 3arm-PEG ((Na⁺)₂[3PEG₁₈-OH]). Isotope pattern of (Na⁺)₂[2PEG₁₈-2OH] and (Na⁺)₂[3PEG₁₈-OH] are perfectly consistent with theoretically calculated one.

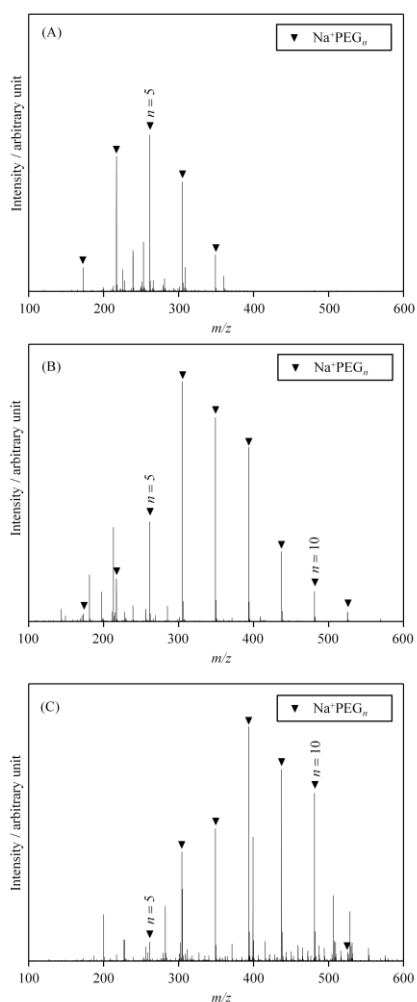


Figure 7.3

TOF-MS of singly charged linear (A) PEG200, (B) PEG300 and (C) PEG400. Each polymer was observed as one Na^+ adduct. The triangle corresponds to each polymer with monomer units (n).

7.3.2 Ion mobility spectrometry of singly charged star-PEG

The singly charged star-PEGs were observed as one Na^+ adduct, and their signal intensities were very weak but enough much to get signals on ion mobility spectra. Although, ion mobility chromatogram (IMC) peak maximum of $\text{Na}^+[\text{2PEG}_{18}\text{-2OH}]$ was observed in slightly higher *CCS* region (**Figure 7.4 (A)**), *CCS* of all other singly charged star-PEGs did not depend on the number of PEG-arm (Figure 7.4 (B) and (C)). Similar phenomena were observed in singly charged star-PEGs with different number of monomer units (See **Figure S1** in Appendix II). Several former studies reported that linear type PEG chain coil is known to form contracted structure around Na^+ in vacuum^{82,98,126}. This state can be regarded as globule state in which all monomer units aggregate into spherical dimension. Conformations from MD simulation of Na^+ adducted star-PEG with 18 monomer units are depicted in Table 7.2. MD simulation was started from initial structure of star-PEG in which each PEG-arm has average number of monomer unit. For instance in case of $\text{2PEG}_{18}\text{-2OH}$, two arms are grafted with PEG chain with 9 monomer units and the residual two arms are simply terminated with OH. As for $\text{3PEG}_{18}\text{-OH}$ and 4PEG_{18} , PEG monomer units are grafted as depicted in Table 7.2. The MD simulation results showed each star-PEG forms globule around Na^+ and calculated *CCS* showed good accordance with experimentally obtained ones (**Table 7.2**). Each type of star-PEG was grafted with different arm length but same total number of monomer units. The spacious size of globule state with almost symmetrically spherical dimension can be determined only by the number of monomer unit but not their arrangement and topology. This thus causes no distinguish between all types star-PEG with the *CCS* values from their singly Na^+ adduct. The singly charged star-PEG is not applicable to examine whether commercial 4arm-PEG (4cPEG_n) contain isomers or not (Figure 7.4 (D)). According to former studies^{24,65,115,126}, multiply charged species can take asymmetric conformation which is possible to clarify the difference of chemical structure of isomers, hence, IMC for doubly charged species were measured in this study.

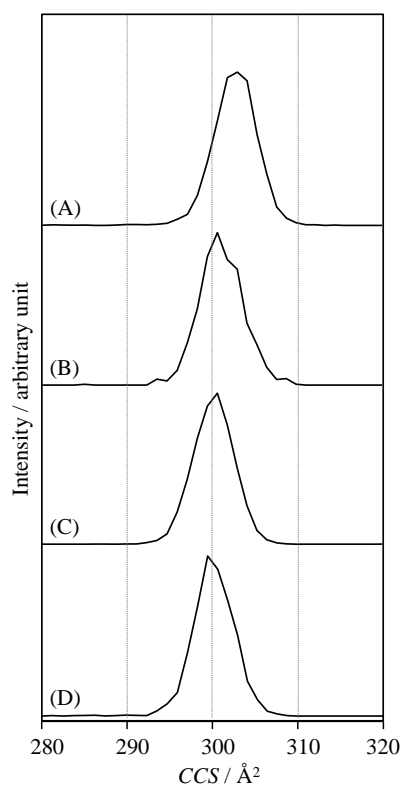


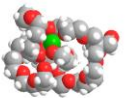
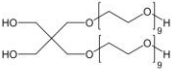
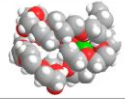
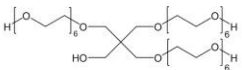
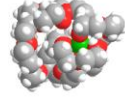
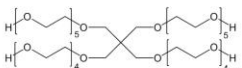
Figure 7.4

IMC of singly charged (A) $\text{Na}^+[\text{2PEG}_{18}\text{-2OH}]$,

(B) $\text{Na}^+[\text{3PEG}_{18}\text{-OH}]$, (C) $\text{Na}^+[\text{4PEG}_{18}]$ and (D) $\text{Na}^+[\text{4cPEG}_{18}]$.

Table 7.2

The snapshot of MD simulated structure of singly charged (A) $\text{Na}^+[\text{2PEG}_{18}\text{-2OH}]$, (B) $\text{Na}^+[\text{3PEG}_{18}\text{-OH}]$ and (C) $\text{Na}^+ [\text{4PEG}_{18}]$ are depicted with same scale. CCS_{exp} and CCS_{calc} stand for the experimentally and theoretically obtained collision cross section (CCS), respectively. The chain length of each star-PEG was set as the structural formula on the right hand side column. Carbon, hydrogen, oxygen, and Na^+ indicated in grey, white, red, and green, respectively.

	MD simulated structure	CCS	Structural formula
(A)		$\text{CCS}_{\text{exp}} = 302.3 \text{ \AA}^2$ $\text{CCS}_{\text{calc}} = 301.5 \text{ \AA}^2$	
(B)		$\text{CCS}_{\text{exp}} = 299.9 \text{ \AA}^2$ $\text{CCS}_{\text{calc}} = 294.9 \text{ \AA}^2$	
(C)		$\text{CCS}_{\text{exp}} = 299.5 \text{ \AA}^2$ $\text{CCS}_{\text{calc}} = 300.3 \text{ \AA}^2$	

7.3.3 Ion mobility spectrometry of doubly charged star-PEG

The peak maximum position of IMC for doubly charged star-PEG obviously depends on the number of PEG-arm, less number of PEG-arm gave larger *CCS* on IMC (Figure 7.5, See also Figure S2 in Appendix II).

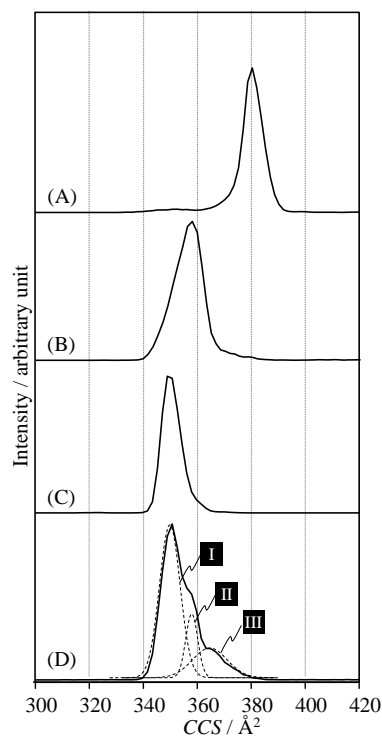
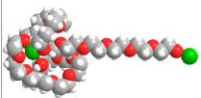
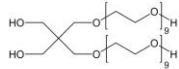
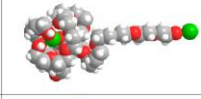
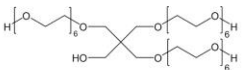
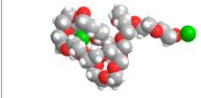
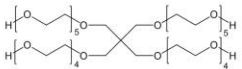


Figure 7.5

IMC of doubly charged (A) $(\text{Na}^+)_2[2\text{PEG}_{18}\text{-2OH}]$, (B) $(\text{Na}^+)_2[3\text{PEG}_{18}\text{-OH}]$, (C) $(\text{Na}^+)_2[4\text{PEG}_{18}]$ and (D) $(\text{Na}^+)_2[4\text{CPEG}_{18}]$. Peak I–III in (D) are Gaussian functions obtained via IMC deconvolution of $(\text{Na}^+)_2[4\text{CPEG}_{18}]$.

Table 7.3

The snapshot of MD simulated structure of doubly charged (A) $(\text{Na}^+)_2[2\text{PEG}_{18}\text{-2OH}]$, (B) $(\text{Na}^+)_2[3\text{PEG}_{18}\text{-OH}]$ and (C) $(\text{Na}^+)_2[4\text{PEG}_{18}]$ are depicted with same scale. CCS_{exp} and CCS_{calc} stand for the experimentally and theoretically obtained CCS , respectively. The chain length of each star-PEG was set as the structural formula on the right hand side column. Carbon, hydrogen, oxygen, and Na^+ indicated in grey, white, red, and green, respectively.

	MD simulated structure	CCS	Structural formula
(A)		$\text{CCS}_{\text{exp}}=387.2 \text{ \AA}^2$ $\text{CCS}_{\text{calc}}=380.2 \text{ \AA}^2$	
(B)		$\text{CCS}_{\text{exp}}=363.6 \text{ \AA}^2$ $\text{CCS}_{\text{calc}}=364.6 \text{ \AA}^2$	
(C)		$\text{CCS}_{\text{exp}}=346.0 \text{ \AA}^2$ $\text{CCS}_{\text{calc}}=334.8 \text{ \AA}^2$	

To compare their conformation, MD simulations were performed for two Na^+ adducted star-PEG with 18 monomer units using the initial structure as well as the singly charged case (**Table 7.3**). Calculated CCS showed good agreement with experimental results. All simulated conformations gave asymmetric structures which were composed of two different parts of globule and stretch-out chain / rod¹²⁶. One Na^+ locates at the end of the rod part with one arm, whereas the other Na^+ sits in globule part. The rod part of $(\text{Na}^+)_2[2\text{PEG}_{18}\text{-2OH}]$ is longer than that of $(\text{Na}^+)_2[4\text{PEG}_{18}]$, because more number of monomer units are allocated to each PEG-arm. Comparing the conformation of doubly charged system to singly charged one, the rod part mainly enlarges CCS in comparison with singly charged one due to the Coulomb repulsion energy between two Na^+ ions¹²⁶. The distances between two Na^+ were measured with 16.6 Å, 21.4 Å, and 24.0 Å for $(\text{Na}^+)_2[4\text{PEG}_{18}]$, $(\text{Na}^+)_2[3\text{PEG}_{18}\text{-OH}]$ and $(\text{Na}^+)_2[2\text{PEG}_{18}\text{-2OH}]$ respectively. We assume that dielectric constant were approximately same among all isomers due to same elemental composition, the distance between two Na^+ could directly affect the Coulomb repulsive energy in doubly charged system. It means that doubly charged star-PEG with

smaller CCS captures two Na^+ under less stabilized state. Herein, one fundamental question arises; *which structural factor plays the key role for determining the distances of two Na^+ in doubly charged system?* The end to end distance of PEG chain with rod state was theoretically obtained with 15.7 Å, 22.8 Å, and 33.5 Å for PEG₄, PEG₆ and PEG₉, respectively by MD simulation. These PEG_{*n*} correspond to averaged PEG-arm in 4PEG₁₈, 3PEG₁₈-OH and 2PEG₁₈-2OH, respectively. These values are very close to the distances of two Na^+ in the corresponding doubly charged system. The Coulomb energy inherently depends on distance of two Na^+ , therefore, Na^+ prefers to locate at the end of the longest PEG-arm. Evaluation of Coulomb energy can increase the reliability in classifying homogeneity of star-PEG depending on graft pattern of PEG-arm. This can be supported by experimental validation with IM-MS, by adding excess energy to sample ion via CID process¹²⁸. By monitoring the amount of singly charged star-PEG against CID energy, it is possible to classify molecular structure of star-PEG.

Based on this idea, tolerance of doubly charged ion against external excess energy was examined by following procedure. First, doubly charged star-PEG with particular monomer units was selected at quadruple mass filter (upstream of ion mobility tube). Second, after traveling through ion mobility tube, selected doubly charged sample was introduced into transfer cell setting downstream of ion mobility tube. Transfer cell is equipped with electrodes and purged with argon gas. Controlling electrode voltage from 0–45 V with 5 V of stepwise, CID experiment was performed. In CID process, an adducted Na^+ ion could dissociate from the polymer. At the third step, the signal intensity of product ion; singly charged ion was monitored. As for all types of star-PEG₁₈, the singly charged ion started to be detected from 25 V. Its signal intensity reached maximum at 40 V and the fragment of star-PEG started to be detected on TOF-MS at more than 45 V. The relative IMC peak area of singly charged ion was thus evaluated against collision energy at 40 V. Relative intensity of each type of star-PEG were plot against collision energy as so-called energy resolved ion mobility spectrum³² (ER-IMS) (**Figure 7.6**).

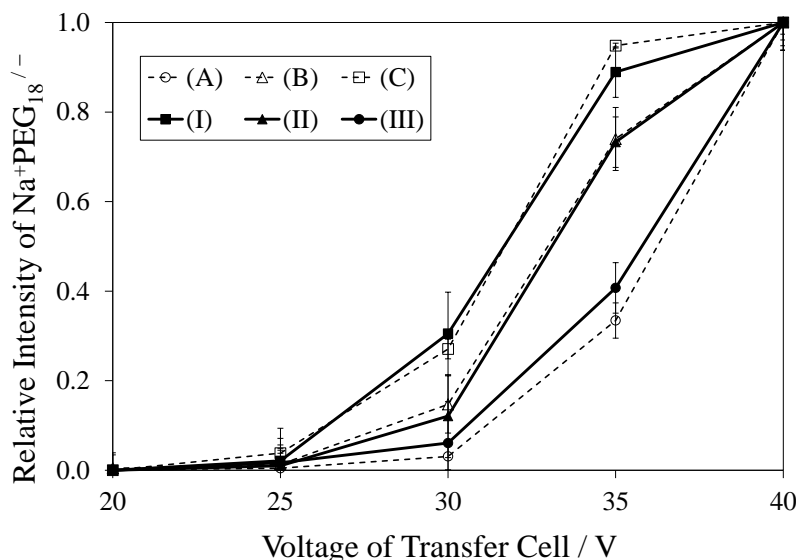


Figure 7.6

ER-IMS of (A) $(\text{Na}^+)_2[2\text{PEG}_{18}\text{-}2\text{OH}]$, (B) $(\text{Na}^+)_2[3\text{PEG}_{18}\text{-OH}]$ and (C) $(\text{Na}^+)_2[4\text{PEG}_{18}]$, respectively are depicted with dotted line. ER-IMS of (I), (II) and (III) Gaussian function obtained via peak deconvolution of $(\text{Na}^+)_2[4\text{PEG}_{18}]$. Standard deviations of three times measurements are depicted on each data point.

The incremental tendency of product singly charged ion obviously depended on grafting pattern in star-PEG. The star-PEG grafted with longer PEG-arm is more stable than shorter one, and the similar results were obtained with other star-PEG_n (See also **Figure S3** for $n = 16$ and $n = 20$ in Appendix II). ER-IMS also works for classification of isomeric isomer based on the longest arm chain in star-PEG.

Applying IMC analysis to general sample, for example commercially available product or other synthetic approach enables a detailed analysis on coexistence of isomers with different grafting pattern of PEG-arm. Here, sample mixture with $2\text{PEG}_n\text{-}2\text{OH}$, $3\text{PEG}_n\text{-OH}$ and 4PEG_n were prepared and measured IMC to confirm that IMC peak profile represented by its position, the full width at half maximum (FWHM) are not disturbed by other isomers (**Figure 7.7**). Experimentally obtained IMC profile was perfectly matched with synthesized IMC profile that was obtained by summation of individual IMC data of all components. IMC analyses of doubly charged star-PEG via peak position and ER-IMS should be helpful to analyze and classify the longest PEG-arm

in star-PEG. Based on this idea, IM-MS experiment of doubly charged commercial star-PEG; $4cPEG_n$ was demonstrated.

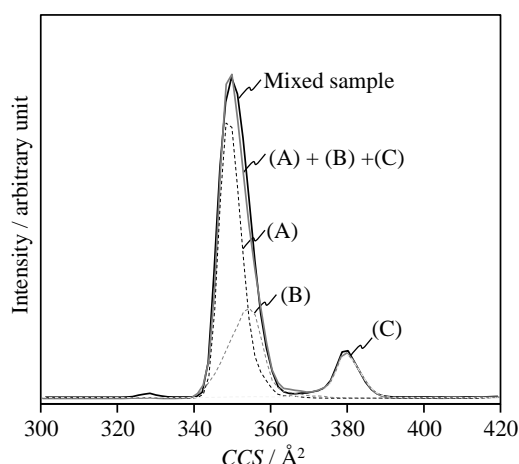


Figure 7.7

Black color solid line represents IMC of mixture sample containing (A) $2PEG_{18}-2OH$, (B) $3PEG_{18}-OH$ and (C) $4PEG_{18}$ described with dotted lines. Synthesis of (A)–(C) were mathematically obtained and depicted on the IMC with gray color solid line.

7.3.4 IMC profile analysis of commercial star-PEG

The IMC profile of $(Na^+)_2[4cPEG_{18}]$ was observed as asymmetric profile without any isolated peaks. Using data analysis software of OriginPro (OriginLab, ver.8.5), peak deconvolution of IMC peak for $(Na^+)_2[4cPEG_{18}]$ were performed with three Gaussian functions; Peak I, II and III (see insertion in Figure 7.6). Peak I ($CCS = 348.0 \text{ Å}^2$, $FWHM = 8.6 \text{ Å}^2$) was obtained with very similar position and width to $4PEG_{18}$ ($CCS = 346.0 \text{ Å}^2$, $FWHM = 8.3 \text{ Å}^2$), neither peak II ($CCS = 356.8 \text{ Å}^2$, $FWHM = 5.3 \text{ Å}^2$) nor peak III ($CCS = 363.9 \text{ Å}^2$, $FWHM = 15.0 \text{ Å}^2$) match with peak of $(Na^+)_2[3PEG_{18}-OH]$ ($CCS = 356.9 \text{ Å}^2$, $FWHM = 12.7 \text{ Å}^2$) and $(Na^+)_2[2PEG_{18}-OH]$ ($CCS = 380.7 \text{ Å}^2$, $FWHM = 8.1 \text{ Å}^2$). IMC profile analysis based on CCS does not work enough to classifying molecular structure of the commercial star-PEG.

Next, ER-IMS measurement was applied to 4cPEG. $(\text{Na}^+)_2[4\text{cPEG}_{18}]$ at $m/z = 487.26$ was selected by the Q-MS and propelled into the ion mobility tube. After traveling through the ion mobility tube, $(\text{Na}^+)_2[4\text{cPEG}_{18}]$ comes into transfer cell and then be transferred under CID at 0–40 V. Precursor ion; $(\text{Na}^+)_2[4\text{cPEG}_{18}]$ and product ion; $\text{Na}^+4\text{cPEG}_{18}$ were detected by time of flight mass spectrometer. Using data analysis software (DriftscopeTM), IMC of $\text{Na}^+4\text{cPEG}_{18}$ produced from precursor doubly charged $(\text{Na}^+)_2[4\text{cPEG}_{18}]$ was extracted. Both peak center position and FWHM of all Gaussian functions are proceeded as followed: peak I–III were fixed and used for peak fitting of IMC obtained at each CID voltage in transfer cell. The peak area I–III was measured for each collision energy, and relative area to CID = 40 V was plot on the ER-IMS (Figure 7.6). The EM-IMS profile of peak I and II could be plot with very close to 4PEG₁₈ and 3PEG₁₈-OH. Taken into account both results from CCS and ER-IMS, peak I can be classified as a homogeneous star-PEG in which all arms are grafted with PEG₄ and PEG₅. Peak II could be classified as slightly inhomogeneous star-PEG in which the longest arm being PEG₆. In comparison to peak I, monomer units are uneven distributed to 4 arms. In both CCS and ER-IMS, peak III locates between 3arm- and 2arm-PEG, which means that longest PEG arm is composed with PEG₇ or PEG₈. FWHM of peak III (15.0 \AA^2) is larger than peak I (8.3 \AA^2) and peak II (5.3 \AA^2). This indicates that peak III could contain some isomers in which the longest PEG-arm should be PEG₇ or PEG₈ whereas the other three of PEG-arms be constituted with different number of monomer units. Considering these matters, peak III can be classified most inhomogeneous star-PEG in 4cPEG₁₈. Resolution of IMC is not enough to distinguish isomers. However, the cross-check in conjunction with CCS and ER-IMS analysis assist to get semi-qualitative insight for isomers and their molecular structure.

7.4 Conclusions

To develop analytical method for investigating existence of isomer in star-polymer, isomeric star-PEGs having different number of PEG-arm was synthesized to evaluate dependency of collision cross-section (*CCS*) on their molecular structure by IM-MS.

Beyond the *CCS* measurement, tolerance of collision induced dissociation is also studied by energy resolved-ion mobility spectrometry (ER-IMS) process of doubly charged star-PEG. This method can elicit subtle difference in molecular structure among isomers. At MD simulation, we observed the doubly charged star-PEG forming asymmetric conformation with globule and rod part played key role to classify isomer for their structure. A commercial star-PEG with uncertain molecular structure was also examined to analyze profile of ion mobility chromatogram (IMC). Its profile of IMC was observed with some shoulder peaks but no isolated peaks, deconvolution with Gaussian function is utilized for extracting IMC for each isomer. Applying both IM-MS and ER-IMS analysis to all extracted peaks, we are able to classify isomers based on their grafting pattern of PEG-arm length in a semi-qualitatively manner. IM-MS simultaneously provides molecular weight and spacious size of synthetic polymer, which is proved to be a crucial method for classifying star-polymer.

Conclusion Remarks

In this work, IM-MS was performed to develop novel analytical methods by focusing on the spacious contribution of each monomer unit to whole size of the macromolecule under the influence of different number of charge. All proposed methods enable extremely swift and precise measurements of these intrinsic properties of synthetic polymers with free of solvent or impurities. IM-MS is a powerful tool for evaluating various types of physical and chemical property of polymer in general, which is a suitable as a routine work for even non-specialists in MS to obtain quantitative and reliable data. The results give a predominant impact on characterization of polymer properties with easy-to-follow protocol and facilitate development of polymer science in the future.

1. Characteristic ratio

IM-MS experiments was performed on PEG, PPG, PMMA and PS, the increment of the collision cross section of the polymer with the degree of polymerization was analyzed in detail in order to evaluate the intrinsic stiffness of the polymer chains. According to MD simulations and experimental results, the globule model is excellently suited for describing the conformational dimensions of PEG and PPG under experimental conditions. The experimentally obtained values of the characteristic ratio C_n of 3.96 for PEG, 5.76 for PPG, respectively, showing excellent agreement with earlier reported values. To verify versatility of proposed method, IM-MS experiment were demonstrated with Na^+ adducted PMMA and PS. From the experiment, C_n is given as 8.65 for PMMA and 7.85 for PS. These results also showed good agreement with reported values.

2. Surface tension

The surface tension of PEG, PPG, PMMA and PS was determined by applying Rayleigh model on critical stable droplet measured from ESI experiment with Li^+ and Na^+ salt. It is noted that two regulations should be considered.

- 1) Sphericity: The minimum polymer ion, which gave the smallest CCS , does not always take spherical dimension. To verify dimension of polymer ion, MD simulation is used here as assistance to characterize steric structure and discriminate sphericity.
- 2) End group correction: CCS containing contribution of polymer chain and end group. If necessary, end group have to be substituted with a hydrogen atom.

Taken into two matters, surface tension can be obtained in good agreement with literature values for PEG with 45.0 mN/m, PPG with 33.1 mN/m, PMMA with 40.0 mN/m and PS with 34.3 mN/m, respectively. This result shows that IM-MS in conjunction with MD simulation enables to evaluate surface tension of synthetic polymer.

3. Relative dielectric constant

IM-MS of doubly charged PEG, $(\text{Na}^+)_2\text{PEG}_n$ ($n = 14-77$), and PPG, $(\text{Na}^+)_2\text{PPG}_n$ ($n = 11-64$) was demonstrated to evaluated the increment dependency of CCS_{eff} on n with the help of MD simulation. From this dependency, the relative dielectric constant (ϵ_r) can be derived. The obtained values for ϵ_r were 7.98 and 6.18 for PEG and PPG, respectively. Although no available reference data for PPG, result of PEG showed relatively good agreement with earlier reported values. As for larger doubly charged polymer, which corresponding $(\text{Na}^+)_2\text{PEG}_n$ ($n = 64-77$) and $(\text{Na}^+)_2\text{PPG}_n$ ($n = 59-64$), can form globule structure. By fitting experimentally measured CCS_{eff} data to globule model, the characteristic ratio C_n of 4.30 and 5.46 for PEG and PPG, respectively, were obtained, which also showed excellent agreement with earlier reported values. The proposed methodology enables the evaluation of intrinsic dielectric properties of polymer. In addition to the high sensitivity and accuracy of MS experiment, combination with ion mobility raises further analytical possibility of MS in polymer science field.

4. Classification structure of isomer in a star-shape polymer

Isomeric star-PEGs with different number of PEG-arms was synthesized to evaluate dependency of collision cross-section (*CCS*) on their molecular structure by IM-MS. As an crosscheck method, tolerance of collision induced dissociation was studied using energy resolved-ion mobility spectrometry (ER-IMS) process for doubly charged star-PEG. This method can elicit subtle difference in molecular structure among isomers. In conjunction with MD simulation, it became apparent that doubly charged star-PEG forming asymmetric conformation with globule and rod part played key role to classify isomers under their structure. A commercial star-PEG with uncertain molecular structure was also examined and analyzed with ion mobility chromatogram (IMC). Although profile of IMC was observed with some shoulder peaks but no isolated peaks, deconvolution with Gaussian function could be utilized for extracting each isomer from IMC. Applying IM-MS and ER-IMS analysis to all extracted peaks, we are able to classify isomers based on their grafting pattern of PEG-arm length in a semi-qualitatively manner. IM-MS simultaneously provides molecular weight and spacious size of synthetic polymer, which is proved to be a crucial method for classifying star-polymer.

Bibliography

- (1) Aston, F. W. *Philos. Mag.* **1919**, 38 (228), 707–714.
- (2) Sharma, K. S. *Int. J. Mass Spectrom.* **2013**, 349–350 (1), 3–8.
- (3) H.W.Kroto, J.R.Heath, S.C.O’Brien, R.F.Curl, R. E. S. *Nature* **1985**, 313 (14), 162–163.
- (4) T.D. Maerk, G. H. D. *Electron Impact Ionization*; Springer-Verlag: Wien, 1985.
- (5) Hoffmann, E. de; Stroobant, V. *Mass Spectrometry: Principals and Applications*, 3rd ed.; John Wiley and Sons: England, 2007.
- (6) Tanaka, K.; Waki, H.; Ido, Y.; Akita, S.; Yoshida, Y.; Yoshida, T.; Matsuo, T. *Rapid Commun. Mass Spectrom.* **1988**, 2 (8), 151–153.
- (7) Karas, M.; Hillenkamp, F. *Anal. Chem.* **1988**, 60 (20), 2299–2301.
- (8) Yamashita, M.; Fenn, J. B. *J Phys.Chem.* **1984**, 88 (20), 4451–4459.
- (9) Barner-Kowollik, C., Gruendling, T., Falkenhagen, J., Weidner, S. *Mass spectrometry in polymer chemistry*, 1st ed.; Wiley: Germany, 2012.
- (10) Hanton, S. D. *Chem. Rev.* **2001**, 101 (2), 527–569.
- (11) Montaudo, G. , Lattimer, R. P. *Mass spectrometry of polymers*; Montaudo, G. , Lattimer, R. P., Ed.; CRC Press: US, 2002.
- (12) Hunt, D. F.; Buko, A. M.; Ballard, J. M.; Shabanowitz, J.; Giordani, A. B. *Biol. Mass Spectrom.* **1981**, 8 (9), 397–408.
- (13) Crecelius, A. C.; Baumgaertel, A.; Schubert, U. S. *J. Mass Spectrom.* **2009**, 44 (9), 1277–1286.
- (14) Buback, M.; Frauendorf, H.; Günzler, F.; Huff, F.; Vana, P. *Macromol. Chem. Phys.* **2009**, 210 (19), 1591–1599.
- (15) Buback, M.; Günzler, F.; Russell, G. T.; Vana, P. *Macromolecules* **2009**, 42 (3), 652–662.
- (16) Buback, M.; Frauendorf, H.; Günzler, F.; Vana, P. *Polymer (Guildf).* **2007**, 48 (19), 5590–5598.

- (17) Buback, M.; Frauendorf, H.; Vana, P. *J. Polym. Sci. Part A Polym. Chem.* **2004**, *42* (17), 4266–4275.
- (18) Vana, P.; Albertin, L.; Barner, L.; Davis, T. P.; Barner-Kowollik, C. *J. Polym. Sci. Part A Polym. Chem.* **2002**, *40* (22), 4032–4037.
- (19) *Characterization and Analysis of Polymers*; John Wiley and Sons: New Jersey, 2007.
- (20) Wilkins, C. L.; Trimpin, S. *Ion Mobility Spectrometry - Mass Spectrometry*; CRC Press, 2011.
- (21) Hiraoka, K. *J. Mass Spectrom. Soc. Japan* **2013**, *58* (4), 139–154.
- (22) von Helden, G.; Wyttenbach, T.; Bowers, M. T. *Int. J. Mass Spectrom. Ion Process.* **1995**, *146–147*, 349–364.
- (23) Wyttenbach, T.; Von Helden, G.; Bowers, M. T. *Int. J. Mass Spectrom. Ion Process.* **1997**, *165–166*, 377–390.
- (24) Trimpin, S.; Plasencia, M.; Isailovic, D.; Clemmer, D. E. *Anal. Chem.* **2007**, *79* (21), 7965–7974.
- (25) Trimpin, S.; Clemmer, D. E. *Anal. Chem.* **2008**, *80* (23), 9073–9083.
- (26) Foley, C. D.; Zhang, B.; Alb, A. M.; Trimpin, S.; Grayson, S. M. *ACS Macro Lett.* **2015**, *4* (7), 778–782.
- (27) Hoskins, J. N.; Trimpin, S.; Grayson, S. M. *Macromolecules* **2011**, *44* (17), 6915–6918.
- (28) Fischer, J. L.; Lutomski, C. A.; El-Baba, T. J.; Siriwardena-Mahanama, B. N.; Weidner, S. M.; Falkenhagen, J.; Allen, M. J.; Trimpin, S. *J. Am. Soc. Mass Spectrom.* **2015**, *26* (12), 2086–2095.
- (29) Woodall, D. W.; Wang, B.; Inutan, E. D.; Narayan, S. B.; Trimpin, S. *Anal. Chem.* **2015**, *87* (9), 4667–4674.
- (30) El-Baba, T. J.; Lutomski, C. A.; Wang, B.; Trimpin, S. *Rapid Commun. Mass Spectrom.* **2014**, *28* (11), 1175–1184.
- (31) Urner, L. H.; Thota, B. N. S.; Nachtigall, O.; Warnke, S.; von Helden, G.; Haag, R.; Pagel, K. *Chem. Commun.* **2015**, *51* (42), 8801–8804.
- (32) Hoffmann, W.; Hofmann, J.; Pagel, K. *J. Am. Soc. Mass Spectrom.* **2014**, *25* (3),

- 471–479.
- (33) Pagel, K.; Harvey, D. J. *Anal. Chem.* **2013**, 85 (10), 5138–5145.
 - (34) Warnke, S.; Baldauf, C.; Bowers, M. T.; Pagel, K.; von Helden, G. *J. Am. Chem. Soc.* **2014**, 136 (29), 10308–10314.
 - (35) Struwe, W. B.; Benesch, J. L.; Harvey, D. J.; Pagel, K. *Analyst* **2015**, 140 (20), 6799–6803.
 - (36) Hofmann, J.; Hahm, H. S.; Seeberger, P. H.; Pagel, K. *Nature* **2015**, 526 (7572), 241–244.
 - (37) Harvey, D. J.; Scarff, C. A.; Edgeworth, M.; Struwe, W. B.; Pagel, K.; Thalassinou, K.; Crispin, M.; Scrivens, J. *J. Mass Spectrom.* **2016**, 51 (3), 219–235.
 - (38) Göth, M.; Lermyte, F.; Schmitt, X. J.; Warnke, S.; von Helden, G.; Sobott, F.; Pagel, K. *Analyst* **2016**, 141 (19), 5502–5510.
 - (39) Struwe, W. B.; Baldauf, C.; Hofmann, J.; Rudd, P. M.; Pagel, K. *Chem. Commun. Chem. Commun* **2016**, 52 (52), 12353–12356.
 - (40) Göth, M.; Pagel, K. *Anal. Bioanal. Chem.* **2017**, 409 (18), 4305–4310.
 - (41) Hofmann, J.; Stuckmann, A.; Crispin, M.; Harvey, D. J.; Pagel, K.; Struwe, W. B. *Anal. Chem.* **2017**, 89 (4), 2318–2325.
 - (42) Lanucara, F.; Holman, S. W.; Gray, C. J.; Evers, C. E. *Nat. Chem.* **2014**, 6 (4), 281–294.
 - (43) May, J. C.; Morris, C. B.; McLean, J. A. *Anal. Chem.* **2016**, acs.analchem.6b04905.
 - (44) Strobl, G. *The Physics of Polymers*, Third Edit.; Springer-Verlag: Berlin, 2007.
 - (45) Rubinstein, M.; Colby, R. H. Polymer physics. *Polymer International*, 2003, 440.
 - (46) Brandrup, J.; Immergut, E. H. *Polymer Handbook*, 3rd ed.; John Wiley: New York, 1989.
 - (47) Jenkins, A.D., Kratochvil, P., Stepto R.F.T., S. U. W. *Pure Appl. Chem.* **1996**, 68 (12), 2287–2311.
 - (48) Krone, N.; Hughes, B. A.; Lavery, G. G.; Stewart, P. M.; Arlt, W.; Shackleton, C. H. L. *J. Steroid Biochem. Mol. Biol.* **2010**, 121 (3–5), 496–504.
 - (49) Carvalho, V. M. *J. Chromatogr. B Anal. Technol. Biomed. Life Sci.* **2012**, 883–884,

- 50–58.
- (50) Ahonen, L.; Fasciotti, M.; Gennäs, G. B. af; Kotiaho, T.; Daroda, R. J.; Eberlin, M.; Kostiaainen, R. *J. Chromatogr. A* **2013**, *1310*, 133–137.
 - (51) Hiraoka, K. *Fundamentals of Mass Spectrometry*, 1st ed.; Springer New York: New York, 2013.
 - (52) Mason, E. A.; McDaniel, E. W. *Transport Properties of Ions in Gases*; Wiley: New York, 1988.
 - (53) Rokushika, S.; Hatano, H.; Bairn, M. A.; Hill, H. H. *Anal. Chem.* **1985**, *57* (9), 1902–1907.
 - (54) Silveira, J. A.; Ridgeway, M. E.; Park, M. A. *Anal. Chem.* **2014**, *86* (12), 5624–5627.
 - (55) Shvartsburg, A. a; Tang, K.; Tolmachev, A. V; Anderson, G. a; Smith, R. D. *Anal. Chem.* **2004**, *77*, 3330–3339.
 - (56) Merenbloom, S. I.; Koeniger, S. L.; Valentine, S. J.; Plasencia, M. D.; Clemmer, D. E. *Anal. Chem.* **2006**, *78* (8), 2802–2809.
 - (57) Giles, K.; Pringle, S. D.; Worthington, K. R.; Little, D.; Wildgoose, J. L.; Bateman, R. H. *Rapid Commun. Mass Spectrom.* **2004**, *18* (20), 2401–2414.
 - (58) Tolmachev, A. V.; Kim, T.; Udseth, H. R.; Smith, R. D.; Bailey, T. H.; Futrell, J. H. *Int. J. Mass Spectrom.* **2000**, *203* (1–3), 31–47.
 - (59) Pringle, S. D.; Giles, K.; Wildgoose, J. L.; Williams, J. P.; Slade, S. E.; Thalassinou, K.; Bateman, R. H.; Bowers, M. T.; Scrivens, J. H. *Int. J. Mass Spectrom.* **2007**, *261* (1), 1–12.
 - (60) Waters Corporation. *Instrument Specifications of SYNAPT G2-S High Definition MS (HDMS) System*; U.S.A., 2013.
 - (61) Flory, P. J. *Stat. Mech. Chain Mol.* **1967**.
 - (62) Sugai, T. *J. Mass Spectrom. Soc. Jpn.* **2010**, *58* (2), 47–73.
 - (63) Bush, M. F.; Campuzano, I. D. G.; Robinson, C. V. *Anal. Chem.* **2012**, *84* (16), 7124–7130.
 - (64) Shvartsburg, A. A.; Smith, R. D. *Anal. Chem.* **2008**, *80* (24), 9689–9699.
 - (65) Larriba, C.; Fernandez De La Mora, J. *J. Phys. Chem. B* **2012**, *116* (1), 593–598.

- (66) Leach, A. R. *Molecular modelling : principles and applications*, 2nd ed.; Prentice Hall: England, 2001.
- (67) Allinger, N. L. *J. Am. Chem. Soc.* **1977**, *99*, 8127–8134.
- (68) Allinger, N. L.; Zhou, X.; Bergsma, J. J. *Mol. Struct. THEOCHEM* **1994**, *312* (1), 69–83.
- (69) PerkinElmer. *ChemBio3D User Guide*.
- (70) Shvartsburg, A. A.; Jarrold, M. F. *Chem. Phys. Lett.* **1996**, *261* (1–2), 86–91.
- (71) Mesleh, M. F.; Hunter, J. M.; Shvartsburg, A. A.; Schatz, G. C.; Jarrold, M. F. *J. Phys. Chem.* **1996**, *100* (40), 16082–16086.
- (72) Mack, E. *J. Am. Chem. Soc.* **1924**, *47* (1920), 2468–2482.
- (73) Williams, J.P., Lough, J. A., Campuzano, I., Richardson, K., Sadler, P. J. *Rapid Commun. Mass Spectrom.* **2009**, *23*, 3563–3569.
- (74) Downard, K. M.; Kokabu, Y.; Ikeguchi, M.; Akashi, S. *FEBS J.* **2011**, *278* (21), 4044–4054.
- (75) Allen, G.; Booth, C.; Price, C. *Polymer (Guildf)*. **1967**, *8*, 397–401.
- (76) Beech, D. R.; Booth, C. *J. Polym. Sci. Part A-2* **1969**, *7*, 575–586.
- (77) Boucher, E. a; Hines, P. M.; Sciences, M. **1978**, *16*, 501–511.
- (78) Ataman, M.; Boucher, E. A.; Sciences, M. **1982**, *20*, 1585–1592.
- (79) Kienberger, F.; Kienberger, F.; Pastushenko, V. P.; Pastushenko, V. P.; Kada, G.; Kada, G.; Gruber, H. J.; Gruber, H. J.; Riener, C.; Riener, C.; Schindler, H.; Schindler, H.; Hinterdorfer, P.; Hinterdorfer, P. *Single Mol.* **2000**, *1* (2), 123–128.
- (80) Lee, H.; Venable, R. M.; Mackerell, A. D.; Pastor, R. W. *Biophys. J.* **2008**, *95* (4), 1590–1599.
- (81) Wyttenbach, T.; Pierson, N. a; Clemmer, D. E.; Bowers, M. T. *Annu. Rev. Phys. Chem.* **2014**, *65*, 175–196.
- (82) Memboeuf, A.; Vekey, K.; Lendvay, G. *Eur. J. Mass Spectrom.* **2011**, *17* (1), 33–46.
- (83) Lewalter, J.; Skarping, G.; Ellrich, D.; Schoen, U. *MAK Collect. Occup. Heal. Saf.* **2012**, *10*, 248–270.
- (84) Bleiholder, C.; Johnson, N. R.; Contreras, S.; Wyttenbach, T.; Bowers, M. T. *Anal.*

- Chem.* **2015**, 87, 7196–7203.
- (85) Lide, D. R. *CRC Handbook of Chemistry and Physics, 94th Edition, 2013-2014*; 2013; Vol. 53.
- (86) Chirot, F.; Calvo, F.; Albrieux, F.; Lemoine, J.; Tsybin, Y. O.; Dugourd, P. *J. Am. Soc. Mass Spectrom.* **2012**, 23 (2), 386–396.
- (87) Abe, A.; Hirano, T.; Tsuruta, T. *Macromolecules* **1979**, 12 (2), 1092–1100.
- (88) Smith, G. D.; Yoon, D. Y.; Jaffe, R. L. *Macromolecules* **1993**, 26 (19), 5213–5218.
- (89) Sasanuma, Y. *Macromolecules* **1995**, 28 (25), 8629–8638.
- (90) Boucher, E. A.; Hines, P. M. *J. Polym. Sci. Polym. Phys. Ed.* **1978**, 16 (3), 501–511.
- (91) Fox, T. G. *Polymer (Guildf)*. **1962**, 3, 111–128.
- (92) Brandrup, J.; Immergut, E.H.; Grulke, E. A. *Polymer Handbook*, 4th ed.; John Wiley and Sons: Canada, 1999.
- (93) Rayleigh, Lord. *Philos. Mag. Ser. 5* **1882**, 14 (87), 184–186.
- (94) Gomez, A.; Tang, K. *Phys. Fluids* **1994**, 6 (1), 404–414.
- (95) Cole, R. B. *Electrospray and MALDI Mass Spectrometry: Fundamentals, Instrumentation, Practicalities, and Biological Applications*, 2nd ed.; John Wiley and Sons: New Jersey, 2010.
- (96) Helfand, E.; Tagami, Y. *J. Chem. Phys.* **1972**, 56 (7), 3592–3601.
- (97) Wesdemiotis, C. *Angew. Chemie - Int. Ed.* **2017**, 56 (6), 1452–1464.
- (98) Kokubo, S.; Vana, P. *Macromol. Chem. Phys.* **2017**, 218, 1600373.
- (99) Pauling, L. *The Nature of the Chemical Bond*, 3rd ed.; Cornell University Press: New York, 1960.
- (100) Fujii, T. *Ion/molecule attachment reactions: Mass spectrometry*, 1st ed.; Springer New York: London, 2015.
- (101) Gidden, J.; Bowers, M. T.; Jackson, A. T.; Scrivens, J. H. *J. Am. Soc. Mass Spectrom.* **2002**, 13 (5), 499–505.
- (102) Wu, S. J. *Macromol. Sci. Part C Polym. Rev.* **1974**, 10, 1–73.
- (103) Roe, R.-J. *J. Colloid Interface Sci.* **1969**, 31 (2), 228–235.
- (104) Kasemura, T.; Suzuki, K.; Uzi, F.; Kondo, T.; Hata, T. *Kobunshi Ronbunshu* **1978**,

- 35 (12), 779–786.
- (105) Roe, R. J. *J. Phys. Chem.* **1968**, 72 (6), 2013–2017.
 - (106) Kasemura, T., Hata, T. *Kobunshi Ronbunshu* **1976**, 33 (4), 192–200.
 - (107) Kasemura, T., Yamashita, N., Suzuki, T., Hata, T. *Kobunshi Ronbunshu* **1978**, 35 (4), 263–268.
 - (108) Rastogi, A. K.; St. Pierre, L. E. *J. Colloid Interface Sci.* **1971**, 35 (1), 16–22.
 - (109) Rastogi, A. K.; Pierre, L. E. *J. Colloid Interface Sci.* **1969**, 31 (2), 168–175.
 - (110) Legrand, D. G.; Gaines, G. L. *J. Colloid Interface Sci.* **1973**, 42 (1), 181–184.
 - (111) Omenyi, S. N.; Neumann, A. W.; Martin, W. W.; Lespinard, G. M.; Smith, R. P. *J. Appl. Phys.* **1981**, 52 (2), 796–802.
 - (112) Blott, S. J.; Pye, K. *Sedimentology* **2008**, 55 (1), 31–63.
 - (113) Cole, R. B. *J. Mass Spectrom.* **2000**, 35 (7), 763–772.
 - (114) Ude, S.; Fernández De La Mora, J.; Thomson, B. A. *J. Am. Chem. Soc.* **2004**, 126 (38), 12184–12190.
 - (115) Larriba, C.; De La Mora, J. F.; Clemmer, D. E. *J. Am. Soc. Mass Spectrom.* **2014**, 25 (8), 1332–1345.
 - (116) Mao, Y.; Burin, L. A.; Ratner, M. A.; Jarrold, M. F. *J. Chem. Phys.* **2002**, 116 (22), 9964–9974.
 - (117) Koizumi, N.; Hanai, T. *Bull. Inst. Chem. Res. Kyoto Univ.* **1964**, 115–127.
 - (118) Sengwa, R. J. *Polym. Int.* **2004**, 53 (6), 744–748.
 - (119) Wohlfarth, C. *Landolt-Börnstein-Group IV Physical Chemistry*, 2008, 568–570.
 - (120) Doi, M.; Edwards, S. F. *The Theory of Polymer Dynamics*; Oxford Univ Press: New York, 1988.
 - (121) Fetters, L. J.; Andrea, D. K.; J, D. S. P.; Vitus, F. J. *Macromolecules* **1993**, 26, 647–654.
 - (122) Ren, J. M.; McKenzie, T. G.; Fu, Q.; Wong, E. H. H.; Xu, J.; An, Z.; Shanmugam, S.; Davis, T. P.; Boyer, C.; Qiao, G. G. *Chem. Rev.* **2016**, 116 (12), 6743–6836.
 - (123) Gao, H. *Macromol. Rapid Commun.* **2012**, 33 (9), 722–734.
 - (124) Lapienis, G. Star-shaped polymers having PEO arms. *Progress in Polymer Science (Oxford)*, 2009, 34, 852–892.

Bibliography

- (125) Kuki, Á.; Nagy, L.; Nagy, T.; Zsuga, M.; Kéki, S. *J. Mass Spectrom.* **2013**, *48* (10), 1125–1127.
- (126) Kokubo, S.; Vana, P. *Macromol. Chem. Phys.* **2017**, *201700126*, 1700126.
- (127) Liu, Y.; Clemmer, D. E. *Anal. Chem.* **1997**, *69* (13), 2504–2509.
- (128) Josse, T.; De Winter, J.; Dubois, P.; Coulembier, O.; Gerbaux, P.; Memboeuf, A. *Polym. Chem.* **2015**, *6* (1), 64–69.

Appendix

Appendix I

Recipe of CCS calibration sample

I-1 General caution

- CCS calibration must be performed 1 hour after turning on ionization source to stabilize gas pressure of ion mobility tube.
- Polyalanine is fragile to heat. Store it in a freezer under -20°C .

I-2 Chemicals

- Poly-alanine : Sigma-Aldrich, Poly-DL-alanine molecular weight : 1000-5000
- Acetonitrile : LC-MS grade
- Water : LC-MS grade, Unavailable with tap water
- Formic acid : Sigma-Aldrich, reagent grade, $\geq 95\%$

I-3 Preparation of poly-alanine calibration solution (Original)

Original poly-alanine calibration solution (PA-sol) is prepared by Poly-alanine dissolving in acetonitrile/water (50/50) solution with 1mg/mL. The PA-sol must be stored in refrigerator (Do not keep it at room temperature).

I-4 Preparation of poly-alanine calibration solution (Just before calibration)

Just before calibration, 10 μL of PA-sol is collected by pipet with disposable tip. 10 μL of PA is dissolved with 1 mL of 0.1 % formic acid acetonitrile/water (50/50). Eventually, 10 $\mu\text{g/mL}$ of PA solution can be injected into IM-MS by a syringe.

Appendix II

Supporting information of Chapter 7

IM-MS of 2arm-PEG (2PEG_n-2OH), 3arm-PEG (3PEG_n-OH) and 4arm-PEG (4PEG_n) with $n = 16$ and 20 were also performed as well as $n = 18$. Each ion mobility chromatogram (IMC) of singly charged ion; Na⁺[2PEG_n-OH] with $n = 16$ and 20 was observed in slightly higher collision-cross section (CCS) region (Figure S1 (1A) and (2A)), CCS of all other star-PEGs did not depend on the number of PEG-arm (Figure 4 (1B)-(1C) and (2B)-(2C)). On the other hand, as for doubly charged ion, the peak maximum position of IMC obviously depend on the number of PEG-arm, the less number of PEG-arm gives larger CCS on IMC (Figure S2 (1A)-(1C) and (2A)-(2C)). In addition to spacious size of doubly charged ion, ER-IMS also works well for discriminating the number of grafting PEG-arm. IMC and ER-IMS measurement of doubly charged star-PEG were performed for commercial star-PEG (4cPEG) with molecular structure unknown isomers.

IMC of doubly charged 4cPEG showed asymmetric profile with some shoulders but no isolated peaks. Using data analysis software of OriginPro (OriginLab, ver.8.5), peak deconvolution of IMC peak were performed by three Gaussian functions; Peak I–III (see insertion in Figure S2). Extracted peaks could be originated from isomer with different arm number.

Two peaks were extracted from IMC of (Na⁺)₂[4cPEG₁₆], and profile of peak I (CCS = 334.9 Å², FWHM = 11.5 Å²) showed closer to (Na⁺)₂[4PEG₁₆] (CCS = 331.5 Å², FWHM = 11.2 Å²). In ER-IMS, peak I did not perfectly match with (Na⁺)₂[4PEG₁₆], but it located between (Na⁺)₂[4PEG₁₆] and (Na⁺)₂[3PEG₁₆-OH]. Considering these matters, peak I should be originated from star-PEG constituted of almost same chain length with four PEG4 and/or PEG5, therefore, it can be regarded as a homogeneous star-PEG. Neither CCS and FWHM of peak II (CCS = 346.9 Å², FWHM = 12.6 Å²) were observed with similar values with (Na⁺)₂[3PEG₁₆-OH] (CCS = 342.6 Å², FWHM = 7.1 Å²). In

ER-IMS, peak II located at the almost center between $(\text{Na}^+)_2[3\text{PEG}_{16}\text{-OH}]$ and $(\text{Na}^+)_2[2\text{PEG}_{16}\text{-2OH}]$. Taken into account IMC and ER-IMS, peak II should be assigned to inhomogeneous star-PEG with one of PEG-arm with longer than PEG_5 but less than PEG_8 , possibly, PEG_6 or PEG_7 . Remaining 9–10 monomer units are distributed to other three arms with randomly, therefore, coexisting isomers could make FWHM of IMC broaden.

Three peaks were extracted from $(\text{Na}^+)_2[4\text{cPEG}_{20}]$, and profile of peak I ($\text{CCS} = 369.7 \text{ \AA}^2$, $\text{FWHM} = 9.2 \text{ \AA}^2$) showed very similar to IMC of $(\text{Na}^+)_2[4\text{PEG}_{20}]$ ($\text{CCS} = 367.4 \text{ \AA}^2$, $\text{FWHM} = 8.5 \text{ \AA}^2$). ER-IMS of peak I located between $(\text{Na}^+)_2[4\text{PEG}_{20}]$ and $(\text{Na}^+)_2[3\text{PEG}_{20}\text{-OH}]$, therefore, PEG_5 or PEG_6 forms each arm of 4cPEG_{20} .

Peak II ($\text{CCS} = 378.6 \text{ \AA}^2$, $\text{FWHM} = 8.8 \text{ \AA}^2$) showed very similar to CCS of $(\text{Na}^+)_2[3\text{PEG}_{20}\text{-OH}]$ ($\text{CCS} = 382.9 \text{ \AA}^2$, $\text{FWHM} = 9.0 \text{ \AA}^2$). ER-IMS of peak II located between $(\text{Na}^+)_2[3\text{PEG}_{20}\text{-OH}]$ and $(\text{Na}^+)_2[2\text{PEG}_{20}\text{-2OH}]$. This ER-IMS indicates that the longest PEG-arm corresponds to PEG_6 or PEG_7 .

And last, Peak III ($\text{CCS} = 387.1 \text{ \AA}^2$, $\text{FWHM} = 8.7 \text{ \AA}^2$) was also observed between $(\text{Na}^+)_2[3\text{PEG}_{20}\text{-OH}]$ ($\text{CCS} = 382.9 \text{ \AA}^2$, $\text{FWHM} = 9.0 \text{ \AA}^2$) and $(\text{Na}^+)_2[2\text{PEG}_{20}\text{-2OH}]$ ($\text{CCS} = 407.4 \text{ \AA}^2$, $\text{FWHM} = 7.8 \text{ \AA}^2$) on IMC. On the ER-IMS, peak III located closer to $(\text{Na}^+)_2[2\text{PEG}_{20}\text{-2OH}]$ in comparison to peak II. The longest PEG-arm is composed of PEG_8 or PEG_9 , 11–12 of monomer units were grafted into other three arms. Peak III should be the inhomogeneous star-PEG.

The cross-check analysis with CCS and ER-IMS can detect and identify isomer of star-PEG with more easily and quickly than other analytical methodology.

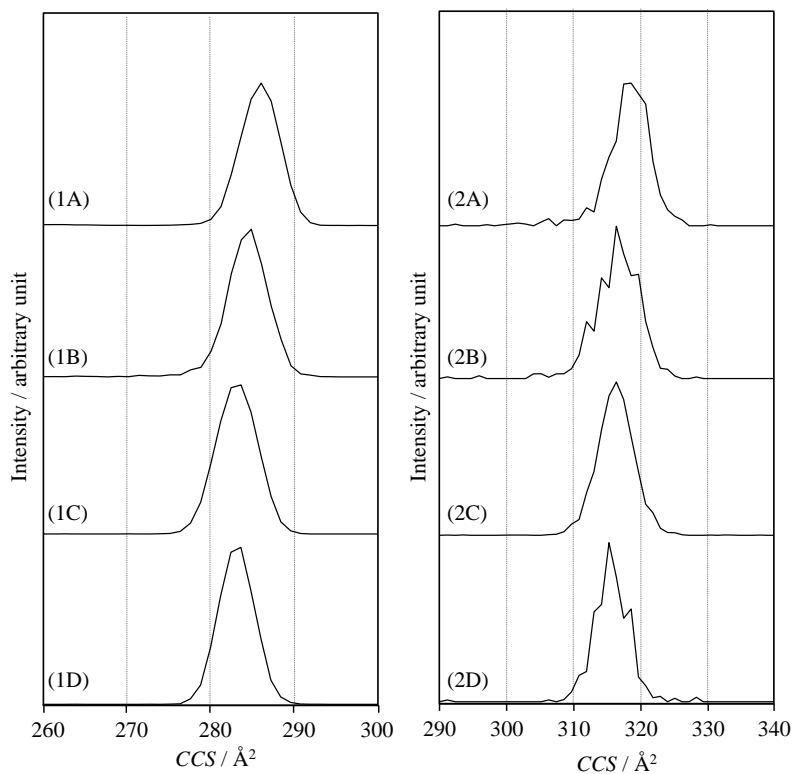


Figure S1

Left hand side IMC of singly charged (1A) $\text{Na}^+[\text{2PEG}_{16}\text{-2OH}]$, (1B) $\text{Na}^+[\text{3PEG}_{16}\text{-OH}]$, (1C) $\text{Na}^+[\text{4PEG}_{16}]$ and (1D) $\text{Na}^+[\text{4cPEG}_{18}]$. Right hand side IMC of singly charged (2A) $\text{Na}^+[\text{2PEG}_{20}\text{-2OH}]$, (2B) $\text{Na}^+[\text{3PEG}_{20}\text{-OH}]$, (2C) $\text{Na}^+[\text{4PEG}_{20}]$ and (2D) $\text{Na}^+[\text{4cPEG}_{20}]$.

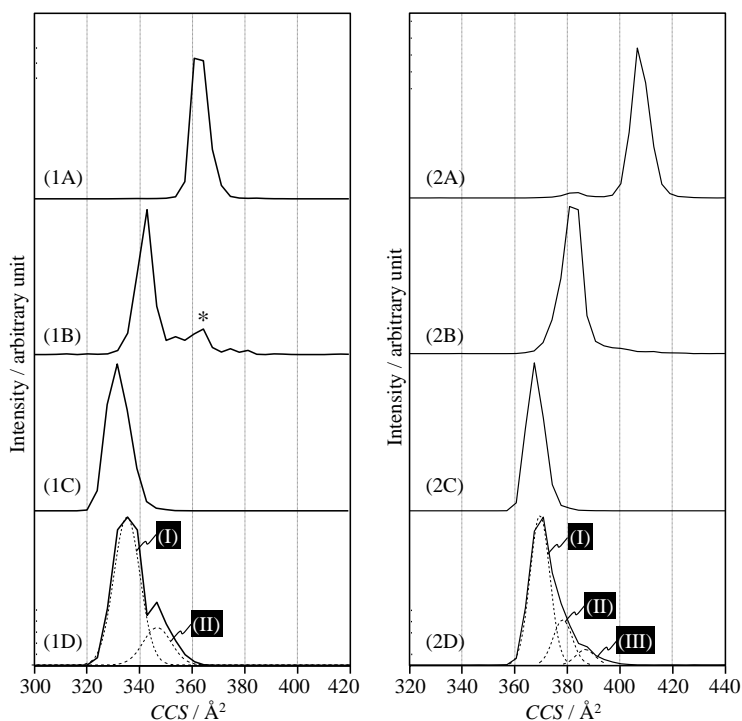


Figure S2

Left hand side IMC of doubly charged (1A) $(\text{Na}^+)_2[2\text{PEG}_{16}\text{-2OH}]$, (1B) $(\text{Na}^+)_2[3\text{PEG}_{16}\text{-OH}]$, (1C) $(\text{Na}^+)_2[4\text{PEG}_{16}]$ and (1D) $(\text{Na}^+)_2[4\text{CPEG}_{16}]$. Right hand side IMC of doubly charged (2A) $(\text{Na}^+)_2[2\text{PEG}_{20}\text{-2OH}]$, (2B) $(\text{Na}^+)_2[3\text{PEG}_{20}\text{-OH}]$, (2C) $(\text{Na}^+)_2[4\text{PEG}_{20}]$ and (2D) $(\text{Na}^+)_2[4\text{CPEG}_{20}]$. An asterisk on (1B) should be originated from isomer which has similar PEG-arm structure to $2\text{PEG}_{16}\text{-2OH}$ according to its CCS. Peak I–III in (1D) and (2D) are Gaussian functions obtained via IMC deconvolution.

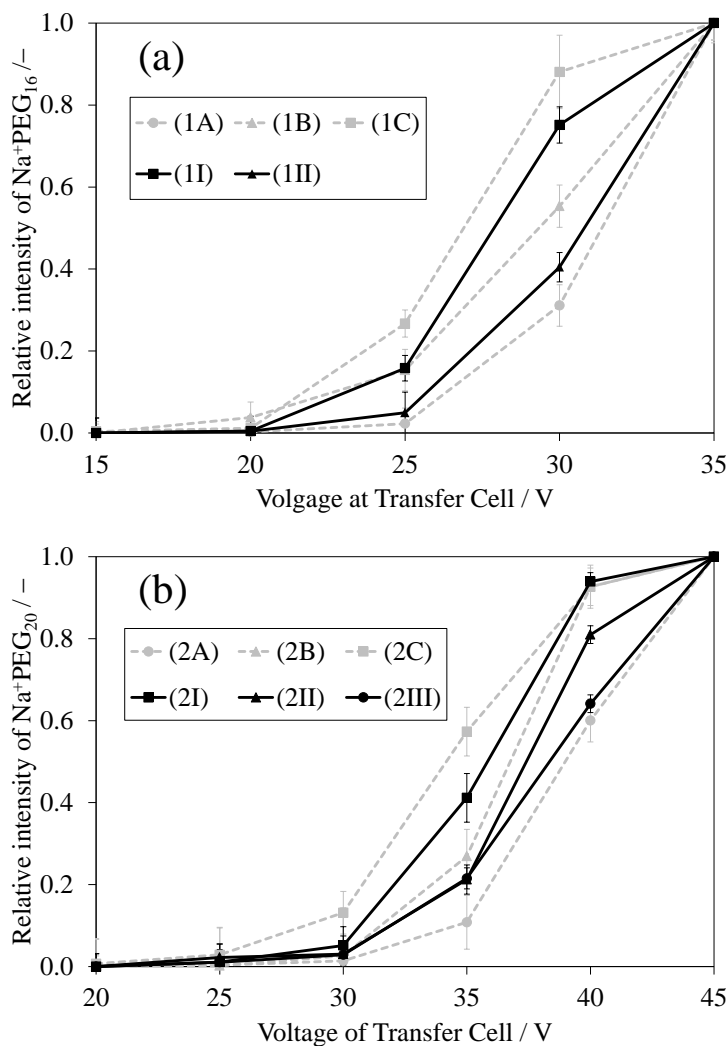


Figure S3

ER-IMS of doubly charged (a) star-PEG₁₆ and (b) star-PEG₂₀.

(1A) (Na⁺)₂[2PEG₁₆-2OH], (1B) (Na⁺)₂[3PEG₁₆-OH], (1C) (Na⁺)₂[4PEG₁₆], (2A) (Na⁺)₂[2PEG₂₀-2OH], (2B) (Na⁺)₂[3PEG₂₀-OH] and (2C) (Na⁺)₂[4PEG₂₀] are depicted with dotted line. ER-IMS of (1I)–(2III) Gaussian functions were obtained by peak deconvolution (See Figure S2). Standard deviations of three times measurements are depicted on each data point.

Appendix III

Abbreviations

α_i	the angles one dipoles form the other vector
b	van der Waals coefficient originated from excluded volume effect
χ	angle between two dipoles
CCS	collision cross section
CCS_{eff}	effective collision cross section
CID	collision induced dissociation
C_n	characteristic ratio
D	diffusion coefficient
DC	direct current
D_c	the smallest circumscribed circle diameter in a particle
d_{gas}	a diameter of vapor gas in the ion mobility tube
D_i	the largest inscribed circle diameter in a particle
d_{ion}	diameter of the sample ion
DMA	differential mobility analyzer
E	electric field of vector in the ion mobility tube
e	elementary charge
ε	dielectric constant
ε_r	relative dielectric constant
ε_0	electric constant
E_{bend}	stiffness of the spring's angle-bending
E_{cc}	charge/charge interaction
E_{cd}	charge/dipole interaction
E_{dd}	dipole/dipole interaction
$ER-IMS$	energy resolved-ion mobility spectrometry
ESI	electro spray ionization

E_{stretch}	bond stretching energy
E_{torsion}	torsion energy
E_{vdW}	van der Waals energy
\mathbf{F}	field force applied to ion in IM tube
ϕ	torsion angle
f_{A}	average collision frequency
f_{e}	Coulomb force of +2 charged polymer
f_{s}	entropy elastic force
FWHM	full width at half maximum
γ	surface tension
h	number of step for MD simulation
HPLC	high performance liquid chromatography
IM	ion mobility
IMC	ion mobility chromatogram
IM-MS	ion mobility-mass spectrometry
IMS	ion mobility spectrometry
IR	infra-red spectroscopy
K	ion mobility
k	Boltzmann constant
K	Kelvin (temperature)
k_{eff}	effective number of bond which contributes to projected \mathbf{R}_p
k_n	number of bond in polymer main chain
k_p	effective number of elements which contribute to projection area
K_s	stiffness of spring's bond-stretching
λ	free drift path of ion in IM drift tube
\mathbf{l}	bond vector consecutive atom in polymer chain
m	mass of sample ion
M	mass of vapor gas in ion mobility tube
M_n	number average molar mass
M_n	weight average molar mass

Appendix

m/z	ratio molar mass to number of charge
MALDI	matrix-assisted-laser-desorption-ionization
MD	molecular dynamics
μ	magnitude of dipole moment
M_n	number average molar mass
MS	mass spectrometer
n	number of monomer unit
N	number of excess charges
N_{gas}	gas density in ion mobility tube
NMR	nuclear-magnetic resonance spectroscopy
$p(t)$	collision event possibility with Poisson's distribution
PA	projection approximation
PEG	polyethylene glycol
PMMA	polymethyl methacrylate
PPG	polypropylene glycol
PS	polystyrene
q	charge
Q	excess charge in charged droplet
θ_0	equilibrium angle
θ_i	projection angle of 3D vector
R	resolution of ion mobility spectrometer
\mathbf{R}	end to end vector of polymer in 3D
r_0	equilibrium length of spring
R_{eff}	effective radius of ion detected by IM-MS
RF	radio frequency
R_g	gyration radius of polymer
R_{globule}	radius of globule coil polymer
$\mathbf{R}_{\text{globule}}$	end-to-end vector of the globular part of polymer
r_i	van der Waals radii for atoms
r_{ij}	an actual distance between two atoms

R_p	end to end vector of polymer on 2D
R_{rod}	end-to-end vector of rod part of polymer
s	the projection area of spherical elements in globule
S	spherical index of aggregated cation adducted polymer
σ	standard deviation of the diffusion process
$S_{p,globule}$	projection area of globule
SRIG	stacked ring Ion guide in traveling wave ion mobility spectrometer
T	temperature
TBMM	tetrakis-bromomethyl-methane
TM	trajectory method
TOF	time of flight
TW	traveling wave
UPLC	ultra performance liquid chromatography
v	velocity of gas in ion mobility tube
V	velocity of sample in ion mobility tube
V	volume of globule coil
v	volume of spherical elements in globule
v_d	drift velocity of ion
V_i	internal potential energy of polymer
V_n	torsional force constant
v_r	relative velocity of the ion to the gas molecule
Ω	collision cross section
W'	width of ion mobility peak
W_h	width of ion packet in ion mobility tube
ξ	parameter determines depth of attractive potential energy well in van der Waals energy
x	particle's position

Acknowledgements

- Prof. Dr. Philipp Vana, MBA

First of all, I appreciate Prof. Dr. Philipp Vana, MBA (Institute of Physical Chemistry, University of Göttingen) for giving a chance to study and supervise for my work in doctor course. Doctor research sometimes brought me new finding which made me extremely excited, on the other hand, sometimes it entailed lonely and hard study to create ideas and develop theory by myself. Prof. Dr. Vana has never denied me, however, always given me helpful suggestions on all my works with warm words of encouragement. I am supremely happy to study under his supervise.

- Prof. Dr. Konrad Koszinowski

I thank Prof. Dr. Konrad Koszinowski (Institute of Organic and Biomolecular Chemistry, University of Göttingen) offering much helpful advice as an expert of Mass Spectrometry. It was very helpful for verifying my hypothesis and building my theory for doctor thesis.

- Dr. Holm Frauendorf

I am grateful to Dr. Holm Frauendorf (Institute of Organic and Biomolecular Chemistry, University of Göttingen) for administrating IM-MS. Thanks to his daily maintenance and troubleshooting, I could carry out IM-MS experiment very smoothly.

- Colleague of the research group; Macromolecular Chemistry Group

I would like to offer my special thanks to Mr. Wantao Peng and Dr. Christian Roßner for synthesizing polymer sample. The polymer was essential to verify my thesis for Chapter 7. I would like to thank Dr. Hendrik Kattner for his supporting and teaching me about many things such as how to serve teaching assistant, earn credit, print a poster at symposium and so on. Besides daily matter, Dr. Hendrik Kattner willingly lent his ear to discussions on my research as a expert of kinetics of polymerization. I also want to

thank all members of Macromolecular Chemistry and Technical and Macromolecular Chemistry group for supporting my research activity and encourage me to study.

- Waters Corporation

I am grateful to the technical staff members of Nihon Waters K.K., particularly, Ms. Mayumi Momma, Mr. Futoshi Sato and Mr. Yosuke Uraga for offering technical and supporting information for the IM-MS.

- Canon, Inc, Japan

During my PhD course enrollment in the University of Göttingen, tuition fee and living costs were fully covered by Canon, Inc. I would like to thank Canon, Inc. for giving an extraordinary precious chance of studying as a PhD student for 3 years (From April 2015 to March 2018).

- My Family

In the end, I am grateful to all my lovely family members, my wife Kaori Kokubo, my elder son Ryosuke Kokubo and my younger son Seisuke Kokubo. Particularly for my sons, they have overcome many difficulties in learning German language and custom. I was always encouraged by their aggressive attitude of doing their best in daily life. And my wife energized me with her cooked delicious meals and warm words of kindness. It was essential for me to keep vigorousness. I am really glad to spend in Germany with all my family. Memory of 3-year-staying in Germany, which is common treasure of all my family, will keep encouraging us in the future.

Acknowledgements

About Author

Shinsuke Kokubo, Japan

Education

1998–2002

Bachelor of Science, Keio University, Japan

Bachelor Thesis: “Negative ion photoelectron spectroscopy of acetonitrile clusters”

Supervisors: Dr. Masaaki Mitsui and Prof. Dr. Atsushi Nakajima

2002–2004

Master of Science, Keio University, Japan

Master Thesis:

“Elucidation of the excess electron states in size selected molecular nano-clusters”

Supervisors: Dr. Masaaki Mitsui, and Prof. Dr. Atsushi Nakajima

2015–2018

Doctoral Studies, University Göttingen, Germany

Supervisors: Prof. Dr. Philipp Vana, MBA and Prof. Dr. Konrad Koszinowski

Awards

- 1) Young Excellent Presentation Award/The 26th Elastomer Symposium (The Society of Rubber Science and Technology, Japan), December 2014, Nagoya, Japan
- 2) Poster Award, 20th European Symposium on Polymer Spectrometry, September 2016, Dresden, Germany

Publications

- 1) Coexistence of solvated electrons and solvent valence anions in negatively charged acetonitrile clusters, $(\text{CH}_3\text{CN})_n^-$ ($n = 10\text{--}100$)
M. Mitsui, N. Ando, **S. Kokubo**, A. Nakajima and K. Kaya, *Physical Review Letters* **2003**, *91*, Art. No. 153002
- 2) Negative ion photoelectron spectroscopy of acridine molecular anion and its monohydrate
K. Kokubo, N. Ando, K. Koyasu, M. Mitsui and A. Nakajima, *Journal of Chemical Physics*, **2004**, *121*, 11112
- 3) Photoelectron spectroscopy of pyrene cluster anions, $(\text{pyrene})_n^-$ ($n = 1\text{--}20$)
N. Ando, **S. Kokubo**, M. Mitsui and A. Nakajima, *Chemical Physics Letters*, **2004**, *389*, 279
- 4) Coexistence of two different anion states in polyacene nanocluster anions
M. Mitsui, **S. Kokubo**, N. Ando, Y. Matsumoto, A. Nakajima and K. Kaya, *Journal of Chemical Physics*, **2004**, *121*, 7553
- 5) Effective Demetalization and Suppression of Coke Formation Using Supercritical Water Technology for Heavy Oil Upgrading
S. Kokubo, K. Nishida, A. Hayashi, H. Takahashi, O. Yokota and S. Inage, *Journal of the Japan Petroleum Institute*, **2008**, *51*, 309
- 6) Easy Access to the Characteristic Ratio of Polymers Using Ion-Mobility Mass Spectrometry
S. Kokubo and P. Vana, *Macromolecular Physics and Chemistry*, **2017**, *218*, 1600373
- 7) Obtaining the Dielectric Constant of Polymers from Doubly-Charged Species in Ion-Mobility Mass Spectrometry
S. Kokubo and P. Vana, *Macromolecular Physics and Chemistry*, **2017**, *218*, 1700018

Presentations at Conference/Symposium

Invited Lecture

- 1) “Characterization of Physical and Chemical Properties of Polymers Using Ion-Mobility Mass Spectrometry”
8th International Symposium on the Separation and Characterization of Natural and Synthetic Macromolecules, February 2017, Amsterdam, Nederland

Oral Presentation

- 1) “Observation of solid-liquid phase transition in giant negatively charged cluster”
(Title in Japanese: 巨大クラスター負イオンにおける固-液相転移の観測)
Annual meetings of Japan society for molecular Science 2003, September 2003, Kyoto, Japan
- 2) “Development of hydro-thermal upgrading treatment for heavy oil”
(Title in Japanese: 水熱処理による重質油改質技術の開発)
36 th Petroleum/Petroleum Chemistry Symposium, The Japan Petroleum Institute, November 2005, Kagoshima, Japan
- 3) “Young’s modulus and chemical properties of electron irradiated butadiene series rubbers”
(Title in Japanese: 電子線照射したブタジエン系ゴムの弾性特性と化学変化に関する研究)
26th Elastomer Symposium, The Society of Rubber Science and Technology Japan, December 2014, Nagoya, Japan
- 4) “Evaluation for physical and chemical properties of rubber material with DEP-MS”
(Title in Japanese: 直接導入型質量分析法によるゴムの物理・化学的特性の評価)
26th Elastomer Symposium, The Society of Rubber Science and Technology Japan, December 2014, Nagoya, Japan

Poster Presentation

- 1) “Photoelectron Spectroscopy of negatively charged hydrogen bonded cluster”
(Title in Japanese: 水素結合性クラスター負イオンの光電子分光)
18th Symposium on Chemical Kinetics and Dynamics, May 2002, Niigata, Japan
- 2) “Study on Production and Photoelectron Spectroscopy of Molecular Aggregate with Nanometer Scale”
(Title in Japanese: ナノメーター領域の分子集合体の生成とその光電子分光)
Annual meetings of Japan society for molecular Science 2002, September 2002, Kobe, Japan
- 3) “Negative ion photoelectron spectroscopy of (benzene)_n⁻ and (toluene)_n⁻ : Solvation energetics of excess electron”
11th International symposium on Small Particles and Inorganic Clusters, September 2003, Strasbourg, France
- 4) “Easy Access to the Characteristic Ratio of Polymers Using Ion-Mobility Mass Spectrometry”
20th European Symposium on Polymer Spectroscopy, September 2016, Dresden, Germany
- 5) “Characterization of Physical and Chemical Properties of Polymers Using Ion-Mobility Mass Spectrometry”
5th International Symposium Frontiers in Polymer Science 2017, Sevilla, Spain

